LBL-3411
c.2

STUDY OF PARTIAL WAVE BRANCHING IN THE ALPHA DECAY OF ^{241}Am, ^{253}Es, AND ^{255}Fm

Arthur James Soinski
(Ph. D. thesis)

September, 1974

Prepared for the U. S. Atomic Energy Commission
under Contract W-7405-ENG-48

TWO-WEEK LOAN COPY

This is a Library Circulating Copy which may be borrowed for two weeks. For a personal retention copy, call Tech. Info. Division, Ext. 5545

LAWRENCE BERKELEY LABORATORY
UNIVERSITY OF CALIFORNIA
BERKELEY

LBL-3411
c.2

DISCLAIMER

This document was prepared as an account of work sponsored by the United States Government. While this document is believed to contain correct information, neither the United States Government nor any agency thereof, nor the Regents of the University of California, nor any of their employees, makes any warranty, express or implied, or assumes any legal responsibility for the accuracy, completeness, or usefulness of any information, apparatus, product, or process disclosed, or represents that its use would not infringe privately owned rights. Reference herein to any specific commercial product, process, or service by its trade name, trademark, manufacturer, or otherwise, does not necessarily constitute or imply its endorsement, recommendation, or favoring by the United States Government or any agency thereof, or the Regents of the University of California. The views and opinions of authors expressed herein do not necessarily state or reflect those of the United States Government or any agency thereof or the Regents of the University of California.

TABLE OF CONTENTS

Abstract v

I. Introduction 1

II. Thermal Equilibrium Nuclear Orientation Theory 6

III. Alpha Particle Angular Distributions 7

IV. Alpha Particle Partial Wave Amplitudes and Phases 10

A. The Bohr, Fröman and Mottelson Method 11

B. Mang Shell Model Theory 14

C. Numerical Integration of Coupled Second-Order Differential Equations 15

1. Mathematical Formulation 17

2. Model-Dependent Nuclear Surface Boundary Conditions 22

3. Results of the Numerical Integration. 24

4. Exclusion of $\ell = 6$ Partial Wave from Coupled Differential Equations 30

5. Correctness of Computer Codes 32

V. Nuclear Orientation Theory

A. Spin Hamiltonian 43

B. Rare Earth and Actinide Ion Electronic Structure. . . . 45

C. Crystal Field Interaction 47

D. Magnetic Hyperfine Interaction 50

E. Electric Hyperfine Interaction 51

VI. Experimental Apparatus and Techniques

A. Cryostat 54

B. Alpha Particle Radiation Detectors 57

C. Neodymium Ethylsulfate Crystals 58

D. Ion Exchange Purification of Actinide Element Ions . . . 60

E. Thermometry and Data Collection and Reduction 61

VII. ^{253}Es Nuclear Orientation Results and ^{253}Es in Neodymium Ethylsulfate Magnetic Hyperfine Interaction Constant 64

VIII. Discussion of ^{253}Es in NES Alpha Particle Angular Distribution

A. Crystal Field Parameters 72

B. Nuclear Magnetic Dipole Moment 75

C. ^{253}Es Alpha Particle Partial Wave Amplitudes and Phases 81

IX. ^{241}Am Nuclear Orientation Results and Discussion 91

A. Quadrupole Coupling Constant 92

B. Alpha Particle Partial Wave Amplitudes and Phases 95

X. ^{255}Fm Nuclear Orientation Results and Discussion 108

XI. Final Remarks on Coupled Channel Calculations 117

XII. Conclusion 119

Acknowledgements 121

Appendix A. Spontaneous Fission Fragment Angular Distributions. 123

References and Footnotes 149

STUDY OF PARTIAL WAVE BRANCHING IN THE ALPHA DECAY OF ^{241}Am, ^{253}Es AND ^{255}Fm

Arthur James Soinski

Nuclear Chemistry Division
Lawrence Berkeley Laboratory
University of California
Berkeley, California 94720

ABSTRACT

Nuclei of ^{241}Am, ^{253}Es and ^{255}Fm were oriented in single crystals of neodymium ethylsulfate at temperatures down to 11 mK. Orientation was detected by alpha particle angular distributions. The temperature dependences of these distributions are consistent with the lowest electronic states of these three actinide ions in the ethylsulfate lattice being similar to those of the corresponding lanthanide ions. Thus magnetic and axial orientation was observed in $Es^{3+}(5f^{10})$, as in $Ho^{3+}(4f^{10})$. Quadrupole orientation was observed in $Am^{3+}(5f^{6})$, as in $Eu^{3+}(4f^{6})$. In $Fm^{3+}(5f^{11})$ the orientation was magnetic and equatorial, as would be expected from the hyperfine interaction in $Er^{3+}(4f^{11})$. The hyperfine interaction constants were determined. For ^{253}Es we report $|A| = 0.26(3)\ cm^{-1}$, for ^{241}Am, $P = -\ 0.0033(6)\ cm^{-1}$, and for ^{255}Fm, $|B| = 0.035(7)\ cm^{-1}$. The ^{253}Es nuclear magnetic dipole moment was determined to be $|\mu| = 2.7(13)\ \mu_N$. The Am^{3+} data are consistent with an anti-shielding constant of $\gamma_\infty \approx -\ 10^2$, in good agreement with theory, and a shielding factor $\sigma_2 = 0.7$, similar to the value for Eu^{3+}. The nuclear results show that the s and d waves are in phase for the favored α decay branch in all three cases. The relative phase of the

g wave was found to be negative for the ^{253}Es decay. Numerical integration of the coupled second-order differential equations describing the favored α decays of ^{253}Es and ^{255}Fm yielded partial wave amplitudes and phases. The results are compared with both intensity and angular distribution data. The measurement of the angular distribution of spontaneous fission fragments from aligned nuclei of ^{253}Es, ^{254}Es and ^{257}Fm are described in a separate appendix. The ^{257}Fm results are consistent with a K quantum number at the outer turning point of either 9/2 or 7/2.

I. INTRODUCTION

An alpha particle emitted by the ground state of an even-even nucleus has a unique angular momentum, ℓ. The even-even parent nucleus has total angular momentum $I_i = 0$, and angular momentum conservation requires that the daughter energy level populated by the alpha particle should have $I_f = \ell$. For odd-odd or odd mass nuclei, $I_i \neq 0$ and more than one value of ℓ is generally permitted. On the basis of angular momentum conservation, Spiers[1] predicted that anisotropic alpha particle emission would take place from oriented nuclei. Subsequent nuclear orientation experiments confirmed this prediction and also yielded information about the relative amplitudes and phases of the observed alpha partial waves.

Hill and Wheeler[2] made the first quantitative estimate of enhanced alpha particle emission from the poles of prolately deformed spheroidal nuclei. Their reasoning can be understood with the aid of Fig. 1. They assumed a uniform probability of alpha particle formation within the nuclear volume. If the barrier set up by the remaining nucleons is simply Coulombic beyond a certain radius, then this barrier is both thinner and lower at the poles than it is at the equator, and tunneling is greatly enhanced at the poles. For moderate nuclear deformation they predicted a sixteen-fold increase of alpha particle intensity from the poles over that from the equator. However, the angular distribution of nuclear radiations is determined primarily by the requirement that angular momentum be conserved in the decay. The greatly enhanced polar emission predicted by Hill and Wheeler could occur only from a nucleus with a large component of angular momentum perpendicular to the nuclear symmetry axis.

Roberts, Dabbs and co-workers[3-5] were the first to test the predictions of Hill and Wheeler experimentally. They oriented ^{233}U and ^{235}U in single crystals of $UO_2Rb(NO_3)_3$ and ^{237}Np in single crystals of $NpO_2Rb(NO_3)_3$. For all three nuclei they observed preferential emission perpendicular to the crystalline c-axis. In the ^{237}Np case they were able to establish that the nuclear spins also tend to orient perpendicular to the c-axis. These two facts taken together imply preferential emission along the nuclear spin vector (i.e., from the poles), thus confirming the predictions of Hill and Wheeler. The data for the uranium isotopes are consistent with this interpretation of the ^{237}Np results, although for uranium the direction of orientation was not established directly. Chasman and Rasmussen[6] have discussed the difficulties in interpreting the ^{233}U data.

Navarro, Rasmussen and Shirley[7] aligned trivalent ^{249}Cf in a single crystal of neodymium ethylsulfate $Nd(C_2H_5SO_4)_3 \cdot 9H_2O$. These authors and also Frankel[8] aligned ^{253}Es in neodymium ethylsulfate (NES). For both isotopes the prediction of Hill and Wheeler was confirmed: Preferential α particle emission from the nuclear poles was observed. Preferential polar emission in these cases reflects the fact that the s and d α particle partial waves (corresponding to orbital angular momentum $\ell = 0$ and 2) are in phase. In this thesis the ^{253}Es nuclear orientation studies are extended to determine the relative phase of the s and g ($\ell = 4$) partial waves. Lower limits are placed on the total relative intensities of the d and g waves with respect to the s wave intensity. Because the experimentally determined relative intensities exceed those given by both the method of Bohr,

Fröman and Mottelson[9,10] and the shell model theory of alpha decay as applied until now,[11,12] numerical integration of the coupled differential equations describing the penetration of the anisotropic barrier by the alpha particles was performed. Any failure of the numerical integrations to yield results consistent with the experimental intensities and angular distributions implies that the alpha particle formation process has not been properly accounted for.

Because the attainment of nuclear orientation depends upon the interaction of the nuclear moments with the environment, the nuclear moments can be regarded as probes of the electronic and crystalline fields. The similarity between the electronic ground states for the f^{10} pair Ho^{3+}-Es^{3+}, as exemplified by similar hyperfine interaction parameters, suggested that actinide candidates for additional nuclear orientation experiments be chosen on the basis of known hyperfine interaction mechanisms in trivalent lanthanides.

Nuclei of trivalent ^{152}Eu and ^{154}Eu ions were aligned in NES by means of the electric hyperfine interaction between the nuclear quadrupole moment and the electric field gradient arising from both the open f-electron shell and the lattice charges.[13] Because the lattice charges are farther from the nucleus than the f-electrons, the f-electron contribution to the field gradient was expected to dominate. Since this was not the case, Judd, Lovejoy and Shirley[13] proposed that distortion of the closed electronic shells by the lattice charges increased or antishielded the crystal field gradient at the nucleus. This unexpected result suggested that americium should also be studied. Sternheimer[14] and later Gupta and Sen[15] predicted that the lattice antishielding factor,

γ_∞, is larger for Am^{3+} than for Eu^{3+}; therefore appreciable alignment of Am^{3+} would be expected. In this thesis nuclear orientation experiments on ^{241}Am are reported. The data are interpreted in terms of both the crystal field parameters and the relative amplitudes and phases of the alpha waves in the favored decay to ^{237}Np. As for ^{253}Es, the relative s-d wave phase in ^{241}Am favored α decay is positive.

I also report results for ^{255}Fm in NES.[16] I find that the s and d waves are in phase in this case. Because of the short half-life (20.1 h) and the limited mass available, the statistical accuracy was not high enough to permit the extraction of the sign of the relative s-g wave phase. The similar electronic ground state of the pair Er^{3+}-Fm^{3+} is confirmed.

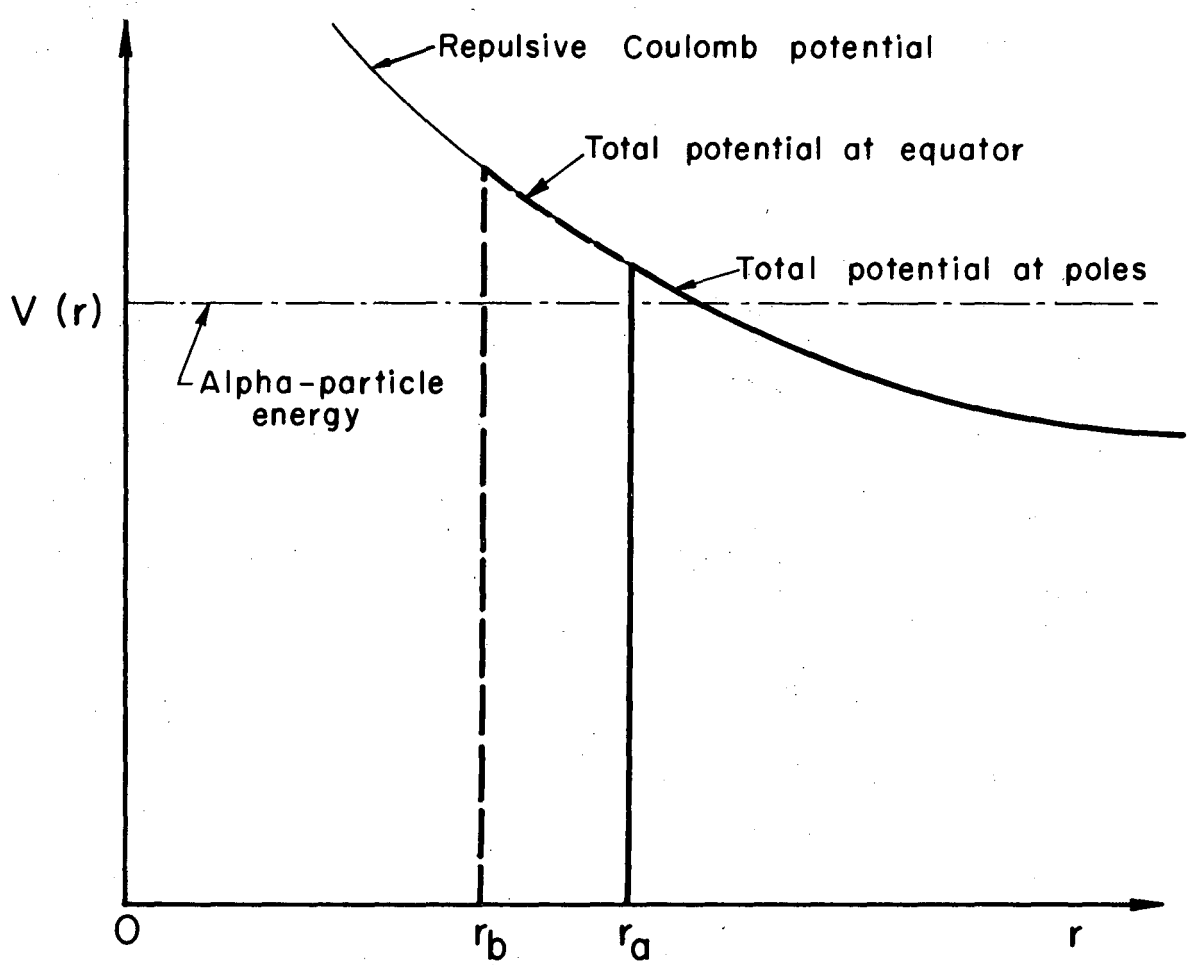

MUB-10078

FIG. 1. Representation of the total (nuclear plus Coulomb) potential of a prolately deformed nucleus, of major (minor) radius r_a (r_b), showing that α particles emitted from polar regions must tunnel through a barrier that is both lower and thinner than at the equator.

II. THERMAL EQUILIBRIUM NUCLEAR ORIENTATION THEORY

As a consequence of the isotropy of three-dimensional space, angular momentum is conserved and the emission of nuclear radiations or particles is anisotropic in the nuclear frame. In order to observe an anisotropic distribution in the laboratory frame, it is necessary to select out one of the nuclear magnetic substates from the ensemble, as in angular correlations, or to preferentially populate certain of the nuclear magnetic substates by either dynamic or static methods. In this thesis only the static or thermal equilibrium method of nuclear orientation (NO) will be considered. Because several good review articles on nuclear orientation[17-20] and magnetic cooling by adiabatic demagnetization[21-23] exist, an abbreviated treatment will be presented here.

In order to prepare a non-uniform ensemble of nuclear substates (labelled by $m_I \equiv I_z$, where I_z is the component of total nuclear angular momentum or spin along a space-fixed axis), the $(2I + 1)$-fold spatial degeneracy must be removed by some external means, and the entropy of the nuclear spin system must be reduced from its maximum value of $R\ln(2I + 1)/\text{mol}$. The entropy reduction is accomplished by adiabatic demagnetization. The removal of the spatial degeneracy by hyperfine interactions will be discussed in some detail, but first the derivation of the angular distribution function will be outlined.

III. ALPHA PARTICLE ANGULAR DISTRIBUTIONS

The angular distribution of alpha particles from oriented nuclei has been developed by Brussaard and Tolhoek,[24] Rose,[25] and Steenberg and Sharma.[26] The formal treatment of nuclear orientation and angular correlations is the same, and Steffen[27] has given an excellent treatment of angular distributions and angular correlations of nuclear radiations. A similar approach with different emphasis has been given by Frauenfelder and Steffen.[28] I summarize Steffen's treatment below.

The directional distribution of α radiation emitted from an axially symmetric oriented state may be expressed in terms of Legendre polynomials as

$$W(\theta) = \sum_k B_k(I_i, T) A_k(\alpha) P_k(\cos\theta). \tag{1}$$

The orientation parameters $B_k(I_i, T)$, which were introduced by Blin-Stoyle and Grace,[18] are given by

$$B_k(I_i, T) = [I_i]^{1/2} \rho_k(I_i) \tag{2}$$

where $\rho_k(I_i)$ is a statistical tensor whose elements are proportional to the relative populations of the nuclear magnetic substates. The notation $[I_i]$ means $2I + 1$. The statistical tensor for α radiation, $A_k(\alpha)$, can be written in terms of F-coefficients as

$$A_k(\alpha) = \sum_{\ell, \ell'} F_k(\ell\ell' I_f I_i) b_k(\ell\ell'; \alpha) \langle I_f \| \mathcal{H}_\ell(\alpha) \| I_i \rangle \langle I_f \| \mathcal{H}_{\ell'}(\alpha) \| I_i \rangle^* e^{i[\delta(\ell) - \delta(\ell')]} \tag{3}$$

where the product of the F-coefficient times the particle parameter for α particles, $b_k(\ell\ell'; \alpha)$, is

$$b_k(\ell\ell';\alpha)F_k(\ell\ell' I_f I_i) = (-1)^{I_i+I_f}\sqrt{[\ell][\ell'][I_i][k]}\begin{pmatrix}\ell & \ell' & k\\ 0 & 0 & 0\end{pmatrix}\begin{Bmatrix}\ell & \ell' & k\\ I_i & I_i & I_f\end{Bmatrix}. \qquad (4)$$

The phase shifts $\delta(\ell)$ arise because the α particles move in the electromagnetic field of the daughter. Thus the α particles must penetrate a predominantly Coulomb barrier and a smaller centrifugal barrier. For deformed nuclei an anisotropic quadrupole barrier also exists. As a consequence of the presence of the quadrupole barrier the α particle is emitted in a non-central potential, and as a result transitions between the angular momentum states of the α particle and the rotational energy levels of the daughter nucleus can occur. If the phase shifts are real (more precisely, if the transition matrix elements are real), the exponential dependence in Eq. 3 reduces to a cosine dependence.

The emission of α radiation is described by the transition matrix $\mathcal{H}(\alpha)$, whose elements are the amplitudes $\langle I_f|\mathcal{H}(\alpha)_{op}|I_i\rangle$ with $\mathcal{H}(\alpha)_{op}$ being the operator for the α particle emission. The emission operator can be expanded in terms of multipole operators $\mathcal{H}_{\ell m}$ that describe the emission of α particles of angular momentum ℓ and projection m on the nuclear symmetry axis. For favored α decay, in which I am interested, $m = 0$. Application of the Wigner-Eckart theorem reduces the matrix elements $\langle I_f|\mathcal{H}_{\ell 0}|I_i\rangle$ to the reduced matrix elements of Eq. 3. These reduced matrix elements, which contain the model-dependent information about the nuclear states $|I_i m_i\rangle$ and $|I_f m_f\rangle$ involved in the decay, reduce to the relative amplitudes of the α particle waves, a_ℓ.

For α decay and other parity conserving processes, only even-order Legendre polynomials occur in Eq. 1. The angular distribution function

can then be written as

$$W(\theta) = 1 + \sum_{\substack{k>0 \\ \text{even}}} \sum_{\ell,\ell'} R a_\ell a_{\ell'} \cos(\phi_\ell - \phi_{\ell'}) Q_k(\theta) b_k(\ell\ell';\alpha)$$

$$\times F_k(\ell\ell' I_f I_i) B_k(I_i, T) P_k(\cos\theta). \tag{5}$$

Solid angle correction factors, $Q_k(\theta)$, have been introduced because neither the source nor the detectors are points. An anisotropy reduction factor, R, accounts for the fact that some radioactive nuclei occupy non-lattice sites and as an ensemble contribute an isotropic distribution. The conservation of angular momentum restricts the α particle angular momentum to $|I_i - I_f| \leq \ell \leq |I_i + I_f|$. The conservation of parity further restricts ℓ to even (odd) values if the parent nucleus and the daughter nucleus have the same (opposite) parity.

The angular distribution function depends on the properties of the decaying nucleus, the nuclear environment, and the temperature. The α decay process and the calculation of partial wave amplitudes and phases will be treated first. Then the solid state aspects of the problem, including such topics as nuclear orientation methods, the spin Hamiltonian, and crystal field parameters, will be treated.

IV. ALPHA PARTICLE PARTIAL WAVE AMPLITUDES AND PHASES

Any theoretical calculation of alpha particle partial wave intensities for the decay of spheroidally deformed nuclei must consider the two separate "events" in the decay. First the alpha cluster is formed from the nucleons of the parent. The boundary conditions are thereby effectively determined on the nuclear surface. Second the α cluster penetrates an anisotropic potential barrier. Because the potential is non-spherical, the α particle and the rotational energy levels of the daughter are coupled, and an exchange of energy and angular momentum can occur.

In no case have both the α cluster formation and the subsequent penetrability been treated rigorously. Three methods for obtaining partial wave intensities will be presented beginning with the simplest. The partial wave phases can be determined either from experimental angular distributions or from the shell model theory to be discussed in section IV.B.

IV.A. THE BOHR, FRÖMAN AND MOTTELSON METHOD

The properties of spheroidally deformed nuclei are best described by the strong coupling model of Bohr and Mottelson.[9,10] In the case of odd-mass nuclei the single particle and nuclear surface oscillations are strongly coupled. The intrinsic angular momentum of the last odd nucleon is not conserved because the nuclear potential is non-spherical, but the projection of intrinsic angular momentum on the nuclear symmetry axis, Ω, is approximately conserved. Because all but the last odd nucleon are paired to given $\Omega = 0$, Ω is equal to K, the projection of total nuclear spin on the nuclear symmetry axis. Rasmussen[29] proposed that those alpha transitions for which K of the parent and daughter, K_i and K_f respectively, are the same are "favored" because the α transition probabilities, at least to the band head, are comparable to those of neighboring even-even nuclei. Favored transitions do not involve the last odd nucleon and do not require the breaking of pairs. The remaining discussion is specialized to favored α decay.

Angular momentum conservation requires that K_i, K_f, and the projection of the alpha particle on the symmetry axis form a triangle. Applying the Wigner-Eckart theorem, the daughter wave function can be expanded in terms of the parent and α particle wave functions as

$$|I_f K_f\rangle = \sum_{\ell} \langle I_i \ell K_i K_f - K_i | I_f K_f \rangle | \ell K_f - K_i \rangle | I_i K_i \rangle \qquad (6)$$

where the Clebsch-Gordan coefficient insures conservation of angular momentum.

Ω is not a constant of the motion during the anisotropic barrier penetration except for the decay of even-even nuclei. However the

only appreciable exchange of angular momentum between the outgoing α particle and the daughter nucleus occurs in the region near the nucleus. Furthermore, the penetration of the α particle takes place in a time short compared to the nuclear rotation period. Therefore the daughter nucleus can be regarded as being stationary during α emission. Then the component of total angular momentum along the nuclear symmetry axis is approximately conserved, and the only α components of importance have $m = K_f - K_i = 0$. Equation 6 then reduces to

$$|I_f K\rangle = \sum_{\ell} \langle I_i \ell K O | I_f K\rangle | \ell 0\rangle | I_i K\rangle . \tag{7}$$

Therefore a given ℓ wave will branch to rotational states built on a given intrinsic state in the ratio of Clebsch-Gordan coefficients. The reduced transition probability P, or decay constant, $\lambda = \ell n 2/t_{\frac{1}{2}}$, for favored decay can be written as

$$P = P_0(Z, E_\alpha) \sum_{\ell} \frac{1}{N} |\langle I_i \ell K O | I_f K\rangle|^2 / HF_\ell \tag{8}$$

where $P_0(Z, E_\alpha)$ is the spherical barrier penetration probability,[30,31] N is a normalization factor of order unity, and HF_ℓ is the hindrance factor of the ℓth partial wave averaged from neighboring even-even nuclei. Hindrance factors account for the fact that decays to excited states of the daughter are slower than would be predicted on the basis of simple barrier penetration calculations.

The Bohr, Fröman and Mottelson prediction of partial wave branching is exact only when the rotational term in the interaction Hamiltonian vanishes; that is, in the limit of infinite nuclear moment of inertia or

vanishing nuclear quadrupole moment. Because the actinides typically have large intrinsic quadrupole moments of the order of 10 b., deviations from the Bohr, Fröman and Mottelson prediction are expected.

IV.B. MANG SHELL MODEL THEORY

The microscopic shell-model theory of α decay of deformed nuclei has been developed by Mang and Rasmussen.[32,33] The most extensive calculations for odd-mass nuclei have been performed by Poggenburg, Mang and Rasmussen.[12] Details of the calculations can be found in the latter publication and in the references cited therein.

The decay constant, $\lambda = \ell n\, 2/t_{\frac{1}{2}}$, is written as the product of (a reduced width $\gamma^2_{I_i I_f \ell}$ of R-matrix theory which contains all information about the alpha cluster formation) times (a penetrability factor, $P_\ell(E_\alpha)$, which accounts for the penetration of the predominantly Coulomb barrier by the α particle). Thus

$$\lambda = \frac{1}{\hbar} \sum_{I_f, \ell} P_\ell(E_\alpha)\, \gamma^2_{I_i I_f \ell} \tag{9}$$

where E_α is the energy of the alpha particle.

The reduced width is proportional to the square of a time-dependent probability amplitude which measures the probability that an α cluster with the proper quantum numbers is projected from the shell model product wave functions of the constituent nucleons.

Because of quadrupole coupling effects the penetrability factor becomes a penetrability matrix which relates α amplitudes on the nuclear surface to α amplitudes (or experimentally observed intensities) at infinity. A Fröman matrix[34] was used by Poggenburg, Mang and Rasmussen to account for the anisotropic barrier penetration in an approximate way.

IV.C. NUMERICAL INTEGRATION OF COUPLED SECOND-ORDER DIFFERENTIAL EQUATIONS

In the α decay of spheroidal nuclei, the noncentral electromagnetic field permits the exchange of energy between internal nuclear excitation and the external alpha particle. The only noncentral couplings of importance are those involving the collectively enhanced intra-band E2 transitions of deformed nuclei. Starting with boundary conditions set at the spheroidal nuclear surface, the formal problem involves the outward propagation of the alpha particle wave function through the anisotropic barrier out to some distance where coupling effects are negligible.

Both Nosov[35] and Fröman[34] have proposed an approximate method for accounting for the anisotropic barrier penetration. However the more exact formulation of the anisotropic barrier penetration problem leads to a set of coupled second-order linear differential equations in the radial separation variable.

Although several researchers have performed the numerical integration of coupled channel equations for the α decay of even-even nuclei, only Chasman and Rasmussen[6] have considered the more involved problem of the α decay of an odd-mass nucleus. In the latter case the conservation of angular momentum permits an α particle partial wave of a given orbital angular momentum, ℓ, to branch to more than one energy level of the daughter nucleus. Thus for the favored alpha decay of ^{233}U Chasman and Rasmussen considered the decay of the s wave to the 5/2 level and the branching of the d wave to the 5/2, 7/2 and 9/2 levels of ^{229}Th. Channel coupling effects were expected to be most significant for the case of a relatively weak wave, such as the typically

highly hindered g wave, coupled to a strong wave such as the s wave. Therefore we have extended the work of Chasman and Rasmussen by considering the branching of the s, d and g waves in the favored α decays of both ^{253}Es and ^{255}Fm.

The nuclei ^{253}Es and ^{255}Fm, both spin 7/2, are ideal cases for applying an exact numerical treatment because alpha transitions to the favored bands of the daughters have been well studied,[36-38] and angular distribution data from low temperature nuclear alignment experiments are available.[39,40] Including the ℓ = 0, 2, and 4 partial waves, nine coupled second-order differential equations must be solved for favored decays to the five lowest levels of the daughter rotational band.

The experimental intensities are sensitive only to the relative partial wave intensities whereas the α particle angular distributions are sensitive to both the relative partial wave intensities and phases. However the angular distribution data yield directly a maximum of two numbers to compare with theory whereas the intensity data yield four.

IV.C.1. MATHEMATICAL FORMULATION

The Coulombic potential energy interaction, considered at distances beyond the nuclear surface, can be expanded in terms of Legendre polynomials of order n divided by r^{n+1}, where r is the distance to an external charge.[41] The n = 0 term is the central Coulombic term. The magnetic multipole terms should be small for charged particle decay. Perlman and Rasmussen[41] considered the E1 interaction in the ^{241}Am favored α decay and concluded that E1 coupling is unimportant. Therefore the E2 interaction contributes the first important coupling term. For nuclei with large hexadecapole deformations, E4 coupling might also be important; however, both ^{249}Bk and ^{251}Cf have small hexadecapole deformation.[42,43] Therefore the coupled differential equations in the radial separation variable can be written in general as[44]

$$u''_{I_d,\ell} - \frac{2M}{\hbar^2}\left(\frac{2Ze^2}{r} + \frac{\hbar^2 \ell(\ell+1)}{2Mr^2} - Q_{I_d}\right) u_{I_d,\ell}$$

$$= \sum_{I'_d,\ell'} K^2_{I_d \ell I'_d \ell'}\, u_{I'_d,\ell'} . \qquad (10)$$

M is the reduced mass, Z is the charge of the daughter nucleus, Q_{I_d} is the effective Q value for the alpha particle with electron screening and daughter recoil energy corrections, and the $K^2_{I_d \ell I'_d \ell'}$ are matrix elements of the quadrupole coupling operator which is proportional to the intrinsic nuclear quadrupole moment of the daughter times $P_2(\cos\theta)$ divided by r^3. For ^{249}Bk the value for the intrinsic quadrupole moment, Q_0, was taken to be the same as that for the parent,

^{253}Es; namely, 13.1 b.[45] For ^{251}Cf and ^{255}Fm we used approximately the same value; namely, 13.0 b.

Explicit expressions for the quadrupole coupling matrix element were given for α decay by Perlman and Rasmussen[41] (see Rasmussen[44] for a trivial correction to these equations) and for optical model scattering applications by Tamura.[46] For α decay (and nuclear reactions and scattering) most numerical integrations of the coupled equations have been confined to a spinless parent (target) nucleus and a spinless emitted particle (projectile) because the coupled equations then have a simple form. For the alpha decay problem the potential barrier is so large that only one of the two linearly independent solutions of each equation (specifically the one that is exponentially increasing in the direction of integration) is stable in numerical integration, even with the large word sizes and small integration intervals feasible in the largest available computers.

The general solutions of the uncoupled differential equations can be written as $U_L(\eta,\rho) = G_L(\eta,\rho) + iF_L(\eta,\rho)$ where G_L and F_L are the irregular and regular Coulomb functions[47] respectively. This form for writing the solutions is chosen because it becomes purely real near the nuclear surface. Solutions of the coupled differential equations approach the Coulomb functions asymptotically at large radius. For notational convenience the indices (I_d, ℓ) used to label the solutions will sometimes be replaced by a single index j or k which varies from 1 to 9. The relation between these indices is given in Table IVA. The previously used, and more common, notation of I_i and I_f to designate the

parent and daughter nuclear spins respectively are not used in this section in order to avoid ambiguity. Because of the channel coupling an α wave starting off in one (initial) channel can be scattered into another (final) channel.

The physical information is contained in the real components which are outwardly decreasing functions (reducing to irregular Coulomb functions in the uncoupled case). The square of an oscillation amplitude in the far region may be related to the experimental intensity divided by the α particle velocity.

In general the phase of an oscillating coupled-channel solution in the far region will differ from the phase of the corresponding Coulomb function. This phase difference will be referred to as the quadrupole phase shift, $\phi_{I_d \ell}$. Although phase shifts do not affect intensity data, they do affect angular distribution data through the interference terms between α components of differing ℓ going to the same final state I_d.

The set of nine second-order coupled differential equations can be transformed into a set of eighteen first-order coupled differential equations having eighteen linearly independent solutions or, equivalently, nine complex solutions. Because the physically meaningful solutions are exponentially decreasing going outward through the barrier, it was not possible to obtain stable solutions by outward numerical integration. Instead I used Coulomb functions as starting conditions at a radius sufficiently large (150 fm) such that the coupling forces were small and integrated inward. The solutions of interest then increased in the direction of integration and were thus stable. The Coulomb function and its derivative was initialized to zero in all but the kth of the nine

channels, while the kth channel was initialized with the value of the complex Coulomb function corresponding to that channel. I label the linearly independent set of complex solutions resulting from the integration as $u_{jk}(r) = g_{jk}(r) + if_{jk}(r)$, representing the jth channel of the kth linearly independent solution.

Any general solution of the coupled differential equations may be expressed as a linear combination of the solutions just described; that is, the general solution for the jth channel may be written as

$$\Psi_j(r) = \sum_{k=1} c_k u_{jk}(r) \tag{11}$$

where the coefficients $c_k = a_k + ib_k$ are complex numbers. Because an α particle is assumed to exist in a quasi-stationary state prior to emission, the imaginary part of each wave function Ψ_j must essentially vanish near the nuclear surface. Using nuclear model constraints, which will be discussed in the next section, values for the real parts of the wave functions at the nuclear surface can be obtained. Then the set of nine complex simultaneous equations, $\Psi_j(r)$, can be solved for the coefficients c_k.

The system of simultaneous equations is most conveniently handled as the matrix equation

$$\underset{\sim}{U}\,\underset{\sim}{C} = \underset{\sim}{\Psi} \tag{12}$$

where the matrix elements u_{jk} of the 9×9 complex matrix $\underset{\sim}{U}$ are the amplitudes of the linearly independent solutions on or near the nuclear surface. The elements of the column vector $\underset{\sim}{C}$ are the unknown complex coefficients c_k, and the elements of the column vector $\underset{\sim}{\Psi}$ are the purely real nuclear model surface amplitudes. The problem is formally solved

by the matrix inversion

$$\underset{\sim}{C} = \underset{\sim}{U}^{-1} \underset{\sim}{\psi} . \tag{13}$$

From the c_k values thereby obtained, and in view of the starting conditions of the pure Coulomb functions, the relative α partial wave intensities $\mathcal{I}_k$ can be written as

$$\mathcal{I}_k = |c_k|^2 Q_\alpha^{\frac{1}{2}} = (a_k^2 + b_k^2) Q_\alpha^{\frac{1}{2}} \tag{14a}$$

and the quadrupole phase shifts ϕ_k can be written as

$$\phi_k = \arg c_k = \tan^{-1}(b_k/a_k) \tag{14b}$$

where Q_α is the α decay energy in that channel.

IV.C.2. MODEL-DEPENDENT NUCLEAR SURFACE BOUNDARY CONDITIONS

In the similar work of Rasmussen and Hansen[48] on even-even ^{242}Cm favored α decay, the boundary conditions for the real part of the solutions could be imposed by demanding agreement with experimental relative intensities to the rotational band levels in ^{238}Pu. For odd-mass nuclei there are insufficient relative intensity data to provide the required boundary conditions. For the problem considered here, eight boundary conditions are required. For the five levels of the daughter there are only four relative intensities, and there are no direct experimental measurements of the mix and relative phases of the partial waves. The low temperature angular distribution data provide two experimental numbers (the coefficients of the $P_2(\cos\theta)$ and $P_4(\cos\theta)$ terms in the angular distribution), but they do not determine uniquely relative partial wave amplitudes and phases.

Because there are insufficient experimental data to completely fix the boundary conditions, nuclear model constraints were used instead. I used the fundamental assumption underlying the leading order intensity relationships of the strong coupling model[9,10] that near the nuclear surface the projection of any partial wave's angular momentum along the cylindrically-symmetric 3-axis of the daughter nucleus, m_ℓ, has a value of $K_d \pm K_p$ where K_d and K_p are the projections of the daughter and parent total nuclear angular momentum on the 3-axis. For $(K_d + K_p) \rangle \ell$ only one value of m is allowed; for favored α decay $m_\ell = 0$. The condition of only $m_\ell = 0$ components on a sphere of radius R_0 near the nucleus provides six boundary conditions, tying

together the components of a given ℓ wave in proportion to Clebsch-Gordan coefficients. Bohr, Fröman and Mottelson[10] and Asaro et al.[36] have, in some applications, constrained the relative s, d and g wave intensities to the average of nearest neighbor even-even nuclei, but such a constraint is not as fundamental as the $m_\ell = 0$ constraint. The remaining two boundary conditions were left as free parameters and are denoted by α_2, the ratio of total d and s wave amplitude at R_0, and α_4, the ratio of total g to s wave amplitude at R_0. Therefore the wave functions at R_0 can be written as

$$\bar{\Psi}_j(R_0) = \alpha_\ell \langle \ell I_p 0 K | I_d K \rangle \tag{15}$$

with the trivial normalization condition $\alpha_0 = 1$. The steady state real part of the wave function is exponentially decreasing going out through the barrier region and oscillatory in the far region.

The numerical integration of the coupled differential equations permits us to test two assumptions of the strong coupling model as usually applied. The first is that near the nuclear surface only $m_\ell = 0$ α partial waves occur. Subject to this $m_\ell = 0$ constraint, I wish to determine if the coupled channel treatment can reproduce both the experimental relative intensities to the five lowest rotational levels (with spins 7/2, 9/2, 11/2, 13/2 and 15/2) of the daughter and the angular distribution data.

The coupled channel treatment can also test the usual approximate handling of anisotropic barrier penetrability in setting the relative intensity of a given ℓ wave to a given level equal to (the square of a Clebsch-Gordan coefficient) times (a calculated spherical barrier penetrability factor for the alpha group). This approximation is exact only in the limit of infinite moment of inertia or vanishing nuclear quadrupole moment.

IV.C.3. RESULTS OF THE NUMERICAL INTEGRATION

The most general way to present the results of the numerical integration is in the form of the complex matrix U^{-1}; the real and the imaginary components of U^{-1} for ^{253}Es are given in Tables IVB and IVC respectively and for ^{255}Fm in Tables IVD and IVE respectively. These matrices reduce to unit matrices for vanishing nuclear quadrupole moment. Operation with either complex matrix on any boundary conditions on a sphere near the nuclear surface will yield partial wave amplitudes and quadrupole phase shifts at large distances. If boundary conditions are fixed on the spheroidal nuclear surface, then a Fröman matrix[35] can be used to transform them to boundary conditions on a sphere at 10 fm.

Let us now consider the determination of the two free parameters α_2 and α_4. The value for α_2 is most stringently determined by the requirement that the α intensity to the 9/2+ level be reproduced because this level receives the largest d wave component. In general there are two values for α_2, one positive and one negative, that give satisfactory agreement with experiment. The sign of the anisotropy in the α particle angular distributions for both ^{253}Es and ^{255}Fm requires that the s and d waves be in phase; that is, that they interfere constructively near the nuclear poles. Therefore only positive values for α_2 are acceptable.

In like manner the α intensity to the spin 13/2+ level fixes the value for α_4. The phase of the g wave is less well determined by the angular distribution data, but the ^{253}Es angular distribution data and alpha decay systematics suggest that the g wave is out of phase. Therefore only negative values for α_4 are considered.

From nuclear model considerations the values of both α_2 an α_4 can be estimated. Using the shell model theory of α decay, Poggenburg[11] calculated partial wave amplitudes on a Nilsson coordinate surface to be 1.035, 0.309 and -0.376 for the ℓ = 0, 2 and 4 waves respectively of ^{253}Es and 1.135, 0.406 and -0.353 for the s, d and g waves respectively of ^{255}Fm. Applying a Fröman matrix of argument B = 2, which is approximately correct for the transformation from the Nilsson surface to a sphere near the nuclear radius, I obtain $\alpha_0:\alpha_2:\alpha_4$ = 1.0:1.0:0.05 for ^{253}Es and 1.0:1.1:0.18 for ^{255}Fm.

The values of α_2 and α_4 were obtained by minimizing the weighted root mean square logarithmic errors in the theoretical intensities. The weighting reflects the uncertainties in the experimental intensities. The values that give the best fit to the experimental intensities are $\alpha_0:\alpha_2:\alpha_4$ = 1.0:0.8580:-0.0977 for ^{253}Es and $\alpha_0:\alpha_2:\alpha_4$ = 1.0:0.7918:-0.1794 for ^{255}Fm. The microscopic theory predicts that the d wave amplitude increases with both Z and N for the heavier actinides.[12] The minimization procedure fails to reproduce this trend, probably because of the unusually large measured intensity to the 9/2+ level of the ^{253}Es daughter. I will return to this point later. The g wave is weak compared to the s and d waves; therefore the difference in α_4 values found by the minimization procedure from those predicted by the microscopic theory are expected.

The partial wave intensities, Coulomb phase shifts and quadrupole phase shifts are summarized in Tables IVF and IVG for ^{253}Es and ^{255}Fm respectively. The Coulomb phase shift difference for α decay is given by[49]

$$\sigma_{\ell+2} - \sigma_\ell = \tan^{-1} \frac{\eta}{\ell+1} + \tan^{-1} \frac{\eta}{\ell+2} + \pi. \tag{16a}$$

The phase shifts themselves are given by

$$\sigma_\ell = \arg \Gamma(\ell + 1 + i\eta). \tag{16b}$$

The values of η and $k(=\rho/r)$ that we used are given in Table IVH.

I will emphasize the ^{253}Es results; however, the general comments are also applicable to the ^{255}Fm results.

Examination of the best fits to the intensities for both ^{253}Es and ^{255}Fm reveals a systematic discrepancy. The experimental intensity ratio of the second to the first excited state in the rotational band is significantly larger than theory for both nuclei. These states are populated primarily by d waves, and no combination of initial $\ell = 0, 2, 4$ ratios reproduces the experimental intensity ratio if the constraint to $m_\ell = 0$ components in the nuclear frame is maintained. This same systematic deviation from Bohr, Fröman and Mottelson theory has been noted for favored bands of many α emitters, but it is only now clear that the coupled channel treatment does not affect the discrepancy.

In order to exhibit the systematics of this discrepancy I have plotted the ratio of the hindrance factors of the second to the first excited state for odd-mass actinide nuclei in Fig. 2. The experimental hindrance factors were taken from the compilation of Ellis and Schmorak.[50] If the α groups populating these two states were pure $\ell = 2$, then, by the Bohr, Fröman and Mottelson intensity relations, the ratios would be equal to the ratio of squares of Clebsch-Gordan coefficients shown as dashed lines. Actually the ratio points are lower limits because the correction for a g wave admixture would raise the

points thereby increasing the discrepancy. Note that all points except the one for ^{245}Cm lie above the theoretical line and that the points for ^{253}Es and ^{255}Fm are not exceptional.

The degree of deviation from the Clebsch-Gordan ratio does not seem to correlate with the amount of Coriolis mixing in the ground band. Two nuclei shown in Fig. 2, ^{237}Np and ^{253}Es, have the odd nucleon in a large j shell model orbital which should be appreciably mixed by the Coriolis interaction, and the other nuclei should have smaller admixtures. The three americium isotopes shown have the same odd-proton state, but they show a discrepancy that is sharply increasing with neutron number.

A related discrepancy with the zero-order BFM intensity relations was found in α-γ angular correlation measurements on ^{243}Am. Falk et al.[51] performed a decoupling experiment in order to obtain an unattenuated correlation. Their results require a larger admixture of d wave relative to s wave in the main α group than the BFM model predicts. The nuclear orientation results on ^{253}Es require that the d wave intensity of the main α group be increased by approximately 20% over the BFM estimate.[39] Therefore both hindrance factor ratios and angular correlation and angular distribution data indicate a systematic deviation of d wave branching from Clebsch-Gordan ratios. The d wave intensity to the two lowest levels of the daughter rotational band is increased while the d wave intensity to the upper level(s) is decreased with respect to the Clebsch-Gordan ratios.

The coupled channel treatment of ^{233}U α decay by Chasman and Rasmussen[6] reproduced the experimentally observed skewing of the d

wave toward the lower spin levels of the rotational band. Their calculation involved four coupled channels with only the s and d waves included, whereas our calculation involves nine coupled channels with s, d and g waves included. It is not clear why the earlier calculations produced the skewing while the present calculations do not. The $\ell = 4$ groups are so weak that coupling to them should not significantly alter the $\ell = 2$ groups. Chasman and Rasmussen may have made a sign error in setting the boundary conditions at the nuclear surface for the d wave component to the first excited level of ^{229}Th. Table II of Ref. 6 shows a negative sign for the quadrupole phase shift of this group. The present work always gives the same sign for the quadrupole phase shift of the d wave; the reason for which can be readily explained. The quadrupole potential is proportional to $P_2(\cos\theta)$ and is therefore highest at the nuclear poles. If the s and d waves are in phase along the axis, then the quadrupole part of the barrier retards the d wave with respect to the s wave; that is, the phase shift is negative.

As a result of the above analysis we conclude that some d wave component with $m \neq 0$ must be included on a spherical surface near the nucleus. When this thesis was being written, various mechanisms for admixing an $m \neq 0$ d wave component into the surface boundary conditions were being investigated. Since these considerations were not finalized at the time of writing, they are not included here but will be in a forthcoming publication.

Table IVJ shows an $\ell = 4$ branching comparison of our coupled-channel results with the BFM formula.[10] Comparison is made with Asaro et al.[36] who calculated the α barrier penetrability for a pure

Coulomb barrier cutting off at a definite radius. The other BFM comparison is from Poggenburg[11] who used an optical model nuclear potential. It is seen that the coupled channel results for $\ell = 4$ branching are very close to the earlier results with the BFM formula, thus confirming the theoretical validity of approximating α branching at infinity by the product of the barrier penetrability times the square of the appropriate Clebsch-Gordan coefficient. However, there is a regime of higher $\ell = 4$ wave hindrance where channel coupling causes deviations from the BFM branching approximation. This can be seen in Fig. 3 where $\ell = 4$ branching ratios are plotted as a function of α_4 with $\alpha_2 = 0.89$. The values at $\alpha_4 = -0.101$ are given in Table IVJ. In the vicinity of $\alpha_4 = 0.2$ the hindrance factors are highest, and the deviations from the BFM branching approximation are substantial.

In summary there seems to be a small but systematic violation of the leading order intensity relations for favored $\ell = 2$ alpha groups. The special effects of channel coupling do not spoil the accuracy of the simple Clebsch-Gordan branching expressions for $\ell = 4$ until higher $\ell = 4$ hindrance factors than are found in either ^{253}Es or ^{255}Fm are encountered.

The effect of the calculated partial wave intensities and phases on the α particle angular distribution function will be discussed later in the appropriate experimental sections, and final comments are made in Section XI.

IV.C.4. EXCLUSION OF ℓ = 6 PARTIAL WAVES FROM COUPLED DIFFERENTIAL EQUATIONS

In order to limit the number of coupled differential equations to be solved, the ℓ = 6 and higher angular momentum waves were excluded from our analysis. The hindrance factor for the ℓ = 6 wave of Cf is approximately 1000 whereas the hindrance factor for the ℓ = 4 wave is approximately 30 (Ref. 50). Therefore the ℓ = 6 wave cannot noticeably affect the ℓ = 4 branching. Because the ℓ = 6 wave was excluded from the theoretical analysis, the i wave component was subtracted from the experimental intensities before making the comparison with theory. This was done as follows. Ahmad[38] has measured the α intensities to the 17/2+ and 19/2+ levels of ^{253}Es to be $4(1) \times 10^{-4}$% and $1.2(4) \times 10^{-4}$% respectively. These levels are populated by ℓ = 6 and higher angular momentum waves only; I assumed that the higher ℓ waves are much weaker than the i wave. The ℓ = 6 penetrability factor for α decay to the 17/2+ level, which was obtained by extrapolating Poggenburg's[11] penetrabilities, was multiplied by the appropriate Clebsch-Gordan coefficient squared in order to obtain a relative theoretical intensity which was normalized to Ahmad's experimental intensity. The process was then reversed to obtain the i wave component to the lower spin states of the favored rotational band. The results are given in Table IVK. For ^{255}Fm α decay the experimental intensity to the 17/2+ level is unknown; therefore I assumed that Poggenburg's calculations correctly predict the relative i wave component. This assumption does not adversely affect the results because my major difficulty is in fitting the α intensities to the 9/2+ and 11/2+ levels for which the i

wave component is small. Although it is true that the intensity to the 13/2+ level determines α_4 to some degree, the weighting factor for this level in our fitting routine is relatively small. The corrections used for the ^{255}Fm experimental intensities are also given in Table IVK. The probable correctness of the calculated i wave components for ^{255}Fm decay is indicated by applying the same method to ^{253}Es. The i wave components would then be 0.0001, 0.0016, 0.0031, 0.0060 and 0.0033 for the 7/2+ through 15/2+ levels. The difference between these values and the ones given in Table IVK suggest that the i wave, like the d wave, may be skewed toward the lower levels of the rotational band.

IV.C.5. CORRECTNESS OF COMPUTER CODES

Several numerical tests on the computer programs were performed. The regular and irregular Coulomb functions were integrated inward from 150 fm to 10 fm with coupling turned off, i.e., with $Q_0 = 0$. The irregular solutions agreed with pure Coulomb functions calculated using two different Coulomb function routines[52] to within a few tenths of a percent. The uncoupled regular solutions, which should be exponentially decreasing going into the barrier, were not stable in to 10 fm, but they were smaller than the irregular solutions by a factor of approximately 10^5, which is more than sufficiently accurate for this problem.

The radial integration interval was varied by an order of magnitude to insure that accuracy was not limited by choice of mesh size.

In order to check the completeness and accuracy of the quadrupole coupling matrix elements, the rotational energy and the centrifugal energy of each group was set equal to zero. The regular Coulomb function $F_0(\eta, \rho)$ with η and ρ appropriate for the $I_d = 7/2$ channel was integrated inward from 150 fm with $Q_0 = 13.1$ b. The d and the g waves were found to branch in the ratio of Clebsch-Gordan coefficients as they should.

A relative penetrability can be approximated by the ratio of the uncoupled regular function at 10 fm to the uncoupled regular function at 150 fm squared. Each squared ratio was divided by the corresponding penetrability given by Poggenburg[11] who used a Fröman matrix to calculate penetrabilities. The resulting numbers should be, and they were, approximately equal.

TABLE IVA. Channels considered in the favored α decay to the first five levels of a $K\pi = 7/2+$ rotational band.

Index	I_d	ℓ
1	7/2	0
2	7/2	2
3	7/2	4
4	9/2	2
5	9/2	4
6	11/2	2
7	11/2	4
8	13/2	4
9	15/2	4

Tables IVB and IVC. Inverse of ^{253}Es Surface Amplitude Matrix.

I_f', ℓ'	7/2, 0	7/2, 2	7/2, 4	9/2, 2	9/2, 4	11/2, 2	11/2, 4	13/2, 4	15/2, 4
					Real Components				
7/2, 0	2.8389E-13	-4.6847E-14	1.9146E-15	4.3804E-14	-3.7024E-15	-2.1475E-14	4.2709E-15	-3.2217E-15	1.4631E-15
7/2, 2	-4.3547E-14	2.0829E-13	-2.3962E-14	1.9060E-14	2.5946E-14	1.1510E-14	-1.0063E-14	-6.9621E-16	-8.9831E-16
7/2, 4	1.4277E-15	-2.0215E-14	1.3146E-13	-8.5929E-15	1.4367E-14	-1.7849E-15	5.4143E-15	9.1879E-16	1.8802E-16
9/2, 2	3.3704E-14	1.5873E-14	-8.4537E-15	1.8553E-13	-4.3859E-15	2.2326E-14	2.0732E-14	-1.5144E-14	-1.9630E-15
9/2, 4	-2.2258E-15	1.8075E-14	1.1941E-14	-3.7263E-15	1.0910E-13	-2.7208E-15	1.2417E-14	4.2887E-15	5.2145E-16
11/2, 2	-1.2974E-14	7.4187E-15	-1.3697E-15	1.7650E-14	-2.5409E-15	1.3910E-13	1.0486E-15	1.0774E-14	-1.6848E-14
11/2, 4	1.9536E-15	-5.5072E-15	3.5009E-15	1.3687E-14	9.8292E-15	8.4889E-16	8.2428E-14	8.0484E-15	2.1089E-15
13/2, 4	-1.0550E-15	-2.6002E-16	4.0641E-16	-7.3796E-15	2.5092E-15	6.7963E-15	6.0775E-15	5.7544E-14	3.9566E-15
15/2, 4	3.1896E-16	-2.0837E-16	5.1909E-17	-5.8781E-16	1.9458E-16	-7.2664E-15	1.1137E-15	2.8357E-15	3.7143E-14
					Imaginary Components				
7/2, 0	-3.0880E-15	7.1623E-15	-6.0093E-16	-5.2612E-15	1.0389E-15	1.8321E-15	-1.0344E-15	6.4430E-16	-2.2668E-16
7/2, 2	9.0650E-15	4.8316E-16	2.8864E-15	-1.8774E-15	-2.1759E-15	-1.9257E-15	3.0429E-16	9.5706E-17	2.0476E-16
7/2, 4	-7.6426E-16	5.0520E-15	-7.1092E-16	2.1082E-15	-1.7815E-15	6.1921E-16	-8.0746E-16	-2.7953E-16	-7.2756E-17
9/2, 2	-8.4270E-15	-2.7345E-15	1.6148E-15	-3.0496E-15	3.5162E-16	-2.8575E-15	-1.8721E-15	7.3266E-16	4.0018E-16
9/2, 4	1.3129E-15	-5.2155E-15	-2.3553E-15	7.6912E-16	-1.4927E-15	4.3253E-16	-1.5535E-15	-5.6217E-16	-1.3488E-16
11/2, 2	3.9184E-15	-2.4771E-15	5.2540E-16	-3.8994E-15	3.2717E-16	-1.4089E-15	-3.7746E-16	-6.6735E-16	8.5652E-16
11/2, 4	-1.2899E-15	1.7539E-15	-1.0952E-15	-4.2999E-15	-2.1287E-15	-4.3671E-16	-1.0788E-15	-8.2390E-16	-1.8860E-16
13/2, 4	7.8883E-16	1.4832E-16	-2.5308E-16	2.7423E-15	-8.2254E-16	-2.0551E-15	-1.2873E-15	-4.2879E-16	-2.6281E-16
15/2, 4	-2.7308E-16	1.8442E-16	-4.7919E-17	4.3275E-16	-1.2334E-16	2.9673E-15	-3.5411E-16	-5.5705E-16	-3.7901E-17

Tables IVD and IVE. Inverse of ^{255}Fm Surface Amplitude Matrix.

I_f', ℓ'	7/2, 0	7/2, 2	7/2, 4	9/2, 2	9/2, 4	11/2, 2	11/2, 4	13/2, 4	15/2, 4
	Real Components								
7/2, 0	1.1870E-12	-1.9486E-13	7.9070E-15	1.8097E-13	-1.5233E-14	-8.7395E-14	1.7438E-14	-1.2998E-14	5.7992E-15
7/2, 2	-1.8115E-13	8.7390E-13	-1.0010E-13	7.9077E-14	1.0760E-13	4.6957E-14	-4.1110E-14	-2.8240E-15	-3.5730E-15
7/2, 4	5.8394E-15	-8.4459E-14	5.5522E-13	-3.5711E-14	5.9097E-14	-7.3058E-15	2.2234E-14	3.7369E-15	7.5245E-16
9/2, 2	1.3100E-13	6.2170E-14	-3.3047E-14	7.2773E-13	-1.7188E-14	8.6398E-14	8.0244E-14	-5.7691E-14	-7.3958E-15
9/2, 4	-8.4032E-15	7.0415E-14	4.6962E-14	-1.4630E-14	4.3090E-13	-1.0639E-14	4.8310E-14	1.6412E-14	1.9783E-15
11/2, 2	-4.5978E-14	2.6245E-14	-4.8311E-15	6.3450E-14	-9.2321E-15	5.0289E-13	3.7216E-15	3.8454E-14	-5.9033E-14
11/2, 4	6.6662E-15	-1.9343E-14	1.2493E-14	4.8987E-14	3.5558E-14	2.9875E-15	2.9989E-13	2.8846E-14	7.4204E-15
13/2, 4	-3.2385E-15	-8.2000E-16	1.2742E-15	-2.3892E-14	8.2094E-15	2.2401E-14	2.0215E-14	1.9240E-13	1.3025E-14
15/2, 4	8.7359E-16	-5.6783E-16	1.4050E-16	-1.6537E-15	5.5735E-16	-2.1403E-14	3.3317E-15	8.6232E-15	1.1340E-13
	Imaginary Components								
7/2, 0	-2.7719E-14	3.4355E-14	-2.8316E-15	-2.3658E-14	4.7344E-15	7.5515E-15	-4.4998E-15	2.6324E-15	-8.4587E-16
7/2, 2	4.2548E-14	-8.1401E-15	1.4189E-14	-8.2482E-15	-1.0082E-14	-8.0857E-15	1.2906E-15	3.7728E-16	7.9411E-16
7/2, 4	-3.5196E-15	2.3561E-14	-9.8289E-15	9.2983E-15	-7.8930E-15	2.6445E-15	-3.3948E-15	-1.1522E-15	-2.9228E-16
9/2, 2	-3.8450E-14	-1.2877E-14	7.5618E-15	-2.1403E-14	1.6768E-15	-1.1604E-14	-7.9200E-15	2.9480E-15	1.4957E-15
9/2, 4	5.7391E-15	-2.3646E-14	-1.0982E-14	3.3762E-15	-1.1519E-14	1.7129E-15	-6.3124E-15	-2.1634E-15	-5.0201E-16
11/2, 2	1.6686E-14	-1.0496E-14	2.2143E-15	-1.6691E-14	1.4947E-15	-1.1395E-14	-1.5150E-15	-2.5743E-15	3.1870E-15
11/2, 4	-5.2252E-15	7.4385E-15	-4.6912E-15	-1.7938E-14	-9.1354E-15	-1.7224E-15	-7.8218E-15	-3.0382E-15	-6.4649E-16
13/2, 4	2.9128E-15	5.5591E-16	-9.5188E-16	1.0483E-14	-3.2108E-15	-7.8825E-15	-5.0751E-15	-3.8616E-15	-8.5954E-16
15/2, 4	-9.0647E-16	6.1223E-16	-1.5937E-16	1.4495E-15	-4.2056E-16	1.0186E-14	-1.2579E-15	-2.0271E-15	-1.4940E-15

Table IVF. ^{253}Es partial wave intensities, quadrupole phase shifts, and Coulomb phase shifts obtained by numerical integration ($a_0 = 1$, $a_2 = 0.8580$, $a_4 = -0.0977$).

I_d	ℓ	Partial wave intensity (%)	Experimental intensity with i wave subtracted (%)	Quadrupole phase shift (radians)	Coulomb phase shift (radians)
7/2	0	81.7983		-0.02102	50.80282
	2	8.9034		-0.13020	53.81583
	4	0.1355		0.12676	56.65920
		90.8372	90.0		
9/2	2	5.2180		-0.15901	54.04699
	4	0.3383		0.13803	56.89128
		5.5564	6.6		
11/2	2	0.7788		-0.19261	54.33783
	4	0.2723		0.15148	57.18327
		1.0511	0.846		
13/2	4	0.0848	0.0810	0.16682	57.53714
15/2	4	0.0085	0.011	0.18423	57.96313

Table IVG. ^{255}Fm partial wave intensities, quadrupole phase shifts, and Coulomb phase shifts obtained by numerical integration ($a_0 = 1$, $a_2 = 0.7918$, $a_4 = -0.1794$).

I_d	ℓ	Partial wave intensity (%)	Experimental intensity with i wave subtracted (%)	Quadrupole phase shift (radians)	Coulomb phase shift (radians)
7/2	0	86.1522		-0.00664	49.49463
	2	7.5837		-0.13561	52.50530
	4	0.2035		0.11033	55.34333
		93.9393	93.4		
9/2	2	3.9054		-0.17933	52.80722
	4	0.4433		0.12150	55.64650
		4.3487	5.05		
11/2	2	0.5004		-0.22613	53.18030
	4	0.3013		0.13352	56.02110
		0.8017	0.62		
13/2	4	0.0787	0.097	0.14564	56.47075
15/2	4	0.0066	0.008	0.15817	56.99444

Table IVH. Values of the effective α particle energy, Coulomb function argument η, and Coulomb function argument ρ/r for ^{253}Es and ^{255}Fm.

$I_d\pi$	^{253}Es Q_{eff} (MeV)	^{253}Es η	^{253}Es k (fm^{-1})	^{255}Fm Q_{eff} (MeV)	^{255}Fm η	^{255}Fm k (fm^{-1})
7/2+	6.78008	23.28794	1.13032	7.176	22.87120	1.16293
9/2+	6.73762	23.36120	1.12678	7.116	22.96742	1.15806
11/2+	6.68482	23.45328	1.12235	7.043	23.08614	1.15210
13/2+	6.62174	23.56473	1.11704	6.957	23.22840	1.14505
15/2+	6.54710	23.69867	1.11073	6.859	23.39375	1.13695

Table IVJ. Theoretical branching of the ℓ=4 alpha groups for ^{253}Es.

I_d	BFM-sharp barrier (Asaro et al.)[36]	BFM-sloping barrier (Poggenburg)[11]	Coupled channel (this work)
7/2	(1)	(1)	(1)
9/2	2.57	2.486	2.499
11/2	2.10	1.994	2.010
13/2	0.65	0.632	0.626
15/2	0.065	0.063	0.063

Table IVK. Correction factors for the i partial wave.

	^{253}Es		^{255}Fm	
I_d^{π}	Experimental intensity[38] (%)	$\ell = 6$ component (%)	Experimental intensity[38] (%)	$\ell = 6$ component (%)
7/2+	90.0(5)	0.0002	93.4(2)	0.0003
9/2+	6.6(2)	0.0014	5.05(7)	0.0022
11/2+	0.85(3)	0.0037	0.62(1)	0.0040
13/2+	0.085(3)	0.0039	0.110(5)	0.0129
15/2+	0.013(1)	0.0018	0.013(2)	0.0049
17/2+	0.0004(1)	(0.0004)		
19/2+	0.00012(4)			

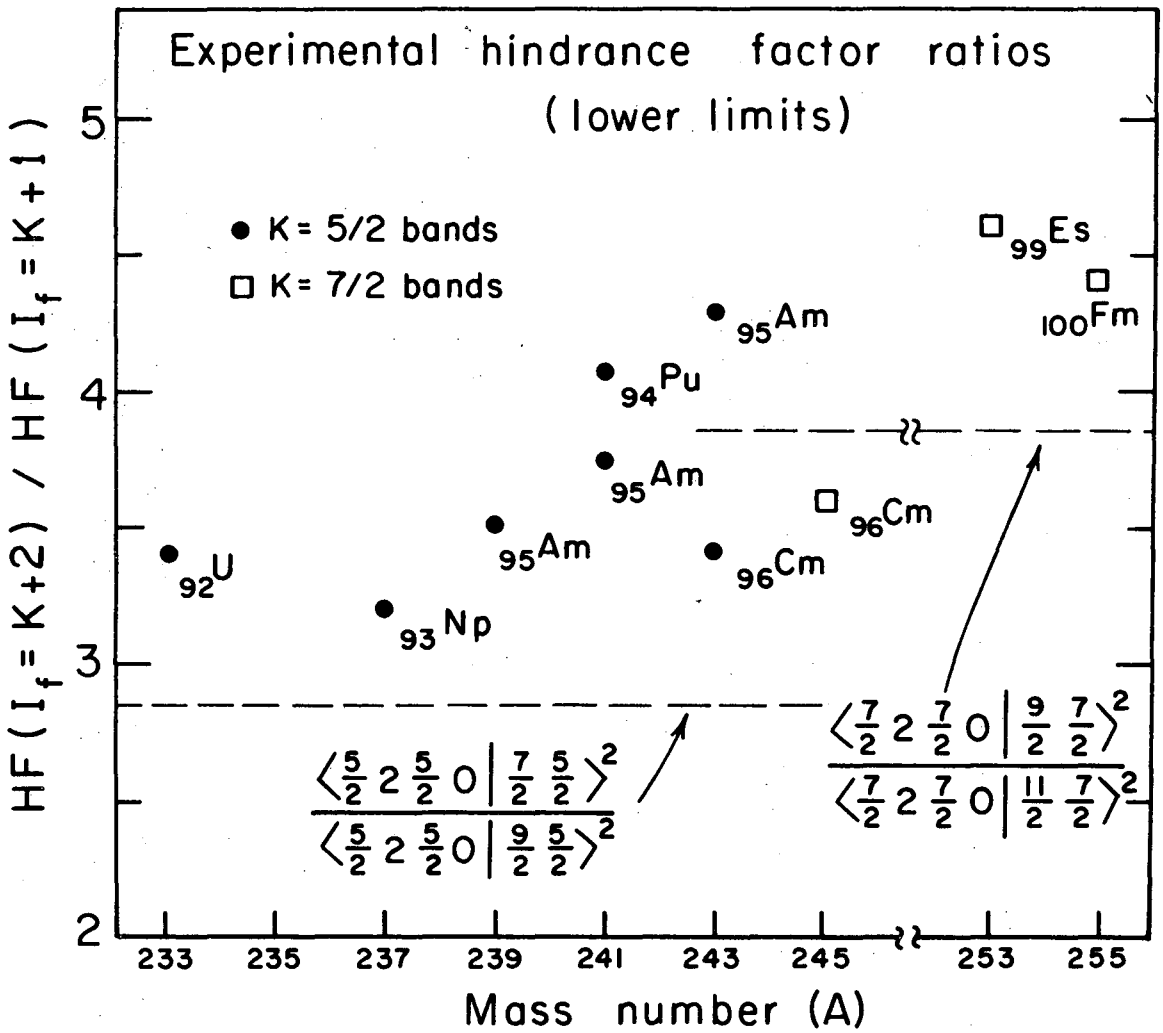

XBL743-2688

FIG. 2. Ratio of the hindrance factor of the second excited level to the hindrance factor of the first excited level in the favored α decay of odd-mass nuclei.

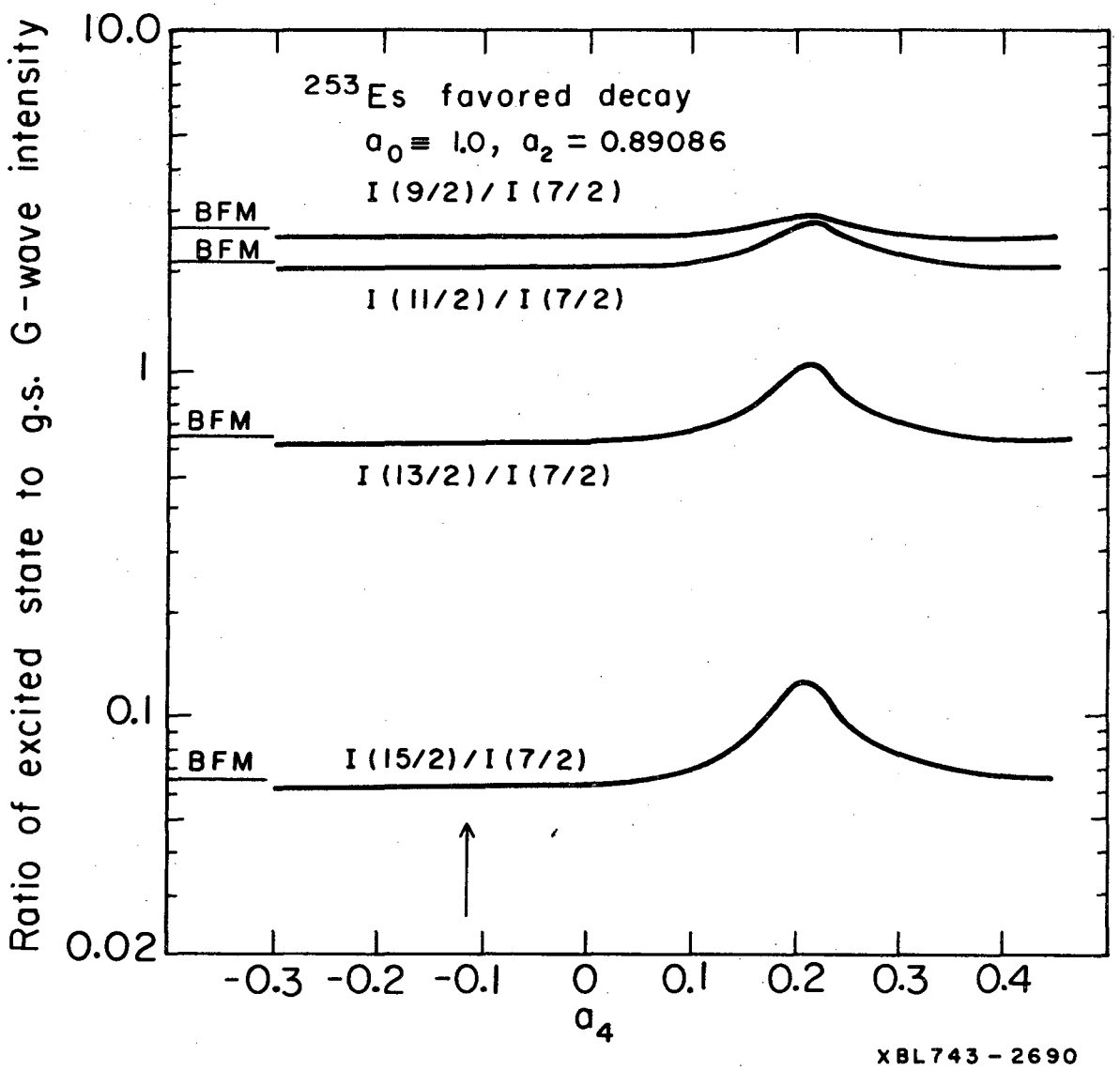

FIG. 3. Logarithm of the ratio of the $\ell = 4$ partial wave intensity in excited states of the 7/2+[633] band of ^{249}Bk to that in the ground state as a function of α_4 with α_2 fixed at 0.89. Bohr, Fröman and Mottelson ratios (Table IVJ) hold for most value of α_4.

V. NUCLEAR ORIENTATION THEORY

V.A. SPIN HAMILTONIAN

The research reported here was restricted to the alignment of nuclei of actinide element ions in paramagnetic salts. Therefore the only NO methods discussed are those specific to a paramagnetic salt host. In the absence of an external magnetic field it is necessary that single crystals of paramagnetic salts be used in order to define a quantization axis. The neighboring atoms of a paramagnetic ion in a crystalline lattice create an electric field at the paramagnetic ion site with strength and direction determined by the crystalline structure. The Stark effect splitting of the unpaired electrons of the paramagnetic ion gives certain orbital states lower energy than others. The overall splitting of the J-manifold of a rare earth ion is of the order of 100 K - 1000 K; therefore only the lowest energy level is populated at NO temperatures. If the crystalline electric field has axial symmetry, alignment of the electronic magnetic moments relative to the crystalline axis will occur. At sufficiently low temperatures nuclear alignment will occur because the nuclear magnetic moment will preferentially align along the electronic field or the nuclear quadrupole moment will align in the electric field gradient arising from the lattice charges and the unpaired electrons.

Hyperfine splitting in the absence of an external magnetic field at a site of axial symmetry is described by a phenomenological spin Hamiltonian[53]

$$\mathcal{H}_{hf} = D(S_z^2 - S(S+1)/3) + AI_zS_z + B(I_xS_x + I_yS_y) + P(I_z^2 - I(I+1)/3). \tag{17}$$

The effective electron spin S is defined such that the multiplicity of the electronic energy levels is equal to (2S + 1). The first term represents the splitting of the electronic levels due to second order effects of the crystalline electric field. It is zero for the most common cases when $S = \frac{1}{2}$. The second and third terms arise from magnetic hyperfine alignment as proposed by Bleaney.[54] The final term describes the electric hyperfine alignment proposed by Pound.[55]

In order to present a more quantitative treatment of magnetic and electric hyperfine interactions, it is necessary to first discuss the free ion and crystal field interactions in the actinides.

V.B. RARE EARTH AND ACTINIDE ION ELECTRONIC STRUCTURE

The actinides are chemically much more complex than the lanthanides. Whereas the lanthanides form 3+ states almost exclusively, numerous charge states occur in the actinides, especially in the lighter actinides, and covalent bonding is important in compounds formed by the more highly valent ions. The 4f electrons are localized and screened by the closed electron shells. The spin-orbit interaction is stronger than the crystal field interaction. Although J remains a good quantum number to first approximation, Russell Sauders or L-S coupling applies only to the ground multiplet, if at all. The 5f electrons are less well shielded, configuration mixing occurs, and J ceases to be a good quantum number because the spin-orbit and crystal field interactions are of comparable importance.[56] W. T. Carnall of Argonne National Laboratory and H. Crosswhite of John Hopkins University are in the process of solving the complete interaction Hamiltonian including Coulombic, spin-orbit, and crystal field interactions for selected actinides. However, in this work I consider the crystal field interaction as a perturbation on the free ion levels.

When the spin-orbit interaction becomes large, states with the same J but different L and S become appreciably mixed, and intermediate coupling occurs. The elements of the spin-orbit interaction matrix were given in general terms by Elliott, Judd and Runciman.[57] The eigenvalues of the interaction matrices are the energy corrections to the levels, and the eigenfunctions are the components of the wavefunctions expressed as linear combinations of L-S coupling wavefunctions.

In this work only pure $5f^N$ configurations are considered. The calculation of energy levels of f electron ions has been treated extensively by both Judd[58] and Wybourne.[59] This thesis treats only the most important points in the calculations.

In only the ^{253}Es case were the experimental results precise enough to justify a detailed study of the actinide ion electronic structure. Therefore some of the comments below will be specialized to ^{253}Es ions.

The electrostatic, spin-orbit, and configuration interaction parameters for Es^{3+} (aquo) have been obtained recently by Carnall et al[60] from an analysis of the solution absorption spectrum. Their values (all in cm^{-1}) are $E^1 = 4445.86$, $E^2 = 21.4464$, $E^3 = 416.638$, $\zeta = 4014.70$, $\alpha = 22.505$, $\beta = -722.53$, and $\gamma = 1000$. The resulting ground state wavefunction is 75.3% ^5I + 21.8% ^3K + 1.2% ^3L + 0.1% ^3M + 1.6% ^1L. At the time I analyzed the data, I used estimates of the ^{253}Es parameters made by John G. Conway;[61] namely, $E^1 = 6682.6$, $E^2 = 30.69$, $E^3 = 620.1$, $\zeta = 2127.1$, $\alpha = 23.5$, $\beta = -811.2$, and $\gamma = 0$. The resulting wavefunction, which was obtained from the program GUESS, is 78.8% $^5I_{20}$ + 14.8% $^3K_{30}$ + 4.3% $^3K_{21}$ + 1.0% $^1L_{22}$ + 0.8% $^3L_{21}$ + 0.1% $^1L_{21}$ + 0.1% $^3M_{30}$. The subscripts are the U quantum numbers which label the irreducible representations of the group G_2. L, S, M_L and M_s do not provide sufficient labels to distinguish terms in ℓ^n configurations when $n > 3$. Since there is little difference between our wavefunction and the one obtained by Carnall et al, no significant changes in my conclusions are expected as a result of the use of the approximate parameters. Only in the case of J-mixing would pronounced changes in the hf interaction parameters occur.

V.C. CRYSTAL FIELD INTERACTION

I next consider the crystal field (CF) interaction as a perturbation on the free ion level and then the hyperfine interaction as a perturbation on the CF levels.

The CF potential can be expanded as

$$\mathcal{H}_{CF} = \sum_i \sum_{k,q} B_q^k (\vec{C}_q^{(k)})_i \sum_k (V_q^k)_i \tag{19}$$

where $\vec{C}_q^{(k)}$ is a tensor operator, B_q^k is a CF parameter that is proportional to a lattice sum times the expectation value of the f electron radial extent, and the summation extends over i electrons of the ion. The CF parameters are usually determined from optical spectra of ions in a crystalline lattice. For f-electrons, $k \leq 6$; and for pure f^N configurations, odd values of k vanish.

The matrix elements of the CF operator can be written as

$$\langle f^N \tau SLJJ_z | \mathcal{H}_{CF} | f^N \tau' SL'J'J_z' \rangle = \sum_{k,q} B_q^k \langle f^N \tau SLJJ_z | \vec{U}_q^{(k)} | f^N \tau' SL'J'J_z' \rangle \times \langle f \| \vec{C}^{(k)} \| f \rangle \tag{20a}$$

where

$$\langle f^N \tau SLJJ_z | \vec{U}_q^{(k)} | f^N \tau SL'J'J_z' \rangle = (-1)^{2J-J_z+S+L'+k} \begin{Bmatrix} J & J' & k \\ L' & L & S \end{Bmatrix} \begin{pmatrix} J & k & J' \\ -J_z & q & J_z' \end{pmatrix} \times \left\{ [J]\ [J'] \right\}^{\frac{1}{2}} \langle f^N \tau SL \| \vec{U}^{(k)} \| f^N \tau' SL' \rangle \tag{20b}$$

and

$$\langle f \| \vec{C}^{(k)} \| f \rangle = -7 \begin{pmatrix} 3 & k & 3 \\ 0 & 0 & 0 \end{pmatrix}. \tag{20c}$$

The reduced matrix elements of $\vec{U}^{(k)}$ can be readily evaluated with the aid of the tables of Nielson and Koster.[62] The CF interaction is diagonal in S. τ stands for all unspecified quantum numbers.

In classifying energy levels in the CF, each energy level can be labelled by a particular irreducible representation of the symmetry group. The ethylsulfates($R(C_2H_5SO_4)_3 \cdot 9H_2O$) have symmetry C_{3h} and a well-known crystal structure.[63] The more highly symmetrical D_{3h} symmetry can be used in describing the CF interaction. The only non-vanishing CF parameters are B_0^2, B_0^4, B_0^6, and B_6^6.

A simple classification scheme for the CF energy levels was proposed by Hellwege.[64] The rotation axis of highest order is taken as the z-axis, and J_z is the projection of J on this axis. The elements V_k^q of the CF potential represent an interaction between the states characterized by J, J_z and J', $J'_z + q$ where $J_z = J'_z$. Obviously when $q \neq 0$, J_z is not a good quantum number. The only non-zero q that occurs in C_{3h} symmetry is 6. The CF interaction matrix factors into a set of irreducible submatrices labelled by the crystal quantum numbers μ where $J_z = \mu (\text{mod } q)$. Only states of the same class can interact with each other. For an odd number of electrons, e.g., Fm^{3+}, there are three classes labelled by $\mu = \pm\frac{1}{2}, \pm\frac{3}{2}, \pm\frac{5}{2}$. In symmetry lower than cubic the levels $\pm\mu$ are doubly degenerate. Kramer's theorem requires that the levels be doubly degenerate in the absence of an external magnetic field or exchange effects. For an even number of electrons, e.g., Am^{3+} and Es^{3+}, there are four classes labelled by $\mu = 0, \pm 1, \pm 2, 3$.

In symmetry lower than cubic the levels may be either singlets or doublets. Further discussion of the CF interaction and the values of the CF parameters will be presented in the results section.

V.D. MAGNETIC HYPERFINE INTERACTION

The magnetic hf interaction is the result of the interaction between the nuclear magnetic dipole moment and the magnetic field produced at the nucleus by the electrons. This can be written as[65]

$$\mathcal{H}_{mhf} = \frac{2\mu_B \mu_N \mu}{I} \sum_{i=1}^{N} \frac{\vec{N}_i \vec{I}}{r_i^3} \tag{21a}$$

with

$$\vec{N}_i = \vec{I}_i - \sqrt{10}\,(\vec{s}\vec{C}^{(2)})_i^{(1)} \tag{21b}$$

where μ_B and μ_N are the Bohr and nuclear magnetons respectively, and μ is the nuclear magnetic dipole moment expressed in units of nuclear magnetons. The problem reduces to finding the matrix elements of $\vec{N}_i$ within a J multiplet. Since $\vec{N}_i$ is a first rank tensor, the Wigner-Eckart theorem can be used to relate its matrix elements to those of $\vec{J}$. Writing the magnetic hf interaction Hamiltonian as $A\vec{I}\cdot\vec{J}$,

$$A_{\parallel} = A = 4\mu_B \mu_N \mu \langle r^{-3} \rangle_{5f} \langle + | J_z | + \rangle \langle J \| N \| J \rangle / I, \tag{22a}$$

$$A_{\perp} = B = 4\mu_B \mu_N \mu \langle r^{-3} \rangle_{5f} \langle + | J_x | - \rangle \langle J \| N \| J \rangle / I \tag{22b}$$

where

$$\langle J \| N \| J \rangle = \frac{\langle f^N SLJ \| \sum_i N_i \| f^N S'L'J \rangle}{\langle f^N SLJ \| J \| f^N S'L'J \rangle} . \tag{22c}$$

$\langle J \| N \| J \rangle$ is proportional to the matrix element $\langle f^N \tau SL \| V^{(12)} \| f^N \tau' S'L' \rangle$ which is tabulated by Nielson and Koster.[62] The wave functions $|+\rangle$ and $|-\rangle$ represent the wave functions of the ground doublet.

V.E. ELECTRIC HYPERFINE INTERACTION

The ehf splitting of the nuclear magnetic substates results from the interaction between the nuclear quadrupole moment, Q, and the electric field gradient (EFG) at the nucleus. In NES there are four sources of an EFG at the rare-earth site: 1) the lattice charges and dipoles, 2) the open f-electron shell, 3 and 4) closed electronic shells that are polarized or distorted by the quadrupole part of the crystal field (CF) and by the unfilled f-shell. The resultant EFG may be written as[66]

$$eq = eq_{nf}(1 - R_Q) + eq_{lat}(1 - \gamma_\infty) \tag{23}$$

where R_Q and γ_∞ are the atomic and lattice Sternheimer[14] anti-shielding factors respectively. Since the quadrupole interaction is proportional to $\langle r^{-3}\rangle$, the lattice term would usually be smaller than the f-electron term were it not for the enhancement of the quadrupole component of the CF potential resulting from distortion of closed shells.

The electric hyperfine interaction between the valence electrons and the nucleus is given by[53]

$$\mathcal{H}_{ehf,nf} = \frac{e^2Q}{2I(2I-1)} \sum_i \left\{ \frac{I(I+1)}{r_i^3} - \frac{3(\vec{r}_i \cdot \vec{I})^2}{r_i^5} \right\}. \tag{24}$$

The elements diagonal in J and J_z are[67]

$$\langle J, J_z | \sum_i \left\{ \frac{I(I+1)}{r_i^3} - \frac{3(\vec{r}_i \cdot \vec{I})^2}{r_i^5} \right\} | J, J_z \rangle$$

$$= -\frac{3}{2} \langle J \| \alpha \| J \rangle \langle r^{-3} \rangle_{nf} \langle + | 3J_z^2 - J(J+1) | + \rangle (I_z^2 - I(I+1)/3) \tag{25a}$$

where

$$\langle J \| \alpha \| J' \rangle = \langle f^N \tau SLJJ_z | \vec{U}_q^{(k)} | f^N \tau' \, SL'J'J_z' \rangle \tag{25b}$$

the matrix elements of which were given previously. The f-electron part of P then becomes

$$P_{5f} = - \frac{3e^2Q}{4I(2I-1)} \langle r^{-3} \rangle_{5f} \langle J \| \alpha \| J \rangle \langle + | 3J_z^2 - J(J+1) | + \rangle (1-R_Q) \tag{26}$$

with the Sternheimer factor included.

Elliott[68] considered the admixture of the J = 2 state into the J = 0 ground state of Eu^{3+} by the crystal field. Using second order perturbation theory he obtained, after allowing for a change from the 4f shell to the 5f shell,

$$P_{5f}^{(2)} = \frac{6e^2Q \, A_2^0 \, (1-\sigma_2) \langle r^2 \rangle_{5f} \langle r^{-3} \rangle_{5f} (1-R_Q) \, | \langle 20 \| \alpha \| 00 \rangle |^2}{I(2I-1) \, E(^7F_{20} - {}^7F_{00})} \, . \tag{27}$$

The ionic shielding parameter σ_2 gives the shielding of the 5f-electrons from the crystal field by the outer electrons, primarily the 6s and 6p shells. A_0^2 is related to the CF parameter introduced earlier by the relationship

$$B_0^2 = 2A_2^0 (1-\sigma_2) \langle r^2 \rangle \, . \tag{28a}$$

A_0^2 is a lattice sum given by

$$A_0^2 = - \frac{e}{4} \sum_i e_i \frac{3\cos^2\theta_i - 1}{r_i^3} \, . \tag{28b}$$

At a site of axial symmetry the quadrupole coupling constant is defined as

$$P = \frac{3e^2Qq}{4I(2I-1)} = \frac{3eQ}{4I(2I-1)} \frac{\partial^2 v}{\partial z^2} \quad . \tag{29a}$$

In the absence of electronic shielding the electrostatic potential is expanded in terms of spherical harmonics as

$$-eV = \sum_{n,m} r^n A_n^m Y_n^m(\theta, \phi) \ . \tag{29b}$$

In cartesian coordinates for crystals of axial symmetry the first non-spherical term is

$$V_2^0 = A_2^0(3z^2 - r^2)/(-e). \tag{29c}$$

Therefore the lattice contribution to P is

$$P_{lat} = - \frac{3Q(1 - \gamma_\infty)A_2^0}{I(2I - 1)} \tag{29d}$$

with the Sternheimer antishielding factor explicitly included.

VI. EXPERIMENTAL APPARATUS AND TECHNIQUES

VI.A. CRYOSTAT

The cryostat used was similar to the one used by Frankel[8] except that the two glass dewars were longer, and an improved high vacuum system was installed. The inner dewar was filled with liquid helium pumped to approximately 1K, and the outer dewar was filled with liquid nitrogen. The dewar tails were constricted to fit within the 6.8 cm gap of an iron yoke electromagnet. The experimental sample chamber was contained in a glass tube 3 cm in diameter and 30 cm long which was attached to a 1 m long thin-walled stainless steel pumping tube by means of a copper-Pyrex housekeeper seal and a soft solder filled gutter seal. A radiation baffle system made of brass was soldered to the lower end of the stainless steel pump out tube, and a 2.54 cm inner diameter brass cage was screwed to the baffle system. The lower half of the brass cage is shown in Fig. 4. The neodymium ethylsulfate crystal is mounted in a yoke formed from a 2 mm diameter Pyrex glass support rod which is anchored near the top of the cage. Its 20 cm of length decreases thermal heat leaks. Technical grade manganous ammonium sulfate (MAS) was crystallized from aqueous solution after being dissolved at 80° C and filtered. The crystals were ground, moistened with a 50-50 glycerol-H_2O solution, and compressed into pills. The MAS cools upon demagnetization before the other paramagnetic salts and cryopumps residual ^{4}He exchange gas. The chromium-potassium alum in glycerine slurry, which is contained in a glass cup, cools upon adiabatic demagnetization to approximately the same temperature as NES and decreases the heat leak down the Pyrex rod to the NES

crystal. The nylon filament damps out vibrations. The α particle detectors are along and perpendicular to the NES c-axis. The error in positioning is estimated to be $\pm 2°$. Because the even order Legendre polynomials entering into the angular distribution function are relatively flat at 0° and 90°, any misalignment results in small errors.

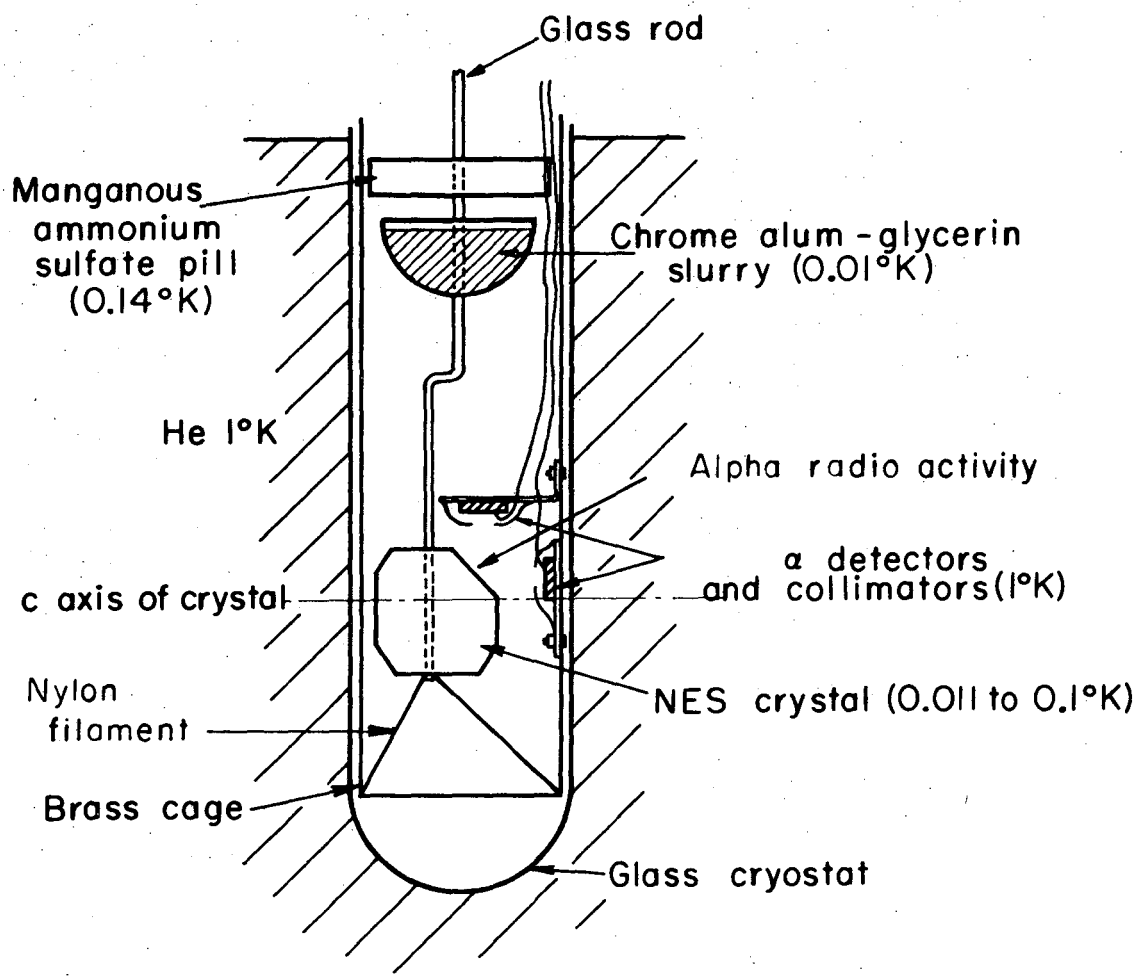

MUB-2999

FIG. 4. Experimental chamber for nuclear orientation studies of α-emitting isotopes.

VI.B. ALPHA PARTICLE RADIATION DETECTORS

The α particle radiation detectors consisted of wafers of silicon 1 cm $\times$ 1 cm $\times$ 0.4 mm that had been lapped and etched. Gold electrodes were evaporated on both the front and back surfaces; the back surface being completely coated and the front surface partially masked prior to evaporation to leave a circle 7 mm in diameter. An electrically conducting silver-containing epoxy was used both to fasten each detector to a 0.25 mm thick molybdenum mounting strip and to secure a fine gold wire to the front electrode. The gold lead was further epoxied to a ceramic stand-off fastened to the molybdenum strip to which a 32 gauge manganin lead had previously been soldered. In order to confine the α particles to the center of the front electrode, where the field gradient is uniform, and in order to permit quantitative solid angle corrections, 2 mm thick brass strips with a 3 mm diameter hole drilled through them were used as collimators.

The detector bias was applied and the output signal removed on a common lead consisting of 32 gauge formex coated manganin wire in the brass cage section and 30 gauge bare constantan wire in the stainless steel pumping tube section. The brass cage served as the electrical and thermal ground.

The detector output pulses were shaped and amplified in an LBL low voltage nuvistor pre-amp (11$\times$1050) and further amplified in an LBL linear amplifier system (11$\times$198). Energy spectra were accumulated on various pulse height analyzers.

VI.C. NEODYMIUM ETHYLSULFATE CRYSTALS

The neodymium ethylsulfate (NES) was prepared in aqueous solution by the reaction

$$Nd_2(SO_4)_3 + 3\ Ba(C_2H_5SO_4)_2 \xrightarrow{H_2O} 2\ Nd(C_2H_5SO_4)_3 \cdot 9H_2O + 3\ BaSO_4\downarrow$$

Single crystals of NES were grown from solution in a refrigerator at approximately 0° C. Although the crystals took a year to grow to useable size (~ 4-7 g), they were almost transparent and free of the visible defects and occlusions characteristic of crystals grown at room temperature. The crystals were stored at 0° C prior to use in order to inhibit dehydration.

One face of each NES crystal was sanded at 45° with respect to the crystalline c-axis in order that both the 0° and the 90° radiation detectors would be exposed to approximately the same source shape and could be placed at approximately the same distance (typically 7-9 mm) from the source spot.

The trivalent actinide ions in the form of the trichloride were dissolved in approximately 3λ (1λ = 10^{-6} ℓ) of quartz distilled water. The solution was taken up in a 2λ micropipette which was held in a micropositioner. From a distance of 0.5mm the 2λ drop was dropped on the sanded crystal face, allowed to remain for one minute in order that the bulk crystal would dissolve permitting the exchange of actinide ions for Nd ions, and then removed to prevent microcrystals from forming. The process was repeated as many times as necessary to leave 1-5× 10^5 α dpm on the crystal. The best samples were prepared in one to three applications. More numerous applications resulted in sources that were deep, irregular craters in the formerly smooth face. The activity must be localized to a spot 1-2mm in diameter in order

to keep the solid angle corrections small. Although this method of sample preparation is crude, no more satisfactory technique was found. The characteristics of a "good" vs. "poor" source will be discussed later.

VI.D. ION EXCHANGE PURIFICATION OF ACTINIDE ELEMENT IONS

Most of the radionuclides used were obtained isotopically pure from the late Prof. Burris Cunningham and his co-workers. However, in some cases it was necessary to purify the activity on α-hydroxy-isobutyrate ("but") and "but" clean-up columns. Details on ion exchange procedures have been given by Fujita.[69]

VI.E. THERMOMETRY AND DATA COLLECTION AND REDUCTION

The final temperature reached after adiabatic demagnetization of the NES crystal was determined from the initial value of H/T using the temperature scale of Blok, Shirley, and Stone.[70] The ratio of the initial magnetic field (measured with a rotating coil gaussmeter[71]) to the pumped helium bath temperature (measured with a dibutylphthalate filled manometer) determines the magnitude of the entropy of the electronic spin system and also the final temperature reached upon adiabatic demagnetization to zero applied magnetic field. Final temperatures measured in this manner are accurate to within ± 6%. Additional details about magnetic temperature determination are given by Ambler and Hudson.[21]

Following adiabatic demagnetization several full spectrum "cold" counts were taken. The NES crystal was then warmed to the ^{4}He bath temperature (approximately 1 K) and a series of "warm" counts were taken for normalization. Because the ^{253}Es in NES α particle angular distribution is anisotropic at 1 K, these warm counts were renormalized to 4 K where the angular distribution is isotropic.

A typical pulse height spectrum is shown in Fig. 5. The α detectors used had an energy resolution (full width at half maximum) of 100 keV or better for 5.5 MeV α particles. The broadening of the peak shown in Fig. 5 is due to energy losses within the NES crystal. The effect of (Rutherford) scattering on the measured anisotropy was determined empirically by dividing typical spectra into several segments and by calculating the anisotropy of each segment. The lowest energy segments should show the smallest anisotropy if large-angle scattering is

important; but, within statistics the anisotropy was constant across each spectrum. However as a safeguard, the lowest 25% of the spectra were not used in calculating anisotropies. The ^{249}Bk daughter β^- activity contributed counts to the lowest part of the energy spectrum but no corrections were necessary because that part of each spectrum was excluded from analysis.

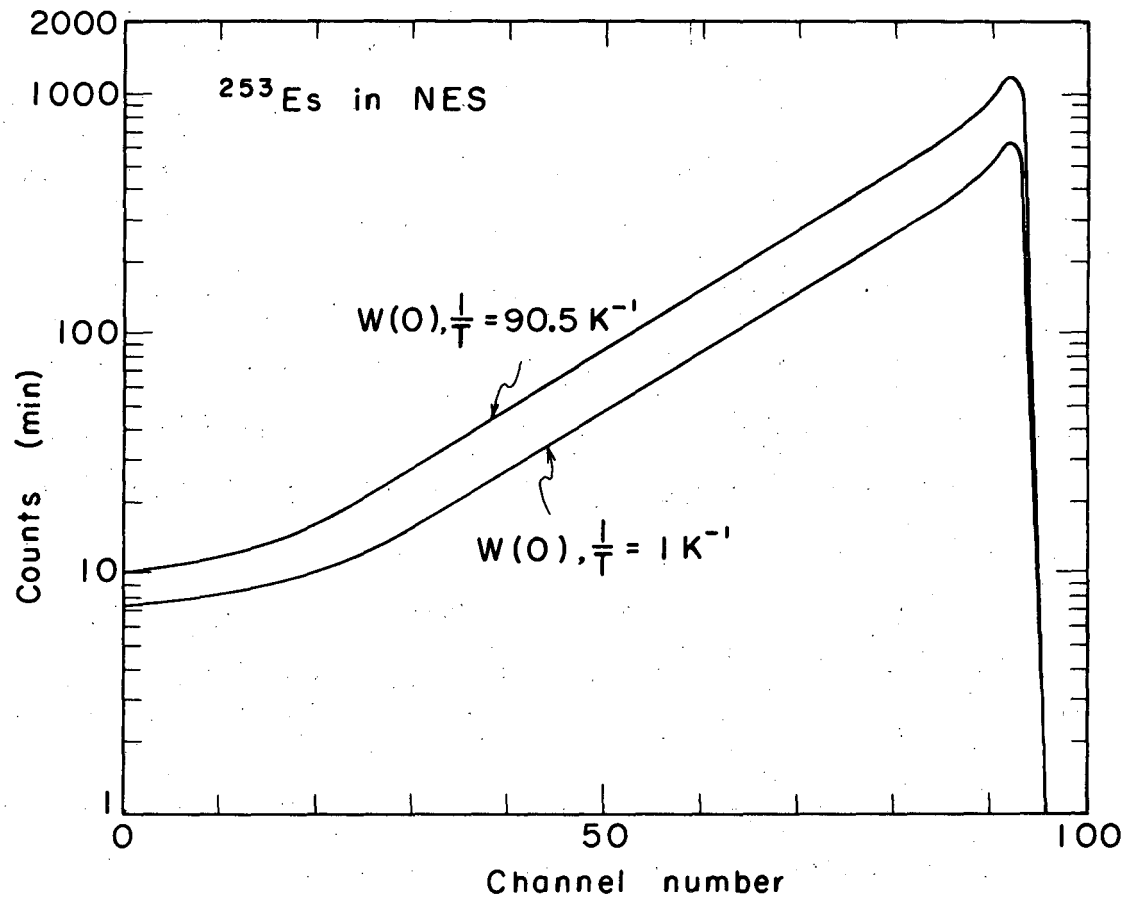

XBL705-2773

FIG. 5. Typical axial counter pulse-height spectrum for ^{253}Es in NES. The cold spectrum was taken at 0.011 K and the warm spectrum at 1 K.

VII. ^{253}Es NUCLEAR ORIENTATION RESULTS AND ^{253}Es IN NES MAGNETIC HYPERFINE INTERACTION CONSTANT

The results and discussion for ^{253}Es, ^{241}Am, and ^{255}Fm will be presented separately. Because the ^{253}Es results are the most quantitative, they will be discussed most completely. The ^{253}Es NO results have been published,[39] but the discussion section has been updated here.

The experimental work on ^{253}Es was carried out in three sets of measurements, which I will denote I[72], II[8], and III.[39] Data from one of my successful runs (designated as set III) are plotted in Fig. 6 and tabulated in Table VIIA. The statistical accuracies are given in parentheses. The quantity $3 - W(0) - 2W(\pi/2)$ in Table VIIA is proportional to the coefficient of $P_4(\cos\theta)$ in the angular distribution function; it will be discussed later. For the run summarized in Table VIIA, the solid angle correction factors are $Q_2(0) = 0.946$, $Q_4(0) = 0.829$, $Q_2(\pi/2) = 0.962$ and $Q_4(\pi/2) = 0.877$. In calculating the solid angle correction factors the radioactivity was assumed to be uniformly distributed throughout the spot. Since the activity probably concentrated at the center of the spot, the corrections may be too large; i.e., the correction factors should perhaps be larger in magnitude.

In discussing these data there are two rather distinct "figures of merit", which are best treated separately: the saturation values of $W(0)$ and $W(\pi/2)$ and their temperature dependences.

Saturation developed in the ^{253}Es in NES α particle angular distribution; that is, the magnetic hyperfine interaction was sufficiently large such that essentially all of the ^{253}Es nuclei were in the $I_z = \pm I$ nuclear magnetic substate below $1/T = 40\ K^{-1}$. The orientation

parameters, B_k, then assume their limiting or maximum absolute values. The saturation values of the orientation parameters for axial magnetic alignment and a parent spin of 7/2 are $B_2 = +1.528$, $B_4 = +0.798$ and $B_6 = 0.174$.

The observed saturation values of W(0) and W(π/2) are affected by the degree to which $^{253}Es^{3+}$ grows into Nd^{3+} lattice sites substitutionally, by scattering in the source crystal, and by the performance of the detectors and counting equipment. Values at saturation of W(0) and W(π/2) from I, II and III are given in Table VIIB. In I the "effect" as measured by the 90° detector, i.e., (1 - W(π/2)), is relatively small; the same is true for the effect at the 0° detector, (W(0) - 1) in II. In III on the other hand large effects are observed with both detectors. We interpret this to mean that III gave the most accurate saturation values for W(0) and W(π/2) because almost any error in a nuclear orientation experiment will act to reduce the observed effect.

Inspection of the discrepancies in Table VIIB suggests that two kinds of errors were present in I and II. First, the smaller effect on even the "better" detector in each case suggests a source preparation problem: perhaps the activity was too deep (leading to excessive scattering) or incompletely substituted into lattice sites. Secondly, the relatively large attenuation of the effect in the "poorer" detector in each case indicates something more grossly wrong either with that detector or with alpha emission in that direction (e.g., more scattering in the source in one direction). In III extreme care was taken to grow ^{253}Es only near the surface of the crystal. Also the detectors and associated circuits were far more reliable than in I and II. The large

effects observed with both detectors in series III were obtained with several sources. For these reasons we take the saturation values of W(0) and W(π/2) from series III as being characteristic of ^{253}Es in neodymium ethylsulfate.

The temperature dependences of W(0) and W(π/2) are affected by different variables than those that affect their saturation values. Immediately after demagnetization the small active volume of the NES crystal is warmed at an appreciable rate by radioactive heating. This can lead to a spurious apparent temperature dependence,[73] with the high-temperature points showing a reduced effect. The hyperfine structure constants derived in such cases are anomalously small. If gamma-ray distributions are studied, the activity can be distributed throughout the host crystal, and the temperature can be monitored through the magnetic susceptibility. For α particle studies, however, the activity must be concentrated in a small volume on the surface, and the resulting intense self-heating can raise the local temperature well above that of the bulk crystal. Ironically, the stronger the source and the shallower its distribution in from the surface (two conditions condusive to reliable measurement of saturation values of W(0) and W(π/2)), the worse will be the self-heating effect. Thus in our experiments, series I and II gave a temperature dependence in W(0) and W(π/2) characteristic of larger values of the magnetic hyperfine interaction constant ($A = 0.28 \pm 0.03$ cm^{-1}) than those that would be derived from series III ($A = 0.18 \pm 0.02$ cm^{-1}). The values of A obtained from several runs are given in Table VIIC. The final adopted value of the magnetic hyperfine interaction constant for ^{253}Es substituted

into neodymium ethylsulfate of $A = 0.26 \pm 0.03\ cm^{-1}$ was decided upon from the entries in Table VIIC on the basis of the above discussion.

Table VIIA. Experimental ^{253}Es in NES α particle angular distribution as a function of the inverse temperature.

$1/T$ (K^{-1})	$W(0)$	$W(\pi/2)$	$3 - W(0) - 2W(\pi/2)$
8.6(1)	1.566(27)	0.698(5)	0.038(28)
11.5(10)	1.712(22)	0.613(14)	0.062(30)
15.0	1.808(18)	0.578(16)	0.036(29)
19.2(5)	1.835(15)	0.544(14)	0.077(25)
25.5(10)	1.881(10)	0.543(5)	0.032(12)
31.2(2)	1.872(9)	0.533(7)	0.062(13)
40.8(13)	1.864(8)	0.524(6)	0.088(12)
49.1	1.864(8)	0.526(6)	0.084(12)
56.1	1.872(8)	0.518(8)	0.092(14)
74.0	1.880(8)	0.514(7)	0.092(13)
90.5	1.896(18)	0.520(4)	0.064(19)

Table VIIB. Saturation values for $W(\theta)$ after solid angle corrections.

Set	$W(0)$	$W(\pi/2)$	Reference
I	1.70	0.68	72
II	1.66	0.55	8
III	1.934	0.497	present work

Table VIIC. Derived magnetic hyperfine interaction constants for ^{253}Es in NES.

Series	Run	A(cm^{-1})	A/k (K)
I	1	0.28(2)	0.40(3)
	2	0.28	0.40
	3	0.25	0.36
II	1	0.28(3)	0.40(5)
	2	0.25(3)	0.36(4)
III	1	0.19(2)	0.28(3)
	2	0.17(2)	0.25(3)

Adopted value: $A = 0.26 \pm 0.03$ cm^{-1}.

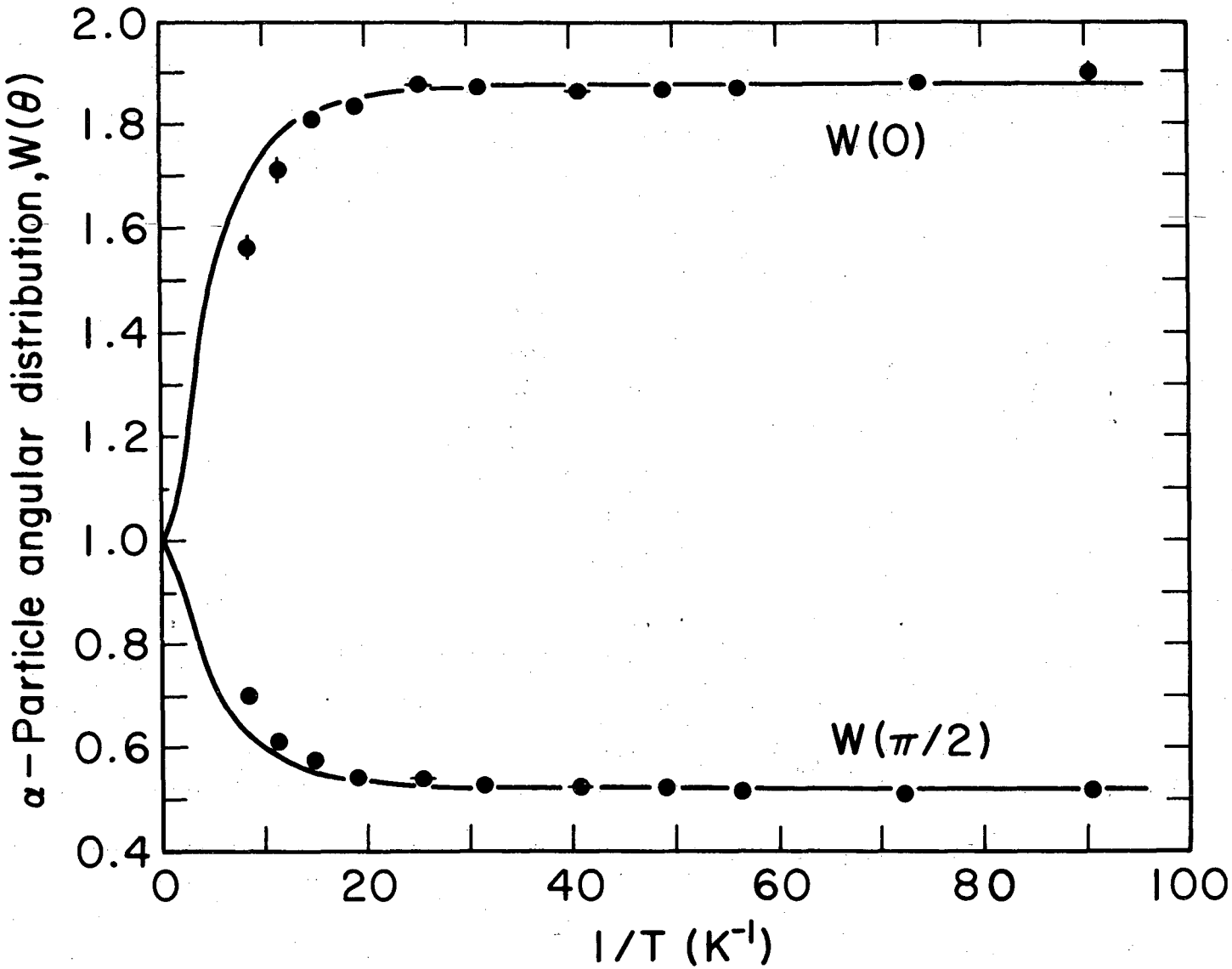

FIG. 6. Experimental α particle angular distribution of ^{253}Es in NES as a function of the inverse temperature. The curves shown are fits to the data with A = 0.26 cm^{-1}. The deviation of the curves from the points at high temperatures is a result of sample self-heating.

XBL 746-3515

VIII. DISCUSSION OF ^{253}Es IN NES ALPHA PARTICLE ANGULAR DISTRIBUTION

VIII.A. CRYSTAL FIELD PARAMETERS

Baker and Bleaney[74] observed the paramagnetic resonance spectrum of Ho^{3+}, the $4f^{10}$ analogue of Es^{3+}, as a 1% impurity in a crystal of yttrium ethylsulfate. The ground CF state is a non-Kramers doublet characterized by $J_z = \pm 7$ with small admixtures of $J_z = \pm 1$ and ∓ 5. A singlet characterized by $J_z = +6, 0$, and -6 lies nearby in energy. The hf interaction constants for ^{165}Ho are $A = 0.334(1)\ cm^{-1}$, $B = 0.02\ cm^{-1}$, $P \approx 10^{-3}\ cm^{-1}$. The dominant term in the CF Hamiltonian is AI_zS_z, which results in alignment along the crystalline c-axis with the nuclear magnetic substate $I_z = \pm I$ lying lowest in energy.

The temperature dependence of W(0) and $W(\pi/2)$ for ^{253}Es indicates that the AI_zS_z term is also dominant in the hfs of the lowest electronic CF state of Es^{3+} in the ethylsulfate lattice. It should therefore be possible to derive a value for the nuclear magnetic moment, μ, of ^{253}Es. To do so, a description of the CF electronic ground state and a value for $\langle r^{-3}\rangle_{5f}$ are required in addition to the value for the magnetic hyperfine interaction constant, A.

Navarro, Rasmussen and Shirley[7] used extrapolated values for the Es^{3+} in NES CF parameters. However, their extrapolation was based on Gruber's CF parameters for $LaCl_3:Am^{3+}$.[75] As pointed out by Conway,[76] Gruber misinterpreted his data, and therefore his CF parameters may be in error. Krupke and Gruber[77] determined that B_0^2 is negative for $LaBr_3:Np^{3+}$. Bishton et al.[78] interpreted this as being a result of a large ligand-n=5 shell overlap exchange charge. However, Carnall[79] has observed

that a more careful analysis of the spectrum and a more detailed theoretical analysis may yield a positive B_0^2. The CF parameters for NES:Es^{3+} were estimated in two different ways. In the first method, we assumed that the A_k^q parameters are the same for analogous lanthanides and actinides and that the only difference is contained in the radial integrals. Using Hüfner's CF parameters for Ho^{3+} in holmium ethylsulfate[80] and ratios of radial integrals obtained from Hartree nonrelativistic wave functions without exchange,[81] the Es^{3+} CF parameters (in cm^{-1}) are $B_0^2 = 430$, $B_0^4 = -1380$, $B_0^6 = -1120$ and $B_6^6 = 960$. For Ho^{3+} in both holmium ethylsulfate[80] and $LaCl_3$ (Ref. 82) the first excited state J = 7 is admixed into the ground state J = 8 by the CF interaction. For the J = 7 excited state we used a truncated wave function given by $0.4279|^5 I_{20}) - 0.3363|^3 K_{21}) + 0.5848|^3 K_{20}) + 0.3750|^3 L_{21})$. For the J = 8 ground state we truncated the wave function given previously and considered only the quintet and the triplet states. Evaluation of $\mathcal{H}_{CF}$ for Es^{3+} with the inclusion of both the J=8 and J=7 wave functions gave a singlet as the ground state. Because alignment would not occur if a singlet were lowest, B_0^2 was increased in magnitude in order to bring a doublet lowest in energy. Using $B_0^2 = 550\ cm^{-1}$, the ground CF state is $0.939|\pm 7\rangle + 0.305|\pm 1\rangle + 0.153|\mp 5\rangle$.

A second estimate of the NES:Es^{3+} CF parameters was obtained from the values of HoES:Ho^{3+} (Ref. 80), $LaBr_3$:Np^{3+} (Ref. 77) and interpolated values for $LaCl_3$:Pm^{3+}. The CF parameters for Np^{3+} in the isoelectronic lattices $LaBr_3$ and $LaCl_3$ should be approximately the same.[83] In $LaCl_3$ a slightly smaller B_6^6/B_0^6 ratio is expected, with both B_6^6 and B_0^6 being larger than in $LaBr_3$. B_0^4 should be slightly smaller in $LaCl_3$ than in $LaBr_3$.[84] The NES:Es^{3+}

CF parameters resulting from this analysis are $B_0^4 = -1440\ cm^{-1}$, $B_0^6 = -760\ cm^{-1}$ and $B_6^6 = 650\ cm^{-1}$. Again it was necessary to vary B_0^2 in order to get a doublet lowest. Using $B_0^2 = 600\ cm^{-1}$, the ground CF state is $0.967\,|\pm 7\rangle + 0.225\,|\pm 1\rangle + 0.120\,|\mp 5\rangle$.

Since this work was published the CF parameters for $LaCl_3:Pm^{3+}$ were determined by Baer, Conway and Davis;[85] however I have not attempted a re-analysis of the resulting NES:Es^{3+} CF parameters with their CF parameters.

VIIIB. NUCLEAR MAGNETIC DIPOLE MOMENT

The difficulties in extracting $\langle r^{-3} \rangle$ from experimental data have been discussed by several authors.[86-91] Because of the lack of experimental data for Es^{3+}, I take a value of $\langle r^{-3} \rangle_{5f} = 10.92$ au which was obtained using relativistic self-consistent Dirac-Fock wave functions.[92] The nuclear magnetic moment was calculated using Eq. 22a which can be written as

$$\mu = \frac{AI}{4\mu_B \mu_N \langle r^{-3} \rangle_{5f} \langle + | J_z | + \rangle} \frac{\langle f^N S\ L\ J \| \ J \ \| f^N S'\ L'\ J \rangle}{\langle f^N S\ L\ J \| \Sigma N_i \| f^N S'\ L'\ J \rangle} . \tag{30}$$

The two values for $|\mu|$ resulting from the two sets of CF parameters are 2.79(32) μ_N and 2.63(30)μ_N. The errors quoted in parenthesis reflect the statistical uncertainty in the value of A only. These values are substantially lower than the value of 4.9 μ_N previously reported[8] because of a change in the electronic ground CF state obtained with a different choice of CF parameters.

The major source of error in my value for the nuclear magnetic dipole moment is the uncertainty of the ground crystal-field state. Both of the predicted ground states have a large $|J_z = \pm 7 \rangle$ component which gives a small derived value for μ. No reasonable choice of CF parameters gave a coefficient for $|\pm 7 \rangle$ of approximately 0.7 which would yield a moment of $\approx 4.0\ \mu_N$. Therefore, I report a nuclear magnetic moment $|\mu| = 2.7(13)\ \mu_N$. The error reflects the statistical accuracy of the measured value of A and the uncertainties in both the CF parameters and the radial integral $\langle r^{-3} \rangle_{5f}$.

Other measurements of the ^{253}Es magnetic dipole moment have been reported. Using the atomic beam nuclear magnetic resonance method, Goodman, Diamond and Stanton[45] obtained $\mu = 4.10(7)\ \mu_N$. Worden et al.[93] measured the emission spectrum of divalent ^{253}Es($5f^{11}7s$) and determined both a_{7s} and a_{5f}. Application of the Goudsmit-Fermi-Segrè formula, which requires large relativistic and nuclear volume corrections, to the value of a_{7s} yielded $\mu = +5.1(13)\mu_N$. However a_{5f} yielded the more accurate value $\mu = +3.6(4)\mu_N$ which, considering the possible error in the value they used for $\langle r^{-3}\rangle_{5f}$, is in excellent agreement with the atomic-beam value. From an analysis of the electron paramagnetic resonance spectrum of divalent ^{253}Es is CaF_2 Edelstein[94] obtained $|\mu| = 3.62(50)\mu_N$.

In summary the atomic beam measured moment, which should be the most accurate value, is larger than that obtained by the other methods. The present NO value is the smallest experimental value, but it should be remembered that Navarro, Rasmussen and Shirley[8] derived $|\mu| = 4.9\mu_N$ from earlier NO data. This situation emphasizes the need for a better understanding of crystal field effects for the actinides.

Lamm[95] calculated the ^{253}Es nuclear magnetic dipole moment using wave functions obtained by diagonalizing a Nilsson Hamiltonian including a pairing force. Using $g_R = 0.40$, $g_\ell = 1.0$ and $g_s^{eff} = g_s^{free}$, she obtained $\mu = +4.239\ \mu_N$. As a result of core polarization g_s is renormalized to a value of approximately $0.6g_s^{free}$. Using this value for g_s^{eff}, Lamm obtained $\mu = +3.650\mu_N$.

In addition to renormalizing g_s, the M1 core polarization, the two-body $\vec{L}$-$\vec{S}$ force, and the mesonic effect result in a renormalization

of g_ℓ. For the deformed nuclei ($150 \leq A \leq 190$) Nagamiya and Yamazaki[96] suggested that $g_\ell = 1.09(3)$ and $g_s^{eff} = 3.7(3) \approx 0.665\, g_s^{free}$. Kalish et al.[97] found $g_R = 0.35(4)$ for shape isomers of ^{237}Pu. The rotational gyromagnetic ratio, g_R, is reduced from its fluid model value of Z/A (= 0.4 for ^{253}Es) as a result of the inability of the protons to follow the rotational motion. Using these renormalized g values, Lamm's calculation gives $\mu = +3.92\,\mu_N$. A g_R value of 0.40 gives $\mu = +3.97\,\mu_N$. A g_s^{eff} larger than 3.7 would also increase the theoretical value for the nuclear magnetic dipole moment and thereby bring it into agreement with the atomic beam value.

Although to my knowledge there have been no other detailed calculations of actinide nuclear magnetic moments, there have been a number of studies of nuclei having single particle states derived from the $i_{13/2}$ neutron shell model orbital. The 7/2+[633] ground state of ^{253}Es is derived from the $i_{13/2}$ proton orbital. I have not made an extensive study of even-odd nuclei with the odd neutron in an $i_{13/2}$ orbital, but the comments below may indicate the direction of future actinide magnetic moment calculations.

In the adiabatic approximation the nuclear magnetic dipole moment is given by[98]

$$\mu(I) = \frac{K^2}{I+1}\,(g_K - g_R) + g_R I \tag{31a}$$

with

$$K g_K = K g_\ell + (g_s - g_\ell)\,\langle K|s_z|K\rangle\,. \tag{31b}$$

The reduced M1 transition probability is given by

$$B(M1, I+1 \rightarrow I) = \frac{3}{4\pi}\,\mu_N^2 \langle I1K0|I{+}1\ K\rangle^2\, K^2\,(g_K - g_R)^2, \tag{32}$$

and therefore both the reduced transition probability and the nuclear magnetic moment depend on g_s, g_ℓ and g_R. Bohr and Mottelson[99] give an explicit equation relating the nuclear magnetic dipole moment and the reduced matrix element of the magnetic moment operator. Therefore both the experimental nuclear magnetic moments and the M1 transition probabilities (which are usually expressed in terms of E2-M1 mixing amplitudes) can serve as checks on calculated g values.

Extensive investigations of high-spin members of rotational bands populated by (α,xn) reactions have been made. Lindblad, Ryde and Barneoud[100] studied the positive parity bands in ^{171}Yb, including the rotational band built on the $\frac{7}{2}$+[633] intrinsic state. Because states with spin up to $\frac{27}{2}$+ are populated by the (α,xn) reaction, it was possible to determine accurately the rotational parameters and the decoupling terms in the expansion of the rotational energy formula in powers of I(I+1). Theoretical calculations within the framework of the non-adiabatic unified model with pairing and Coriolis interactions included can successfully reproduce the irregular spacing in these strongly Coriolis coupled rotational bands provided the strength of the Coriolis interaction is reduced. Unfortunately the choice of the attenuation factor is ambiguous because of the large number of free parameters involved in the fit.

Lindblad and co-workers found that in order to reproduce both the magnetic moments and the reduced M1 transition probabilities in ^{171}Yb it was necessary to reduce the intra-band M1 transition probabilities with $|\Delta K| = 1$ in addition to reducing the Coriolis matrix elements. Once this correction was made, the best fit to the data was

obtained with $g_s = 0.6g_s^{free}$. Hjorth, Johnson and Ehrling[101] studied the rotational-particle coupling in the $\frac{7}{2}$+[633] band in ^{167}Er and also found that the intra-band M1 transition probabilities with $|\Delta K| = 1$ had to be reduced.

Pyatov and co-workers[102-104] have discussed the nonadiabatic corrections to rotational band levels resulting from diagonalizing the Coriolis interaction in the space of several single particle states. The renormalization of matrix elements described in the paragraph above are the result of polarization effects that arise when the residual interactions are accounted for. These methods treat the recoil interaction as a one-body term whereas Pyatov and co-workers treat it as a two-body residual interaction of an outer particle with the nucleons of the core; that is, they consider the coupling of the odd nucleon to both the rotation and the intrinsic excitations of the core. The renormalization of the Coriolis coupling matrix elements, corresponding to a reduction of approximately 30%, then results from the coupling of the odd nucleon to the 1+ excitations of the core and not because of any coupling to the rotational motion of the core. They derive a consistent microscopic formalism for this renormalization. An advantage of the method is the relatively small number of parameters required to fit energy levels, nuclear magnetic dipole moments, and M1 transition probabilities.

Some of the more interesting results of Pyatov's calculations are cited below. The scattering of the odd particle by the 1^+ excitations of the core leads to a renormalization of the spin gyromagnetic ratio, g_s. As a rule g_s^{eff} is not constant within a rotational band; strong oscillatory behavior as a function of spin was found for ^{155}Gd. Therefore

the use of $g_s^{eff} \approx 0.6\ g_s^{free}$ is questionable at least in the calculation of reduced M1 transition probabilities. Pyatov was able to use the g_s values for the free nucleons in his calculations because he explicitly calculated the effects of spin polarization on g_s.

Pyatov and co-workers leave g_R^0 as the only free parameter in the calculation of μ. g_R^0 is roughly related to the effective gyromagnetic ratio by

$$g_R^{eff}(N) < g_R^0 < g_R^{eff}(Z)$$

and has a value of approximately 0.3. g_R^{eff} is also not a constant within a rotational band being smaller by perhaps 50% than g_R^0 for the low spin states and asymptotically approaching g_R^0 as the spin increases.

An excellent review of the current status of nuclear moment measurements and calculations can be found in the 1972 Conference on Nuclear Moments and Nuclear Structure.[105] Unfortunately no reference to Pyatov's work is given in the published Proceedings.

VIII.C. ^{253}Es ALPHA PARTICLE PARTIAL WAVE AMPLITUDES AND PHASES

The partial wave phases are readily determined from the angular distribution. The fact that W(0) increases with decreasing temperature, as shown in Fig. 6, (i.e., enhanced α particle emission occurs along the crystalline c-axis) implies that the relative s-d phase is positive. Because the nuclear alignment is along this axis, the preferential emission is along the nuclear poles thereby confirming the prediction of Hill and Wheeler.[2]

Although the value of the orientation parameter B_6 is not negligible with respect to B_2 and B_4 (see Section VII for the saturation values), the product A_6B_6 is negligible with respect to A_2B_2 and A_4B_4 because $A_6 \approx -0.0025$ for reasonable partial wave amplitudes and phases. Therefore the $P_6(\cos\theta)$ term can be excluded from the analysis. The 0.4% of the α decays that were not included in the calculation of $W(\theta)$ were assumed to give the same angular distribution as the decays that were included.

The relative s-g wave phase can be determined also. If the solid angle correction factors are unity (point source and point detector), the quantity $3 - W(0) - 2W(\pi/2) = -\frac{7}{4} A_4B_4$; however, because they are not, a small component proportional to $P_2(\cos\theta)$ enters. This quantity is tabulated in Table VIIA and is plotted in Fig. 7. Because B_4 is positive, A_4 must be negative. This implies that the s and g partial waves are out of phase.

Next I discuss the partial wave amplitudes and the resulting values of A_2, A_4 and the saturation values of W(0) and $W(\pi/2)$.

For convenience these values are tabulated in Table VIIID. The partial wave intensities given by the BFM theory, the shell model theory, and numerical integration of coupled differential equations are given in Tables VIIIA, VIIIB and VIIIC respectively. The experimental intensities in these latter tables are from Ahmad.[38] In Tables VIIIA and VIIIC the $\ell = 6$ wave contribution has been subtracted by the method described in Section IV.C.4. In all three cases the total theoretical intensity is normalized to equal the total experimental intensity. A partial α decay scheme for ^{253}Es is shown in Fig. 8.

First I examine the intensity predictions. The intensities to the 9/2+ and 15/2+ states are underestimated but the intensity to the 11/2+ state is overestimated by all three theoretical methods. In order to determine if this situation is unique to ^{253}Es decays, I made a study of hindrance factors (HFs) throughout the actinides for favored α decay to states with $I_f = K + 1$ and $I_f = K + 2$ (Cf. Section IV.C). Defining the HF as P_0/P, from Eq. 8 I obtain

$$HF = P_0/P = \frac{1}{N} \sum_{\ell} HF_{\ell} / \langle I_i \ell K0 | I_f K \rangle \tag{33a}$$

and

$$\frac{HF(K+1)}{HF(K+2)} = \frac{\sum_{\ell} \langle I_i \ell K0 | K{+}2\ K \rangle^2 / HF_{\ell}}{\sum_{\ell} \langle I_i \ell K0 | K{+}1\ K \rangle^2 / HF_{\ell}} \ . \tag{33b}$$

If the alpha groups are pure d waves, the summations on the R.H.S. of Eq. 33b reduce to a single term, and the HF ratios reduce to Clebsch-Gordan coefficient ratios. In Fig. 2 the experimental ratios taken form the compilation of Ellis and Schmorak[50] are plotted. The dashed lines indicate the Clebasch-Gordan ratios. Except for ^{245}Cm,

all points are above the dashed lines. Furthermore, the inclusion of $\ell = 4$ admixtures would only increase the discrepancies. This systematic deviation seems to indicate that the d wave branching should be skewed toward the lower energy levels in the rotational band.

From Table VIIID it is seen that the magnitudes of A_2 and A_4 are larger experimentally than they are theoretically. The small theoretical A_2 values suggest that the total d wave intensity, but especially that to the band head, should be increased to approximately 0.15. The BFM value for W(0) agrees well with experiment. The BFM value for $W(\pi/2)$ would be much better if the g wave intensity to the band head were increased from 0.127 to 0.15.

The relative s, d and g wave intensities that fit the NO data best are compared with the theoretical intensities in Table VIIIE. This Table supports the statements made above concerning the total $\ell = 2$ and $\ell = 4$ wave intensities.

Table VIIIA. Intensities for partial waves in favored α decay of ^{253}Es to the ground-state band in ^{249}Bk (Bohr, Fröman, and Mottelson theory [9, 10]).

E_f (keV)	$I_f{}^{\pi}$	s	d	g	Σ(%)	Experimental intensity minus i wave component* (%)
0	$\frac{7}{2}+$	79.6	10.0	0.127	89.7	90.0
41.7	$\frac{9}{2}+$		5.92	0.328	6.24	6.6
93.8	$\frac{11}{2}+$		0.88	0.268	1.15	0.846
155.8	$\frac{13}{2}+$			0.083	0.083	0.081
229.3	$\frac{15}{2}+$			0.0083	0.0083	0.011

*Cf. Section IV. C. 4.

Table VIIIB. Intensities and phases for partial waves in favored α decay of ^{253}Es to the ground-state band in ^{249}Bk (Mang shell-model theory as used by Poggenburg[11]).

I_f^{π}	s	d	g	i	$\Sigma(\%)$	Experimental intensity[38] (%)
$\frac{7}{2}+$	82.28	-8.81	0.078	0.0002	91.11	90.0(5)
$\frac{9}{2}+$		-5.184	0.194	0.001	5.382	6.6(2)
$\frac{11}{2}+$		-0.770	0.156	0.004	0.930	0.85(3)
$\frac{13}{2}+$			0.049	0.004	0.053	0.085(3)
$\frac{15}{2}+$			0.0049	0.0017	0.0066	0.013(1)

Table VIIIC. Intensities and phases for partial waves in favored α decay of ^{253}Es to the ground state band in ^{249}Bk (Numerical integration, this work. $m_\ell = 0$; $a_0 = 1$, $a_2 = 0.8580$, $a_4 = -0.0977$).

I_f^π	s	d	g	Σ(%)	Experimental intensity minus i wave component* (%)
$\frac{7}{2}+$	-81.798	-8.903	0.136	90.837	90.0
$\frac{9}{2}+$		-5.218	0.338	5.556	6.6
$\frac{11}{2}+$		-0.779	0.272	1.051	0.846
$\frac{13}{2}+$			0.085	0.085	0.081
$\frac{15}{2}+$			0.0085	0.0085	0.0110

*Cf. Section IV. C. 4.

Table VIIID. Coefficients A_2 and A_4 for the ^{253}Es in NES angular distribution function and $W(0)$ and $W(\pi/2)$ at saturation with solid angle correction factors included.

	A_2	A_4	$W(0, {}^1/T \to \infty)$	$W(\pi/2, {}^1/T \to \infty)$
Experiment	0.630(5)	-0.059(7)	1.878(7)	0.518(4)
Bohr, Fröman, and Mottelson procedure (Cf. Table VIIIA for intensities)	0.618	-0.019	1.881	0.540
Mang shell model theory as applied by Poggenburg.[11] (Cf. Table VIIIB for intensities)	0.585	-0.013	1.837	0.566
Numerical integration, this work. (Cf. Table VIIIC for intensities)	0.566	-0.035	1.795	0.575

Table VIIIE. Relative α partial wave intensities for the decay of ^{253}Es.

	NO experiment	BFM theory (Table VIIIA)	Poggenburg calculation (Table VIIIB)	Numerical integration (Table VIIIC)
s wave	1.000	1.000	1.000	1.000
d wave	0.216	0.211	0.179	0.182
g wave	0.0078	0.010	0.0052	0.0103

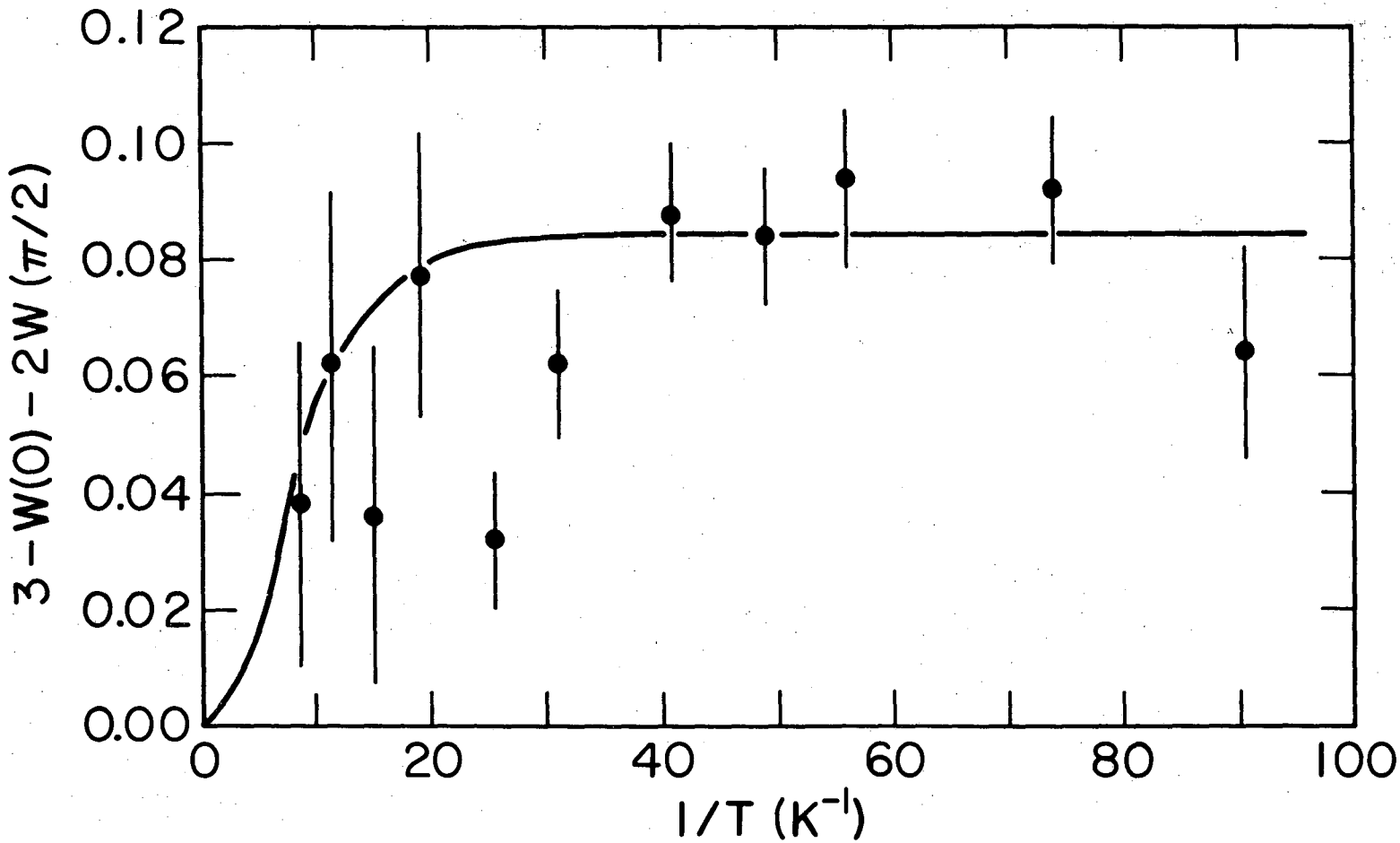

XBL 746-3516

FIG. 7. Temperature dependence of the (negative) coefficient of the $P_4(\cos\theta)$ term in the ^{253}Es α particle angular distribution function. The curve shown is an approximate fit to the data.

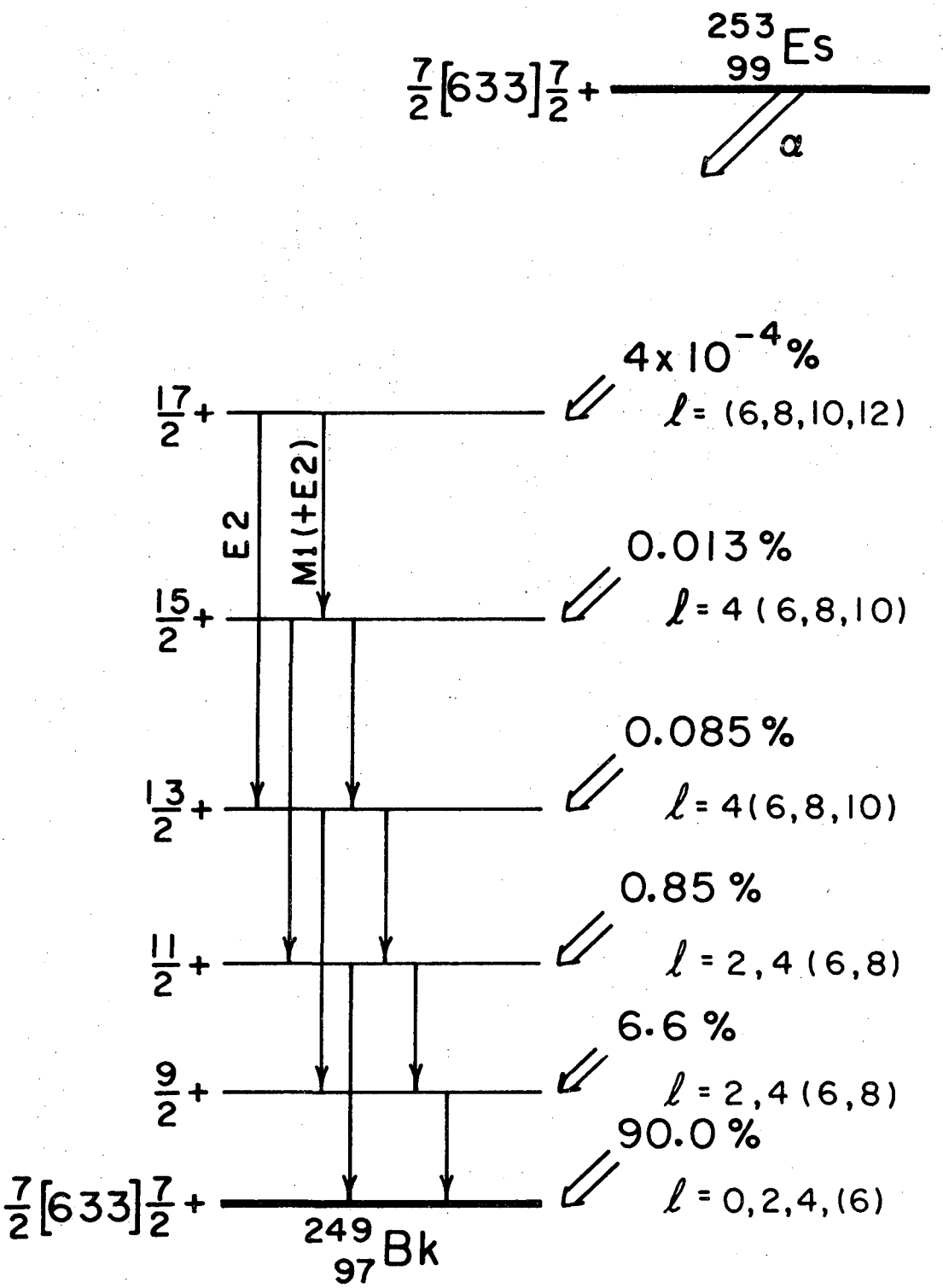

FIG. 8. Partial α decay scheme for ^{253}Es adapted from references 36 and 38. The intensities to each daughter level and the permitted α particle angular momentum values are shown.

IX. ^{241}Am NUCLEAR ORIENTATION RESULTS AND DISCUSSION

The experimental ^{241}Am in NES α particle angular distribution measured at 0° and 90° with respect to the NES c-axis as a function of the inverse temperature is shown in Fig. 9, and the results are tabulated in Table IXA. The numbers shown in parentheses for $W(\theta)$ are the standard deviations based on counting statistics. The inverse temperatures have a possible error of up to 6% in addition to the values shown in parentheses. The linear temperature dependence of $W(\theta)$ at higher NO temperatures is characteristics of electric quadrupole alignment. If the $P_4(\cos\theta)$ term in Eq. 1 is small, the angular distribution function reduces to

$$W(\theta) = 1 + A_2\,(\ell\ell' I_f I_i) Q_2 B_2(I_i, T)\,(3\cos^2\theta - 1)/2, \qquad (34)$$

and $B_2(I_i, T) \propto 1/T$ for low degrees of quadrupole alignment. For the series of adiabatic demagnetizations reported here $Q_2(0) = 0.930$, $Q_4(0) = 0.787$, $Q_2(\pi/2) = 0.955$, and $Q_4(\pi/2) = 0.855$.

IXA. QUADRUPOLE COUPLING CONSTANT

Am^{3+} has a $5f^6$ electronic configuration outside the radon core. The Hund's rule ground state is $^7F_0$, as in $Eu^{3+}(4f^6)$. Since the ground state is a singlet, there is no magnetic hyperfine interaction.

In order to determine accurately the value of the quadrupole coupling constant, P, it is necessary that the temperature be low enough such the $P \approx kT$, where k is Boltzmann's constant. Then curvature develops in the $W(\theta)$ vs. $1/T$ curve. Since sufficiently low temperatures were not possible using NES as a host, my value for P of -0.0033 (6) cm^{-1} (P/k = - 0.0048 (8)K) lacks precision. The negative sign implies that the nuclear magnetic substates $I_z = \pm 5/2$ lies lowest in energy.

In the analysis of the nuclear orientation of ^{152}Eu in NES,[13] $P_{4f}^{(2)}$ could be calculated with reasonable accuracy because the value of the CF parameter $B_0^2 = 2A_2^0(1-\sigma_2)\langle r^2\rangle_{4f}$ had been experimentally determined. A value for the lattice shielding factor, σ_2, was then calculated. Although B_0^2 for Am^{3+} has not been determined, I can make a reasonable estimate and then proceed with the analysis. I write

$$P_{expt} = P_{lat} + P_{5f}^{(2)}. \tag{35a}$$

Then from Eqs. 29d and 27,

$$P_{expt} = -\frac{3QB_0^2}{2I(2I-1)}\left[\frac{1-\gamma_\infty}{\langle r^2\rangle_{5f}(1-\sigma_2)} - \frac{2e^2\langle r^{-3}\rangle_{5f}(1-R_Q)\,|\langle 20\|\alpha\|00\rangle|^2}{E(^7F_{20}-{}^7F_{00})}\right]. \tag{35b}$$

Every term on the right hand side of Eq. 35b either is known or can be estimated with reasonable accuracy except for B_0^2, σ_2, and R_Q. I discuss R_Q first and then return to the CF terms.

The atomic Sternheimer factor R_Q accounts for the shielding of the f-electron generated field gradient by the closed electron shells as measured at the nuclear site. For the lanthanides R_Q is of the order of 0.08 - 0.13 (Ref. 15) and therefore shielding. However Sen[15] calculated a value of $R_Q = -0.087$ for Am^{3+} as a free ion. This is in contrast to the experimental value of $R_Q = 0.35(10)$ for Np^{6+} found by Dunlap, Kalvius and Shenoy.[106] R_Q is not expected to be strongly dependent on either Z or the ionic charge within a period; however, ion-ligand overlap is important for the spatially extended 5f electrons. Therefore the disagreement between the experimental and theoretical values is not surprising. I accept the value of $R_Q = 0.35$ as being valid for Am^{3+}. I will show below that the second expression in brackets in Eq. 35b is smaller than the first; therefore my conclusions are not strongly affected by this choice.

There have been two determinations of B_0^2 for trivalent actinides at trigonal sites. For $LaCl_3:Am^{3+}$ Gruber[75] obtained $B_0^2 = 412\ cm^{-1}$. However, the J-levels in the optical spectra were not properly assigned,[76] and therefore this value may be in error. For $LaBr_3:Np^{3+}$ Krupke and Gruber[77] obtained $B_0^2 = -22.8\ cm^{-1}$ which indicates a value for σ_2 greater than one since A_2^0 should be positive for the actinides. This agrees with both the large values of σ_2 reported for the light rare earths by Blok and Shirley[107] and the calculations of Gupta and Sen.[15] Sengupta and Artman[108] calculated $\sigma_2 = 0.881$ for Np^{3+} whereas Sen[15] calculated $\sigma_2 = 1.091$ for Am^{3+}. Therefore the theoretical calculations do not firmly establish the sign of $(1-\sigma_2)$ and hence the sign of B_0^2 for Am^{3+}. Carnall[79] has suggested that the negative B_0^2 for $LaBr_3:Np^{3+}$

may be the result of using a model that is not sufficiently refined and that σ_2 is probably less than one for both Np^{3+} and Am^{3+}. Preliminary analyses of the optical spectra of Nd^{3+} and U^{3+} yielded $B_0^2(U^{3+}) \approx 4\ B_0^2(Nd^{3+})$.[109] If, as a working estimate, I take $B_0^2(Am^{3+}) = 4B_0^2(Eu^{3+})$, then $B_0^2(Am^{3+}) = 640\ cm^{-1}$ using $B_0^2(Eu^{3+}) = 160\ cm^{-1}$ (Ref. 110).

I can now calculate $1 - \sigma_2$ using Eq. 35b. The ^{241}Am quadrupole moment is 4.9 b. (Ref. 111). The Sternheimer factor $1 - \gamma_\infty$ is calculated to be 112.92,[15] a value which should be accurate to 10%. The radial integrals for free ions were obtained from relativistic self-consistent Dirac-Slater wave functions as given by Lewis et al.;[92] namely, $\langle r^2 \rangle_{5f} = 5.388 \times 10^{-17}\ cm^2$ and $\langle r^{-3} \rangle_{5f} = 5.300 \times 10^{25}\ cm^{-3}$. For a pure $^7F_0$ electronic state the reduced matrix element $\langle 20 \| \alpha \| 00 \rangle = 2/(5\sqrt{3}) = 0.23094$(Ref. 68) whereas for the intermediate coupled state obtained by diagonalizing the combined electrostatic and spin-orbit interaction matrices $\langle 20 \| \alpha \| 00 \rangle = 0.18857$(Ref. 112). For $LaCl_3{:}Am^{3+}$ the $^7F_2$ state lies 5328 cm^{-1} above the $^7F_0$ ground state,[76] and a comparable splitting should occur in an ethylsulfate lattice. When these values are substituted into Eq. 35b I obtain $-0.0032\ cm^{-1} = -\ 0.000985\ cm^{-1}\ (1 - \sigma_2) + 0.000251\ cm^{-1}$ so that $1 - \sigma_2 = 0.285$ or $\sigma_2 = 0.715$. This value may be in error by as much as 50%, but it agrees very well with the value $\sigma_2 = 0.73$ for the lanthanide analogue, Eu^{3+} (Ref. 107). Although this interpretation is not unique, it gives reasonable values for the parameters B_0^2, σ_2, and γ_∞. In particular, it seems clear that $(1 - \gamma_\infty)$ must have a value of $\approx 10^2$. A re-analysis of the $LaCl_3{:}Am^{3+}$ optical data would be especially helpful in establishing both B_0^2 and σ_2.

IX.B. ALPHA PARTICLE PARTIAL WAVE AMPLITUDES AND PHASES

I next discuss the effect of the ^{241}Am α particle partial wave amplitudes and phases on the angular distribution.

The phase shifts in Eq. 5 are the sum of the intrinsic phases on the nuclear surface, which were assumed to be either 0 or π, plus the phase shifts that occur upon transmission through the combined Coulomb and quadrupole barriers. The intrinsic phases are taken from the microscopic shell model theory;[11,12] namely, the s, d, and g waves are all in phase but the i wave is out of phase. The formula for the Coulomb barrier phase shift difference for α decay was given in Eq. 16a. For ^{241}Am the d wave lags the s wave by approximately 7° and the g wave lags the s wave by approximately 23.5°. The quadrupole phase shifts can be obtained only by numerical integration of the coupled differential equations that result from the consideration of the exchange of energy and angular momentum between the outgoing α particle and the daughter nucleus. Since these calculations have not been performed for ^{241}Am, the quadrupole phase shifts were taken to be zero. The quadrupole part of the barrier has the effect of retarding higher ℓ-waves with respect to the lower ℓ-waves if the waves are in phase at the nuclear surface. Therefore the quadrupole phase shifts for ^{241}Am would be additive to the Coulomb phase shifts except for the i wave which was not included in the analysis of the angular distribution because it is too weak to influence the results.

In order to compare theory with experiment I re-write Eq. 4 as

$$W(\theta)_{expt} = 1 + R\,[Q_2A_2B_2P_2(\cos\theta) + Q_4A_4B_4P_4(\cos\theta)]. \qquad (36)$$

Higher order Legendre polynomials are excluded for the decay of a spin 5/2 state. The factor R is an anisotropy reduction factor accounting for the fact that not all ^{241}Am nuclei are at rare-earth sites in the NES lattice. For the results reported here R is between 0.54 and 0.83. The solid curve in Fig. 9 was obtained using $P = -0.0033\ cm^{-1}$, $RA_2 = 0.54$ and $RA_4 = 0.05$. The shape of the experimental angular distribution curves rather than the absolute values are of importance for the determination of hyperfine interaction parameters. The competing requirements for a good nuclear orientation source were discussed in Section VII. There are always radioactive nuclei that either are not at lattice sites or are so deeply imbedded in the crystal that the outgoing alpha particles are excessively scattered. These events contribute an isotropic background with the result that the full theoretical angular distribution is usually not achieved.

I next present three different estimates for the partial wave amplitudes. The resulting A_2 and A_4 coefficients are tabulated in Table IXB. The fact that $W(0) > 1$ means that the s and d waves are in phase for ^{241}Am, in confirmation of the shell model calculations. The experimental results do not establish the relative s-g wave phase (predicted to be positive), primarily because of the weakness of the g wave. Therefore in Table IXB I include the A_2 and A_4 values for both relative g wave phases.

In the theory of Bohr, Fröman, and Mottelson (BFM)[9,10] as it is usually applied the branching of an ℓ-wave is given by the product of (the square of a Clebsch-Gordan coefficient) times (a calculated

spherical barrier penetrability for the alpha group) times (the reciprocal of the hindrance factor averaged from neighboring even-even nuclei). The intensities resulting from the application of this method to ^{241}Am are given in Table IXC. A partial decay scheme for ^{241}Am is given in Fig. 10. The experimental intensities were taken from Nuclear Data,[113] and the band assignments were taken from Lederer et al.[114]

Numerical integration of the coupled differential equations for ^{233}U α decay performed by Chasman and Rasmussen (CR)[6] suggested that the relative intensity for the d wave to the ground state of the daughter would be increased by 40% over the BFM predicted value. Although the application of this correction for other nuclei was never suggested by these authors, it has been used successfully in the analysis of the ^{243}Am α-γ angular correlation as will be mentioned later. This CR correction substantially alters A_2 as can be seen from Table IXB.

In the Mang shell model theory as applied by Poggenburg et al.[12] the anisotropic barrier penetration was calculated using Fröman's method,[34] and assuming a realistic sloping inner barrier. The analysis of the ^{253}Es in NES α particle angular distribution[39] revealed that the BFM intensities more closely fitted the NO data than did the Poggenburg intensities; however the BFM calculations had the advantage of the use of experimental ℓ-wave hindrance factors averaged from neighboring even-even nuclei. In contrast all of Poggenburg's transition probabilities were normalized with respect to ^{238}Pu and are thereby more model dependent. The shell model predicted intensities are given in Table IXD. The $\ell = 6$ wave is included to illustrate its predicted weakness which justifies its exclusion from the analysis.

Let us now try to choose the best A_2-A_4 pair given in Table IXB. The A_k coefficients obtained from the BFM theory and the shell model theory are very similar, and a choice of one over the other will be difficult. As expected the relative s-g wave phase influences A_4 primarily. Because the d wave intensity is fifty times greater than the g wave intensity, the a_2a_2 direct term in A_4 is five times larger than the a_0a_4 interference term. In most other cases the interference term dominates and hence the relative s-g wave phase determines the sign of A_4. For ^{241}Am A_4 is positive for either relative phase and therefore the magnitude of A_4 must be determined accurately in order to extract the phase. In order to decide whether this is feasible, let us consider the ratio A_4B_4/A_2B_2. From Table IXB, A_2 is between 8 and 18 times larger than A_4. Over the temperature range of our experiments $B_4/B_2 \approx 0.03$ at $1/T = 10\ K^{-1}$ and $B_4/B_2 \approx 0.22$ at $1/T = 90\ K^{-1}$. Therefore A_4B_4/A_2B_2 will never be larger than 0.025. I performed a least squares fit to my data with A_2 and A_4 as free parameters but could not get a satisfactory fit. I then tried an iterative procedure of fixing A_2 and leaving A_4 free, followed by fixing the resulting A_4 with A_2 free. Again the accuracy with which A_2 and A_4 were determined was not satisfactory. The basic problem is the small size of the quadrupole coupling constant and the resulting limited curvature that develops in the anisotropy curves at the lowest temperature. Although the present NO results do not provide a basis for choosing between the A_2-A_4 pairs in Table IXB, I note that the Chasman and Rasmussen correction to the d wave branching to ground was required to explain

both the ^{253}Es NO and the ^{243}Am unattenuated angular correlation[51] results. The angular correlation (AC) results are more germane to the present discussion. Although there are only limited results for ^{241}Am, extensive published results exist for ^{243}Am which has the same Nilsson ground state as ^{241}Am; namely, $K\pi[Nn_z\Lambda] = 5/2^-[523]$, and a similar rotational band structure.

Following α decay, time-dependent hf fields develop because of the excitation of the electronic shells caused by both the change in nuclear charge and the approximately 100 keV of recoil energy given the daughter nucleus. These "after effects" have been considered by Thun[115] and by Mang.[116] An objective of α-γ AC experiments is to obtain an unattenuated correlation by eliminating the extranuclear fields during the intermediate state lifetime. The AC function is commonly written as

$$W(\theta) = \sum_k G_k(t) A'_k P_k(\cos\theta) \tag{37}$$

where $G_k(t)$ is a time-dependent attenuation coefficient. As before the A'_k depend on the spins and multipolarities involved in the decays.

For the attenuated (5.486 MeV α - 59.54 keV γ) correlation from ^{241}Am, Krohn et al.[117] determined the upper limit of A'_2 to be -0.36(2). The negative sign in itself implies that the s and d waves are in phase; a result that my experiments confirmed. For this cascade the $P_4(\cos\theta)$ term vanishes and therefore the relative s-g phase cannot be determined.

Asaro and Siegbahn[118] measured the correlation between alpha particles populating the 118 keV level of ^{239}Np and the de-exciting

γ rays in order to determine the relative d-g wave phase. Their results indicate that the phase is negative, but the positive phase could not be excluded.

For the unattenuated (G_k = 1) (5.275 MeV α - 75 keV γ) cascade in the decay of ^{243}Am Falk et al.[51] obtained A'_2 = - 0.404(10). Using liquid sources Hutchinson[119] obtained A'_2 = - 0.41(2) for this same cascade. The 75 keV level of the ^{239}Np daughter is the first member of the 5/2-[523] band and corresponds to the 59.54 keV level of ^{237}Np. The BFM theory predicts that A'_2 = - 0.358 while the CR correction gives A'_2 = - 0.405 in excellent agreement with experiment. The corresponding partial wave amplitudes are a_2/a_0 = (+)0.47 and (+)0.56 for the BFM theory without and with the CR correction respectively. In contrast Poggenburg calculated a_2/a_0 = + 0.42 which yields A'_2 = - 0.33, well outside the experimental error. The effect of the g wave on the theoretical A'_2 by only 1% because of the low g wave intensity.

I comment again on the ratio of the hindrance factor (HF) for the α-decay to the $9/2^-$ state to the HF for decay to the $7/2^-$ state. If these states were populated by pure d waves, BFM theory predicts the ratio to be $\langle \frac{5}{2}\, 2\, \frac{5}{2}\, 0 \mid \frac{7}{2}\frac{5}{2}\rangle^2 / \langle \frac{5}{2}\, 2\, \frac{5}{2}\, 0 \mid \frac{9}{2}\frac{5}{2}\rangle^2$ = 2.857 for decay to a K = 5/2 rotational band. The experimental ratios are 3.50, 3.75 and 4.36 for ^{239}Am, ^{241}Am and ^{243}Am respectively.[50] Because of the different experimental HF ratios for ^{241}Am and ^{243}Am there is no assurance that the CR correction found to be applicable to ^{243}Am will be applicable to ^{241}Am also. The observed trend of HF ratios with increasing neutron number is in the opposite direction to what would be expected. Since the g wave is becoming more highly hindered with increasing N, the HF ratios should decrease rather than increase. I have no explanation

for the observed trend.

In general there is no justification for applying the CR correction to the relative $\ell = 2$ wave intensity throughout the actinides. The BFM assumption that the K quantum number is a constant of motion has not been supported by coupled channel numerical integrations applied to the decay of ^{253}Es and ^{255}Fm (cf. Section IVC.) The channel coupling which spoils the BFM branching ratios depends on the relative strengths of a number of coupling matrix elements. Although the d and g wave branching to the lower states in a rotational band is enhanced over the BFM theory estimates as a result of the channel coupling, the percentage enhancement is not always the same as that found by Chasman and Rasmussen for ^{233}U. In fact, AC experiments[120] on ^{249}Cf showed that the BFM theory overestimates the d wave intensity in the favored branch of α decay to ^{245}Cm, a result which is unexpected.

Table IX A. Experimental ^{241}Am in neodymium ethylsulfate α particle angular distribution as a function of inverse temperature.

$1/T\,(K^{-1})$	W(0)	W(π/2)
10.8(3)	1.060(7)	0.969(9)
15.0	1.104(8)	0.939(10)
19.3(17)	1.132(5)	0.933(7)
31.7(6)	1.193(8)	0.883(9)
43.5(2)	1.274(8)	0.859(10)
55.6	1.330(12)	0.822(13)
74.0	1.412(10)	0.781(10)
88.5	1.460(24)	0.748(16)
90.5	1.500(14)	0.736(17)

Table IXB. Coefficients A_2 and A_4 for the ^{241}Am in NES α particle angular distribution function $W(\theta) = 1 + R[A_2Q_2B_2P_2(\cos\theta) + A_4Q_4B_4P_4(\cos\theta)]$.

	A_2	A_4
BFM theory, s and g waves in phase	0.7747	0.0756
BFM theory, s and g waves out of phase	0.7477	0.0483
BFM theory, Chasman and Rasmussen correction, s and g waves in phase	0.8668	0.1032
BFM theory, Chasman and Rasmussen correction, s and g waves out of phase	0.8390	0.0770
Mang theory, s and g waves predicted to be in phase	0.7838	0.0847
Mang theory but with s and g waves out of phase	0.7398	0.0397

Table IXC. Intensities for partial waves in ^{241}Am favored α transitions to the first excited rotational band in ^{237}Np according to the method of Bohr, Fröman and Mottelson.[9,10] Numbers in parentheses have been modified by the "Chasman and Rasmussen correction."[6]

E_f(keV)	$I_f\ \pi$	s	d	g	i	Σ (%)	Measured intensity[113] (%)
59.54	5/2-	72.56 (67.76)	14.29 (19.08)	0.004		86.85	85.5
102.96	7/2-		10.81	0.017	0.0004	10.83	12.6
158.52	9/2-		1.81	0.018	0.0024	1.83	1.6
226.0	11/2-			0.006	0.0037	0.010	0.015
304.8	13/2-			0.0006	0.0019	0.0025	0.002

Table IXD. Intensities and phases for partial waves in ^{241}Am favored α transitions to the first excited rotational band in ^{237}Np as calculated by Poggenburg.[11]

I_f^{π}	s	d	g	i	Σ(%)	Measured intensity[113] (%)
5/2-	72.74	14.36	0.011		87.12	85.5
7/2-		10.70	0.045	-0.0004	10.74	12.6
9/2-		1.76	0.046	-0.0025	1.81	1.6
11/2-			0.0158	-0.0052	0.0210	0.015
13/2-			0.0015	-0.0020	0.0035	0.002

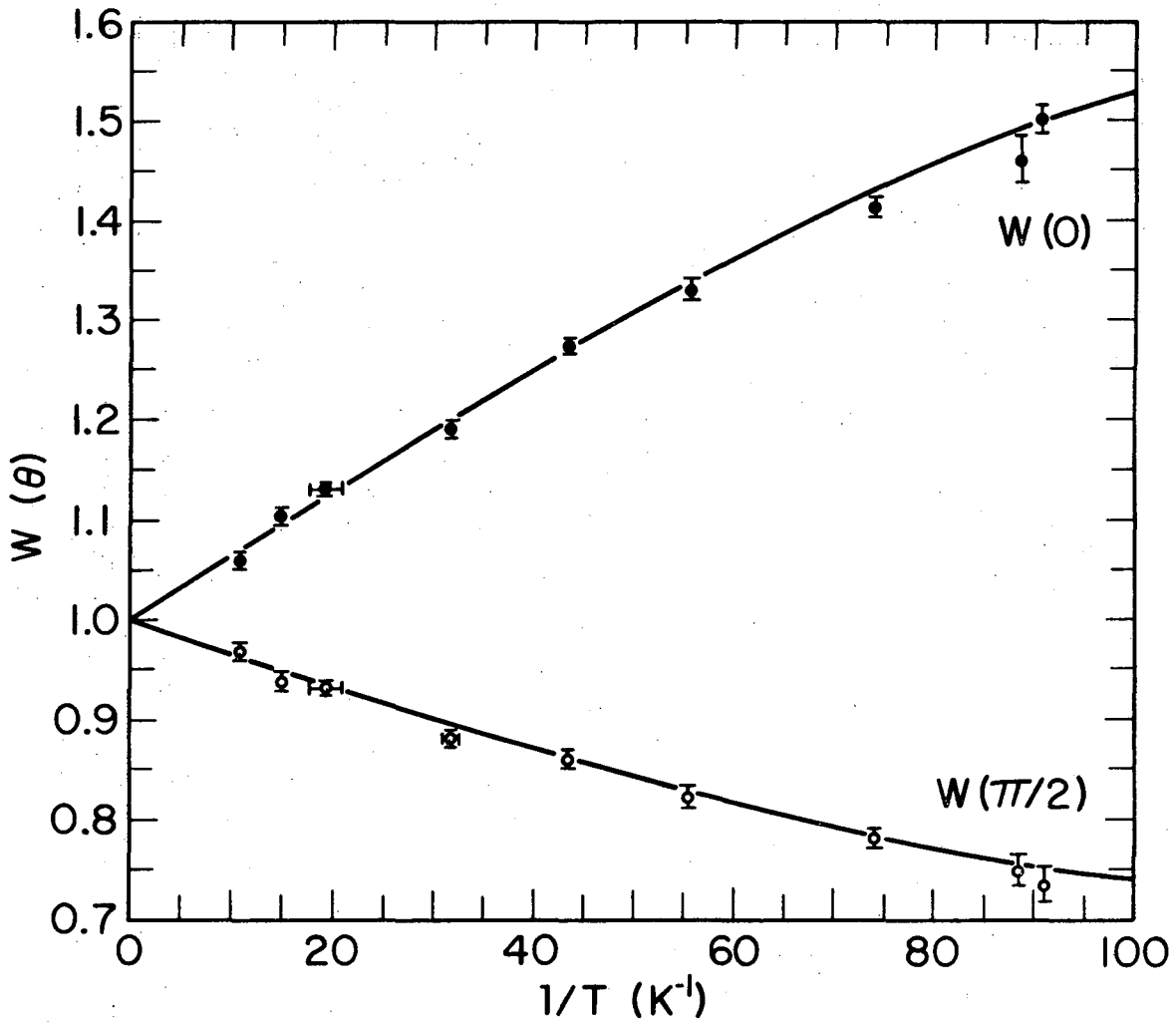

XBL 745-3063

FIG. 9. ^{241}Am in neodymium ethylsulfate (NES) α particle angular distribution at 0^0 and 90^0 with respect to the crystalline c-axis as a function of inverse temperature.

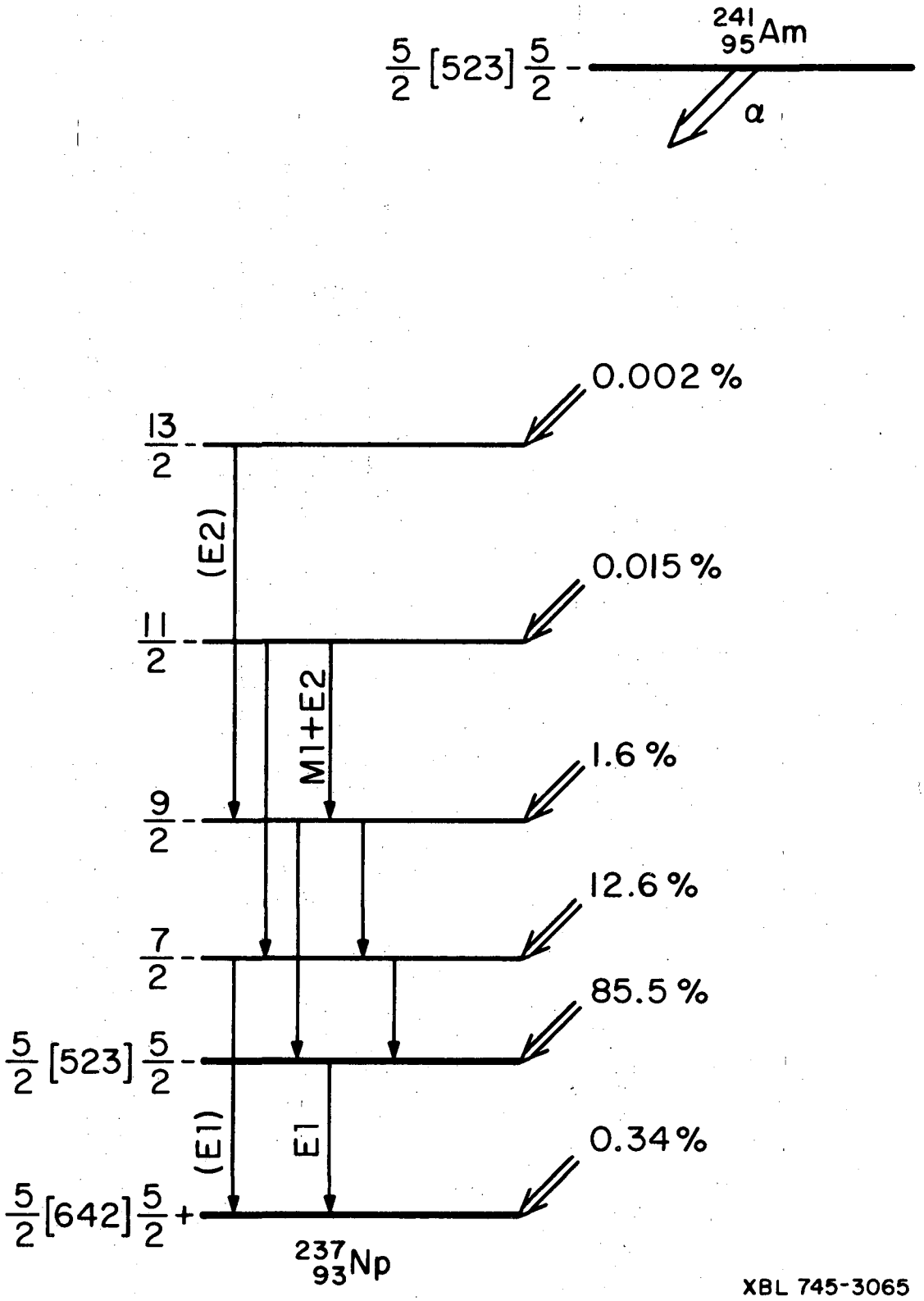

FIG. 10. Partial α decay scheme for ^{241}Am as adapted from references 113 and 114. The favored α decays populate a rotational band built on the 5/2[523] state.

X. ^{255}Fm NUCLEAR ORIENTATION RESULTS AND DISCUSSION

I now briefly discuss the ^{255}Fm NO results. Paramagnetic resonance studies of Er^{3+}, the lanthanide analogue of Fm^{3+}, diluted in lanthanum ethylsulfate, yielded the hf interaction parameters $|A| = 0.0052(1)\ cm^{-1}$, $|B| = 0.0314(1)\ cm^{-1}$ and $|P| = 0.0030(3)\ cm^{-1}$ (Ref. 121). For $|B| > |A|$ the nuclear magnetic substates are admixed except when $|k| = I + 1/2$ where $k = I_z + S_z$ where $S_z = \pm 1/2$. The levels labeled by + k and - k are degenerate except when k = 0. The ground state for a half integral nuclear spin is a singlet ($|1/2, -1/2\rangle - |-1/2, 1/2\rangle)/\sqrt{2}$, and a doublet lies closely above. The alignment may be regarded as being in a plane perpendicular to the crystalline c-axis, and the degree of alignment is relatively small.

The experimental α particle angular distribution from ^{255}Fm nuclei aligned in NES is shown in Fig. 11. The statistical accuracy of the results is limited by the low degree of alignment, the mass of ^{255}Fm available (~ 200 disintegrations/min), and the short half-life. The shape of the anisotropy curve yields a value for $|B|$ of $0.035(7)\ cm^{-1}$ or $|B|/k = 0.05(1)$ K. I could not determine the value of $|B|/|A|$, but the temperature dependence of W(0) establishes that the magnitude of B is greater than that of either A or P as in Er^{3+}. The value of the anisotropy reduction factor R is approximately 0.8. In comparing theory to experiment the reader should note that B_2 is negative and B_4 is positive for non-axial magnetic alignment for a spin 7/2 parent.

For non-axial alignment the counting rate along the c-axis decreases for a positive s-d phase. From Fig. 11 it is seen that this is the case. The solid curve in Fig. 11 was obtained using my value for

$|B|$ with $|A| = 0$ and the relative amplitudes and phases given by Poggenburg[11] for the favored decay to the 7/2+[6[3] rotational band in ^{251}Cf. Poggenburg's predicted intensities and phases are given in Table XA. The resulting A_k parameters are given in Table XB for both relative g wave phases. On the basis of NO experiments on ^{253}Es, the negative relative phase should be correct. A partial decay scheme for ^{255}Fm, as derived from Asaro et al.[122] is given in Fig. 12.

In Table XC I list the intensities given by the BFM theory. The theoretical intensities were taken from Asaro et al.[122] but the d and g wave branching was modified by using the HFs given in the Table of Isotopes.[123] A striking difference between Tables XA and XC is the factor of four difference in total g wave branching. This is reflected in the A_4 parameters given in Table XB. In order to simplify his calculations Poggenburg used a constant nuclear radius parameter and basis wave functions appropriate near the deformation $\eta = 5$. Although this approximation should be good for medium weight actinides, it should break down for the lightest and heaviest actinides. Therefore for ^{255}Fm I expect that the BFM branching rule may be more accurate than the values given by Poggenburg.

The partial wave intensities and phases for ^{255}Fm α decay obtained by numerical integration of the coupled second-order differential equations were presented in Table IVG; these same results are presented in slightly different format in Table XD. The NO results fix α_2 to positive values. The shell model α decay theory[12] and the smooth trend of g wave hindrance factors found for the even-even heavier

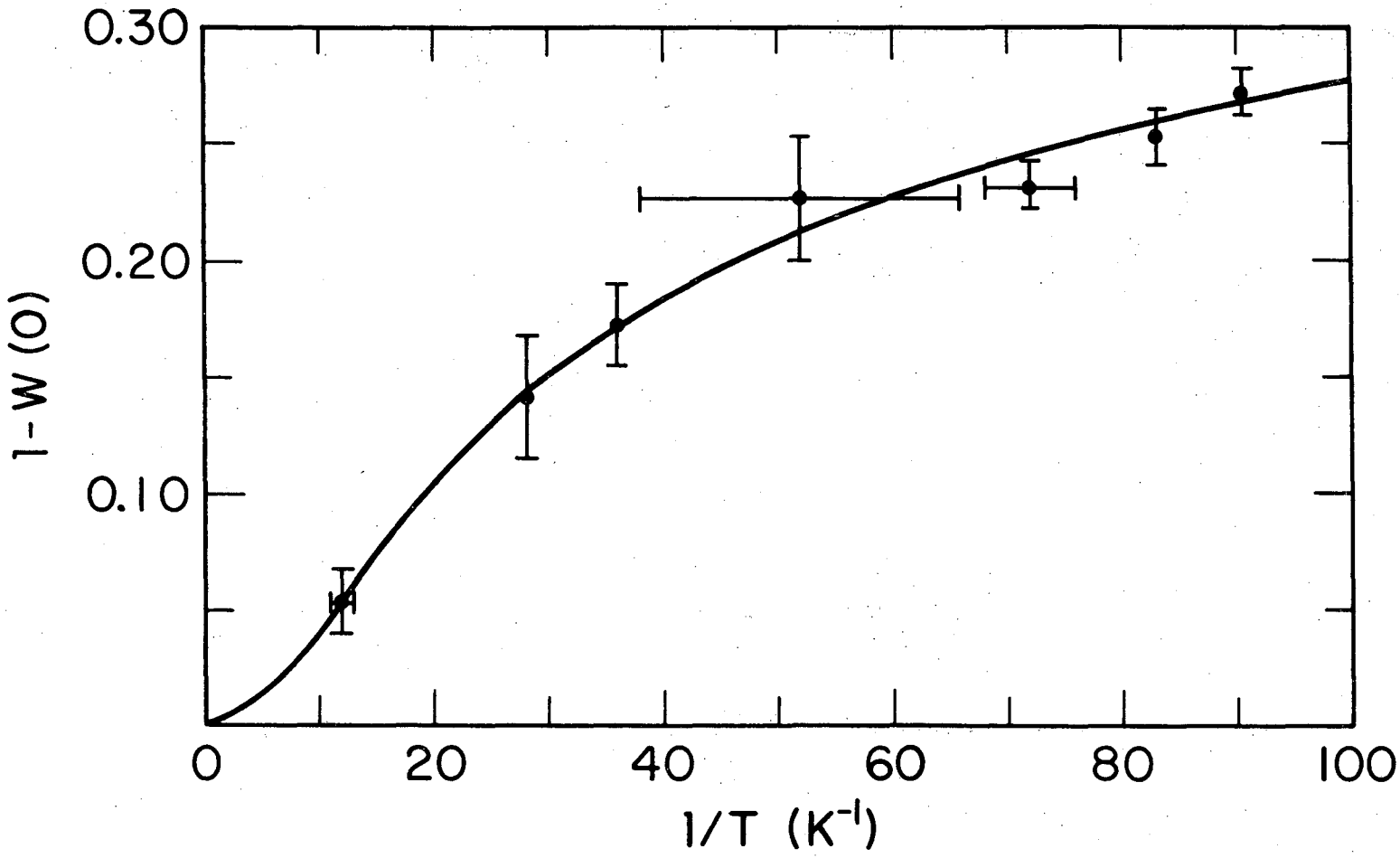

XBL 745-3064

FIG. 11. ^{255}Fm in NES α particle angular distribution at 0° with respect to the crystalline c-axis as a function of the inverse temperature.

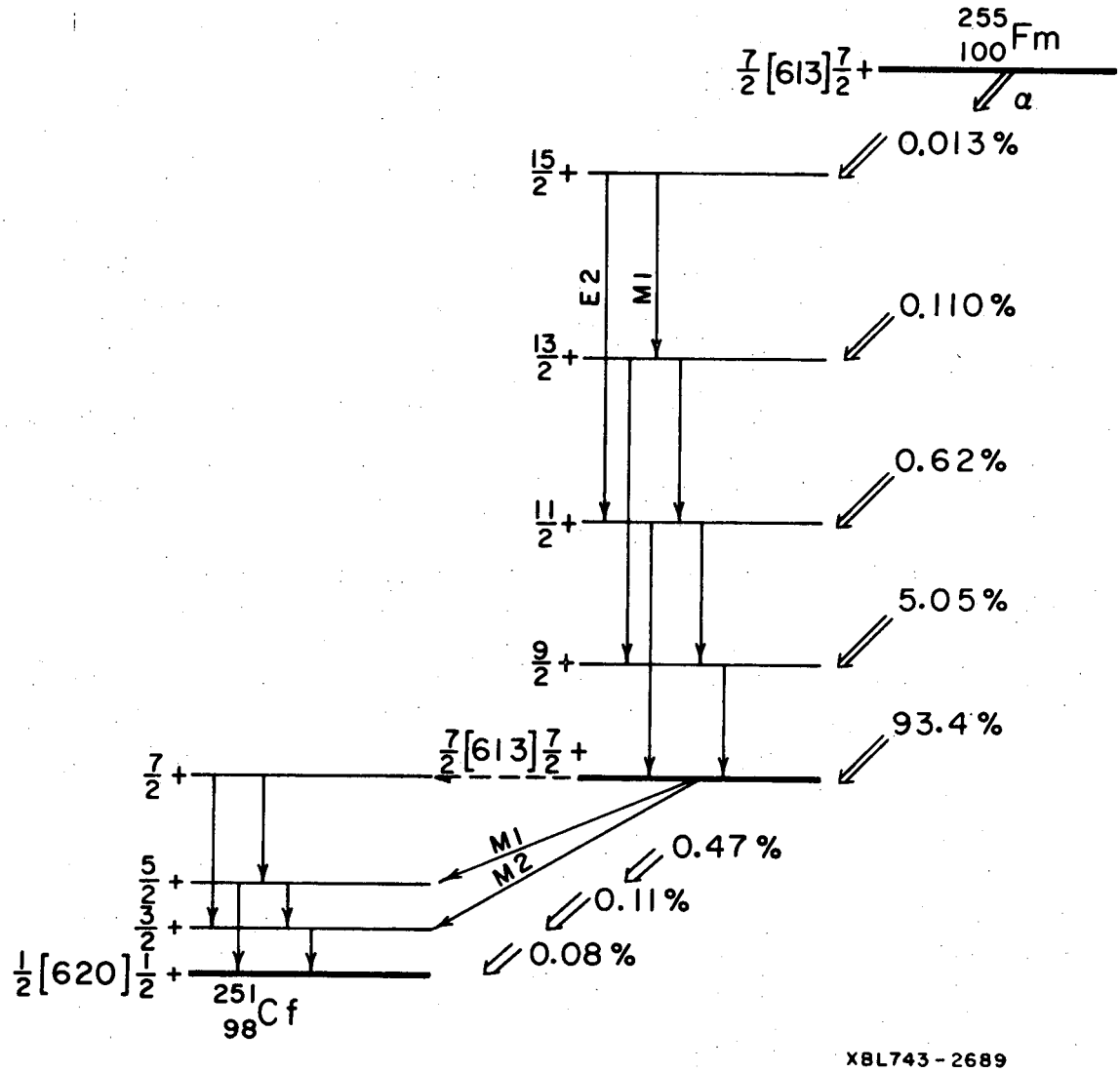

FIG. 12. Partial decay scheme for ^{255}Fm as adapted from reference 122. The favored α decays populate a rotational band built on the 7/2[613] state.

actinides give the relative s-g wave phase as being negative. Therefore only negative α_4 values are of interest. I could not experimentally determine the relative s-g wave phase because the 90° radiation detector failed during the experiment. I experienced the same difficulties in fitting the intensities to the 9/2+ and 11/2+ levels of the ^{251}Cf daughter as I experienced with the ^{253}Es decay. I attempted intensity fits with α_4 positive, but no better intensity fits were obtained than with the negative value.

Even though the ^{255}Fm anisotropy is small, determination of the ratio $W(0)/W(\pi/2)$ would make it possible to decide among the five cases given in Table XB. In Table XB I have tabulated this ratio at $1/T = 90.5\ K^{-1}$ for a point source and a point detector.

Table XA. Intensities and phases for partial waves in ^{255}Fm favored alpha transitions to ^{251}Cf as calculated by Poggenburg.[11]

$I_f\pi$	s	d	g	i	Σ(%)	Measured intensity[38] (%)
7/2+	82.47	10.28	-0.092	-0.0003	92.84	93.4(2)
9/2+		5.231	-0.197	-0.0024	5.43	5.05(7)
11/2+		0.651	-0.132	-0.0052	0.78	0.62(1)
13/2+			-0.0338	-0.0045	0.0383	0.110(5)
15/2+			-0.0027	-0.0017	0.0044	0.013(2)

Table XB. Coefficients A_2 and A_4 for the ^{255}Fm in neodymium ethylsulfate alpha particle angular distribution function and the ratio $W(0)/W(\pi/2)$ at $1/T = 90.5\ K^{-1}$.

	A_2	A_4	$W(0)/W(\pi/2)$
BFM theory, s and g waves out of phase	0.596	-0.0397	0.434
BFM theory, s and g waves in phase	0.695	0.1566	0.400
Poggenburg calculation based on shell model theory, s and g waves predicted to be out of phase	0.634	0.0003	0.413
Poggenburg calculation but with s and g waves in phase	0.700	0.1242	0.390
Numerical integration ($a_0 = 1$, $a_2 = 0.7918$, $a_4 = -0.1794$)	0.514	-0.0552	0.494

Table XC. Intensities for partial waves in ^{255}Fm favored alpha transitions to the first excited rotational band in ^{251}Cf according to the method of Bohr, Fröman, and Mottelson.[9,10]

E_f (keV)	$I_f\pi$	s	d	g	Σ(%)	Measured intensity[38] (%)
106	7/2+	83.4	9.6	0.23	93.2	93.4(2)
165	9/2+		4.89	0.50	5.39	5.05(7)
238	11/2+		0.62	0.35	0.97	0.62(1)
325	13/2+			0.086	0.086	0.110(5)
421	15/2+			0.0066	0.0066	0.013(2)

Table XD. Intensities and phases for partial waves in ^{255}Fm favored α decay to ^{251}Cf as obtained by the numerical integration of coupled differential equations ($a_0 = 1$, $a_2 = 0.7918$, $a_4 = -0.1794$).

$I_f\ \pi$	s	d	g	Σ (%)	Measured intensity minus i wave component* (%)
7/2+	86.1522	7.5837	-0.2035	93.9393	93.4
9/2+		3.9054	-0.4433	4.3487	5.05
11/2+		0.5004	-0.3013	0.8017	0.62
13/2+			-0.0787	0.0787	0.097
15/2+			-0.0066	0.0066	0.008

*Cf. Section IV. C. 4.

XI. FINAL REMARKS ON COUPLED CHANNEL CALCULATIONS

Now that all the experimental results to which the coupled channel calculations can be compared have been presented, a few final comments are in order. The reason for the systematic deviation of hindrance factor ratios from Clebsch-Gordan coefficient ratios shown in Fig. 2 must be explained.

Three mechanisms for the admixture of $m \neq 0$ α partial waves on a sphere near the nuclear surface in the case of favored α decay have been considered. If the symmetry axis of the daughter nucleus tilts with respect to the parent axis as the α particle is leaving the nuclear surface, then $m \neq 0$ projections of the α particle arise. However, reasonable assumptions about the magnitude of the effect produce too small a skewing of the d wave branching.

If the sharp inner potential barrier that I have used is replaced by a sloping barrier, then the higher energy α particles (that is, those to the lower levels of the rotational band) penetrate a thinner barrier and are thereby enhanced. Although this mechanism can reproduce the experimental intensity to the 9/2+ level, it shifts too much intensity out of the 13/2+ and 15/2+ levels. Also for ^{253}Es the degree of slope that gives the best fit to the experimental intensities fails to reproduce the experimental angular distribution.

Gamma vibrational phonon ($\ell = 2$, $m = 2$) admixtures into actinide element nuclear wave functions have been calculated by Soloviev and co-workers.[124,125] It is necessary to postulate $m = 2$ mixing amplitudes larger than the Soloviev theory predicts in order to change the d wave branching to the degree required to fit intensity patterns and

nuclear orientation data.

Certain requirements can be put on any acceptable modification of boundary conditions on the nuclear surface. Since in general four relative experimental intensity ratios are known, there should be no more than three adjustable parameters; a fourth parameter should be introduced only if physically meaningful constraints can be put on it. Both the intensity and NO data on ^{253}Es should be reproduced. The large differences in hindrance factor ratios for the three americium isotopes, ^{239}Am, ^{241}Am and ^{243}Am, should be explained. The ^{233}U case should be re-examined to check the correctness of the Chasman and Rasmussen[6] work.

I would like to close this section with an appropriate quotation from a character who, along with his friends from Okefenokee Swamp, has given me many enjoyable hours during my years as a graduate student: "Nuclear physics ain't so new, and it ain't so clear either."[126]

XII. CONCLUSION

The orientation of trivalent actinide elements in the neodymium ethylsulfate lattice is straight forward. The four elements Am, Cf, Es and Fm have been oriented in this way. It is difficult, however, to study α particle angular distributions with precision. The results reported here for ^{253}Es, ^{241}Am and ^{255}Fm are sufficiently quantitative to establish that the s and d waves in the favored transitions are in phase, but they permit the determination of the relative s-g wave phase only in the ^{253}Es case. The orientation data yielded definitive information about the electronic ground states of these trivalent ions. In $Am^{3+}(5f^6)$, as in $Eu^{3+}(4f^6)$, quadrupole coupling dominates the nuclear orientation, and the antishielded crystal field term A_2^0 is the main contributor to the electric field gradient. The data strongly support a large negative Sternheimer antishielding factor, $\gamma_\infty \approx -10^2$, and they also indicate a shielding constant $\sigma_2 \approx 0.7$, in good agreement with an earlier value for Eu^{3+}. In $Es^{3+}(5f^{10})$, as in $Ho^{3+}(4f^{10})$, the orientation is magnetic and axial. From the derived magnetic hyperfine interaction constant and extrapolated crystal field parameters a value for the nuclear magnetic dipole moment was determined. In $Fm^{3+}(5f^{11})$, as in $Er^{3+}(4f^{11})$, the electronic ground state in the ethylsulfate lattice has $|B| > |A|$.

The formal treatment of the ^{253}Es and ^{255}Fm favored α decay revealed that the assumption of the Bohr, Fröman and Mottelson theory that only $m_\ell = 0$ partial waves occur near the nuclear surface is not strictly true. The approximate treatment of anisotropic barrier penetration that is proportional to a spherical barrier penetration factor

times a Clebsch-Gordan coefficient squared appears to be valid except in the case of very highly hindered partial waves.

ACKNOWLEDGEMENTS

It is a pleasure to acknowledge association with and assistance from members of the Lawrence Berkeley Laboratory staff.

Prof. David A. Shirley directed my research. His suggestions for solving problems and his insights into the implications of the experimental results aided in the maturing of my scientific abilities.

The theoretical α decay studies would not have been successfully completed without the patience and generosity of Prof. John O. Rasmussen. Mr. David Raich wrote most of the computer codes in an elegant manner. Ms. Elizabeth Rauscher encouraged the completion of the studies.

Dr. Stanley Thompson, Prof. Luciano Moretto and Mr. Raymond Gatti collaborated on the spontaneous fission fragment studies and introduced me to the use of dielectric track detectors.

Most of the separated and purified actinide isotopes were provided by the late Prof. Burris Cunningham and his co-workers, especially Dr. Dennis Fujita. Dr. Raymond Dod provided technical advice on the operation of ion exchange columns. Productive discussions about crystal field and hyperfine interactions were carried on with Dr. Norman Edelstein.

I profited from collaboration with Prof. N. J. Stone, Prof. Erik Karlsson, Prof. Günter Kaindl and Dr. Fredrick Bacon.

The following "Rad Lab" staff members have my special gratitude for their help. Ms. Winifred Heppler grew the neodymium ethylsulfate crystals. Ms. Gerda Bolz provided radiochemical assistance, served as the floor shrink, and kept a desk drawer stocked with edibles. Mr. Dimitri "Ed" Voronin and Mr. Henry Teppo assisted in the design and

alignment apparatus. Dr. Richard Pehl and Dr. Eugene Haller provided semiconductor radiation detectors.

Among the former and present graduate students with whom I had especially enjoyable associations are Fred Bacon, John Barclay, Bill Brewer, Jim Holliday, Jim Huntzicker, Steve Rosenblum, Dan Salomon, and Rick Streater.

I might not have completed my research had it not been for the understanding of Ms. Dodie King.

This work was supported by the United States Atomic Energy Commission and therefore by the hard-pressed taxpayers of this country.

APPENDIX A. SPONTANEOUS FISSION FRAGMENT ANGULAR DISTRIBUTIONS

The nuclear potential energy as a function of a deformation parameter has a relative maximum or saddle point.[127] Bohr simplified the consideration of the passage either over or through the barrier by the introduction of the concept of the transition state.[128] The low energy states at the saddle point are expected to be similar to the low energy states of the slightly deformed ground state nucleus. These states are characterized by I, M, K and π where M is the projection of nuclear spin on a space-fixed axis ($M \equiv I_z$ of my earlier notation). Rotational levels built on intrinsic states are expected as the lowest levels at the saddle point, at least for odd-mass and odd-odd nuclei for which single particle excitations are more easily excited than vibrational modes.

Not all of the physics of fission is contained in the statics of the process; that is, the fission process depends on both deformation coordinates and inertial parameters. As the nuclear deformation increases, changes in the K quantum number may occur as different intrinsic energy states of the odd nucleon(s) are crossed.[129] This of course requires a mechanism such as Coriolis or γ vibrational couplings to change K. It is not clear whether K at the saddle point or K at the outer turning point is the relevant K value for spontaneous fission. In either case, two points should be considered. First, K for spontaneous fission may not be the same as K for the nuclear ground state (K = I). Second, K may not be single-valued because of the possible existence of closely-lying states of different K at the outer turning point.

A.1. FISSION FRAGMENT ANGULAR DISTRIBUTION FUNCTION

If it is assumed that the fission fragments separate along the nuclear symmetry axis and that K is a good quantum number in the descent of the nucleus from the transition state to the configuration of separated fragments, then the angular distribution of the fission fragments is the same as the angular distribution of the nuclear symmetry axis.

In the strong coupling model the nuclear wave function is factored into an intrinsic part times a rotational part:

$$\psi = [(2I+1)/16\pi^2]^{\frac{1}{2}}[\chi_K(x)D^I_{MK} + (-1)^{J-K}\chi_K(x)D^I_{M-K}] , \qquad (A.1)$$

where $D^I_{MK} \equiv D^I_{MK}(\alpha,\theta,\gamma)$ is a symmetric top wave function. The distribution of the nuclear symmetry axis is given by

$$W^I_{MK}(\theta) = \int |\psi|^2 \, d\alpha d\gamma dx. \qquad (A.2a)$$

The integration over the intrinsic wave function gives a Kronecker delta. Therefore

$$W^I_{MK}(\theta) = \frac{2I+1}{8\pi}\left[|D^I_{MK}|^2 + |D^I_{M-K}|^2\right]. \qquad (A.2b)$$

The matrices $|D^I_{MK}|^2$ can be reduced to a summation over the complex conjugate matrices $D^{I'\,*}_{MK}$ by using Eq. 1.38 of Rottenburg *et al.*[130] The sum of rotation matrices squared reduces to

$$|D^I_{MK}|^2 + |D^I_{M-K}|^2 = (-1)^{K-M} \sum_{I' \text{ even}} 2(2I'+1)D^{I'\,*}_{00}\begin{pmatrix} I & I & I' \\ M & -M & 0 \end{pmatrix}\begin{pmatrix} I & I & I' \\ K & -K & 0 \end{pmatrix} \qquad (A.3a)$$

and

$$D^{I'\,*}_{00}(\alpha,\theta,\gamma) = P_{I'}(\cos\theta) \qquad (A.3b)$$

from Edmonds[131] Eq. 4.1.26. Equation A.2b can then be written, with

the further reduction of the $P_0(\cos\theta)$ term and the weighting with the population factors p(M), as

$$W(\theta) = \frac{1}{4\pi} + \sum_{\substack{k>0 \\ \text{even}}} \sum_{M} (-1)^{K-M} p(M) \frac{[I]\,[k]}{4\pi} \begin{pmatrix} I & I & k \\ M & -M & 0 \end{pmatrix} \begin{pmatrix} I & I & k \\ K & -K & 0 \end{pmatrix} P_k(\cos\theta) \tag{A.4a}$$

where the normalization is such that

$$2\pi \int_0^{\pi} W(\theta) \sin\theta \, d\theta = 1. \tag{A.4b}$$

The first term in the summation over k in Eq. A.4a can be written in closed form by using the algebraic form for the 3j-symbols which is given by Edmonds:[131]

$$\begin{pmatrix} I & I & 2 \\ K & -K & 0 \end{pmatrix} \begin{pmatrix} I & I & 2 \\ M & -M & 0 \end{pmatrix} = (-1)^{2I-K-M} \frac{4[3K^2-I(I+1)][3M^2-I(I+1)]}{(2I+3)(2I+2)(2I+1)(2I)(2I-1)} . \tag{A.5}$$

For a nucleus with a given I, M and K the fission fragment angular distribution can also be written as[132]

$$W^I_{MK}(\theta) = \frac{2I+1}{4\pi} \left| d^I_{MK}(\theta) \right|^2 . \tag{A.6}$$

The $d^I_{MK}(\theta)$ functions are given in closed form by Wheeler.[133] Both Wheeler and Bekhami[134] have given typical angular distributions to be expected for various I, M and K values. For mixed M states the distribution in Eq. A.6 must be weighted by the appropriate population factors, p(M).

A.2. SUITABLE NUCLEI FOR SPONTANEOUS FISSION ANGULAR DISTRIBUTION STUDIES

There are a number of considerations in choosing isotopes for the study of spontaneous fission fragment angular distributions. First, the nuclear spin must be greater than 1/2, and the hyperfine interaction constant should be large. The angular distribution function is proportional to a weighted sum over $|d^I_{MK}|^2$. Each $|d^I_{MK}(\theta)|^2$ peaks at one angle, but if more than one nuclear magnetic substate is appreciably populated, the distribution broadens and the value of K at the saddle point may be difficult to determine.

Second, the fission branch should be a reasonable fraction of the total decays. The competing mode of decay is usually α decay. The relative number of fission events per α decay is simply the inverse ratio of the corresponding half lives. The α decays are not of any direct interest, although their angular distribution can be useful in monitoring the source temperature, but they raise the source temperature thereby decreasing the anisotropy. The lighter actinides have very small fission branches, typically of the order of one fission per 10^{10} α decays. Also the long total half lives require large masses of the active element. Large masses mean thick sources, internal scattering and adsorption, and broadening of the angular distribution. The alternative of a thin source with large area means poor angular resolution. Therefore only the heavier actinides, which have large fission branches, can be used. The only non-zero nuclear spin isotopes that meet the fission/α branching requirement are ^{249}Cf, ^{253}Es, ^{254}Es, ^{255}Es, ^{255}Fm and ^{257}Fm. ^{255}Fm can be eliminated becuase of its short half

life (20 h). ^{249}Cf can be eliminated because of its small hyperfine splitting.[7] ^{255}Es occurs with ^{253}Es to the extent of 1 part in 10^5; it is not available in sufficient quantity for NO experiments.

Third, the host lattice either should have a high heat capacity or should be maintainable at a low temperature by an external refrigerator. Contact cooling is limited to metallic lattices. Because no research has been done on alloy systems of the heavier actinides, the radioactive element ions were substituted into a neodymium ethylsulfate lattice which was cooled by adiabatic demagnetization.

Fourth, the radioactive isotope must be available, an important consideration in the study of actinide elements.

Experimental results on ^{253}Es, ^{254}Es and ^{257}Fm will be discussed after the experimental apparatus is described.

A.3 APPARATUS

The cryostat that was used to study α particle angular distributions could not be used to study fission fragment angular distributions because the gap between the electromagnet pole faces was too small to accommodate the detectors required for mapping the fragment angular distributions. Therefore the adiabatic demagnetization apparatus named Copernicus which was built by John Barclay[135] was used instead. The cooling magnet, named Stanislaus, is a 40 koe superconducting solenoid 23.3 cm long with a 13.5 cm i.d. and a measured coil constant of 214 oe/amp.

A.3a. CRYOSTAT

The cryostat is a stainless steel can 37 mm high with a 10.2 mm i.d. A flange, tapped for machine screws, was welded to the top. The can is bolted to the pumping tube, which is 82 cm long 3.8 cm o.d. stainless steel with a 0.05 mm wall, with the vacuum seal being made with an indium wire gasket. Two additional tubes, each 3 mm o.d., lead into the can. One of these tubes contains four twisted tripletsof 32 gauge formex coated manganin wire potted in Stycast 2850 GT epoxy in order to minimize heat leaks down the wires. The other tube was soldered to the top of a welded stainless steel bellows the bottom of which was soldered to the can cover flange. The top of this tube was fed through a Wilson seal and capped with a Rad Lab fitting at room temperature. The entire tube can be moved up and down through a distance of 2 cm without breaking the cryostat vacuum. The use of this bellows system will be explained later.

A.3b. SALT PILLS

The salt pills are shown in Fig. 13. The experimental chamber is the space between the innermost salt pills. The two bottom pills are supported by sets of three pitch-bonded graphite legs 3.0 cm long and 6 mm in diameter. The two outer salt pills are filled with a manganous ammonium sulfate (MAS) in glycerol slurry, and the two inner pills are filled with a chromium potassium alum (CPA) in glycerol slurry. The sides of the two lower pills are 0.13 mm thick mylar. The sides of the two upper pills, which extend down to the lower salt pills where they fasten with 0-80 brass screws, are 0.13 mm thick annealed copper sheet. The base plate and the bottoms of the salt pills are epoxy-fiberglass laminate sheet (NEMA G10) either 6.3 mm or 9.5 thick with sections machined out in order to reduce the thermal mass while retaining strength. The top of the lowest pill is an epoxy-fiberglass sheet that is in two pieces anchored together by a split copper section that is thermally anchored within the salt mass thereby providing a long thermal path from the outside of the pill which "sees" 1 K to the inner pill which is at 0.01 K. The top of the lower CPA-filled pill is a split brass plate which is thermally anchored within the CPA slurry.

A.3c. ACTINIDE ION DOPED NEODYMIUM ETHYLSULFATE SOURCES

The radioactivity-containing NES crystal is mounted between two sets of gold-plated copper fins. Each set of fins is composed of fourteen 0.13 mm thick sheets of copper that are silver soldered together at the top end. The bottom section of each fin, which is imbedded in the CPA slurry, is 25 mm high and 45 mm long. The top section, which extends upward through a rectangular hole in the pill's top plate, is 40 mm high and 18 mm wide.

A.3d. FISSION FRAGMENT DETECTORS

The choice of a fission fragment detector was influenced by four considerations. The number of fission events was less than one/min for the source strengths used. The source strength was limited either by the mass of a given isotope available or by the desire to limit α particle heating of the NES crystal. For a source strength of 10^5 α dpm, the particles deposit approximately 1 erg/min. In general heat fluxes of 100 erg/min can be tolerated in the entire NES crystal, but the α particles deposit their energy in a small volume of the crystal, and at 0.01 K the thermal conductivity, which is proportional to T^3, is too low to dissipate the heat input throughout the crystal.

Second, whereas α particle angular distributions peak at either 0° or 90° with respect to the crystalline c-axis, fission fragment angular distributions can, in principle, peak at an intermediate angle. Therefore the fragment distribution must be measured at several angles.

Third, because of the low count rate, very low noise detectors are needed. Few spurious counts on an absolute basis can be tolerated.

Fourth, high reliability is desired because of the long apparatus set-up times.

Semiconductor detectors are not acceptable because of their poor angular resolution, bulkiness, high noise, and poor reliability at ultra-low temperatures. Therefore solid state track detectors[136] are used instead. Both mica and mylar can be used to detect fission fragments. The fission fragments leave sites of high free energy that can be chemically etched to a large enough size for optical microscope scanning. Mylar has the advantage of being a synthetic material and therefore has no background tracks. However, the etched tracks are cylindrical cones that cannot always be distinguished from imperfections. Mica always has background fission tracks from uranium decay. However, if the mica is annealed at 450° C for six hours and then etched in concentrated hydrofluoric acid, the background tracks appear as shallow and broad pyramids that are easily distinguished from the deep and narrow diamonds that develop upon etching the unannealed tracks.

The fission fragments are detected in annealed and pre-etched mica strips 3.92 cm long, 15 mm wide and 0.03 - 0.05 mm thick. The strips are held in a curved brass holder with an inner radius of 12.7 mm that subtends an angle between -40° and 130° with respect to the NES crystalline c-axis. Holes drilled through the holder at 0° and 90° permit pins, which are part of an alignment jig, to protrude from the holder back through to the source spot in order that source-detector alignment errors can be reduced. The holder attaches to the brass salt pill top with brass screws.

In order to prevent the fission fragments from hitting the mica detector at any but the lowest temperatures, a mechanical baffle made of copper mounted on a spring-loaded pivot is used. The spring keeps the baffle out of position unless it is pulled into position over the source spot by a 0.08 mm diameter tantalum wire. The wire is fed through holes drilled through the salt pill copper radiation shields, over a 11 mm o.d. brass wheel, through two guide slots, and then vertically up through the 1.5 mm o.d. thin wall stainless steel tube with the bellows at the bottom. The wire is anchored to the room temperature end of the tube under a Rad Lab fitting. The bellows permits the tube and the tantalum wire to move through 2 cm thereby pulling the fission fragment baffle into position.

A.3e. TEMPERATURE MONITORING

The temperatures of the brass plate and the copper fin assembly are monitored with 15 Ω 1/8 watt Allen-Bradley carbon composition resistors connected to three leads. The resistance is measured with an AC bridge.[137] The principles of carbon resistance thermometry have been given by Black, Roach and Wheatley,[138] Sinclair, Terbeek and Malone,[139] and Kopp and Ashworth.[140]

The temperature of the radioactive source spot following adiabatic demagnetization is monitored either by the α particle anisotropy measured at 90° with respect to the NES c-axis by a solid state detector mounted behind the mica detector holder or by the γ ray anisotropy of the 962, 966 and 1178 keV γ rays of ^{160}Tb which was in some cases grown into the NES crystal bulk.

A.4. ^{253}Es SPONTANEOUS FISSION FRAGMENT ANGULAR DISTRIBUTION

The initial experiments and apparatus development were done with ^{253}Es in NES because ^{253}Es is the most readily available heavy actinide element with a nuclear spin greater than 1/2. Also the hyperfine interaction is known to be large and axial; therefore a sharp fission fragment angular distribution at low temperatures was expected.

In a series of demagnetizations extending over ten days only 20 fission events (too small a number to permit extraction of the K quantum number) were observed from a source measuring 2×10^5 α dpm. The source strength was increased to 1×10^6 α dpm in order to increase the number of events. However, this latter source warmed up within three hours whereas the previous source remained cold for several hours. Therefore a point of diminishing returns was reached. The "colder" source permitted longer counting periods per demagnetization than the "hotter" source did, but because of the fixed length of time required per demagnetization and apparatus cycling, both sources yielded the same number of fission counts per day (two demagnetizations). The hotter source had the significant disadvantage of rapid warm up which required continuous monitoring of the source temperature in order that mica exposure could be terminated prior to warm-up. In order to get reasonable statistics, counting would have to extend over a period of 50 days, which is not practical because of demands on some of the experimental equipment. In any event, ^{257}Fm became available; experiments with that isotope are reported next.

A.5. ^{257}Fm SPONTANEOUS FISSION FRAGMENT ANGULAR DISTRIBUTION

The most extensive fission fragment angular distribution studies were performed with ^{257}Fm (I = 9/2) which has the advantage of a large fission/α branching ratio (475(10)α decays/spontaneous fission decay)[141] but the disadvantage of a small and non-axial hyperfine interaction constant. As was mentioned in the section on the ^{255}Fm in NES α particle angular distribution, the non-axial hyperfine interaction means that the nuclear magnetic substates are mixed; i.e., even at the lowest nuclear orientation temperatures more than one nuclear magnetic substate is appreciably populated. Therefore the fission fragment angular distribution is not expected to be particularly sharp.

The total quantity of ^{257}Fm available for the experiment was 370 α dpm and therefore approximately one fission every 1.5 min. Approximately 1/5th of this activity was substituted into an NES single crystal.

After the ^{257}Fm in NES source was prepared and mounted in the salt pill holder, a strip of cellulose nitrate was placed in the mica holder and exposed at liquid nitrogen temperatures with 50μ of ^{4}He exchange gas in the cryostat for 2430 min. Cellulose nitrate registers both α particles and fission fragments. The cellulose nitrate was removed, etched in 6N NaOH, and a strip 3 mm wide along the center of the strip was otpically scanned in 1 mm long blocks. The number of tracks counted is shown in Fig. 14. There are two points shown per scanned segment because two independent scans were made. The disagreement between the two scans indicates the difficult of positively identifying real tracks that are recorded in an amorphous material.

As an aid in identifying real tracks, a strip of cellulose nitrate that had not been exposed to α particles was etched along with the exposed strip as a blank. The scans indicate that the detector was not precisely centered on the source since the count rate is not constant with angle, but this small misalignment can be corrected for. The fall off in counts beyond the 0° and 90° positions indicates that the source is a shallow crater in the NES crystal surface.

Because of the small mass of ^{257}Fm available, the α particle anisotropy could not be used for monitoring the source temperature. ^{160}Tb was grown into the crystal bulk before adding the ^{257}Fm, and the ^{160}Tb γ ray anisotropy was used to monitor the temperature. Because α particle heating was not a problem, the temperature of the ^{257}Fm source spot and the NES crystal bulk should have been the same.

A mica strip was exposed to the ^{257}Fm in NES source for a total of 84 hr. following eight separate adiabatic demagnetizations. The baffle position was determined by two electrical contacts, one in the closed position and one in the open position. The mica was also exposed to an isotropic distribution for 8 hr. during cryostat assembly and disassembly. I will refer to this mica strip as the anisotropic mica. The optical scan of the etched anisotropic mica is shown in Fig. 15. For comparison, a scan of a mica strip that was exposed to the ^{257}Fm in NES source at liquid nitrogen temperatures, where the fission fragment angular distribution is isotropic, is shown in Fig. 16. I will refer to this mica strip as the isotropic mica.

The isotropic data indicate, as did the cellulose nitrate that was exposed to the ^{257}Fm α particles, that the mica strip is closer to the

source at 0° than it is at 90°. Although the number of events recorded from the spontaneous fission of ^{257}Fm nuclei in the NES lattice at low temperatures is small, comparison of Figs. 15 and 16 reveals a difference in the fission fragment track distribution. In Fig. 16, the isotropic case, the events are more concentrated near 0° than they are at 90°. In Fig. 15, the anisotropic case, the opposite is true; i.e., the events are more concentrated near 90° than they are at 0°. Because of the low degree of alignment expected, the results can be analyzed initially in terms of a $P_2(\cos\theta)$ term only. The experimental results can then be compared with the theoretical angular distribution given by Eqs. A.4a and A.5.

The second-order Legendre polynomial is zero near 55°, and $P_2(\cos\theta)$ is positive for $\theta < 55°$ and $P_2(\cos\theta)$ is negative for $\theta > 55°$. Because of the limited number of events recorded in the anisotropic mica, the events are divided into two groups, those for which $\theta < 55°$ (group 1) and those for which $\theta > 55°$ (group 2). Some events beyond 0° and 90° are also included in the analysis. The average values of $P_2(\cos\theta)$ over the mica strip are 0.60 for $-15° < \theta < 55°$ and -0.35 for $55° < \theta < 105°$.

For the anisotropic case, there are 16 events in group 1 and 24 events in group 2. For the isotropic case, there are 76 events in group 1 and 63 events in group 2. Using the number of isotropic events for normalization, the "effect" at 0° with respect to the "effect" at 90° is $(16/76)/(24/63) = 0.552 \pm 0.284$. That is, the fission fragment angular distribution at low temperatures peaks at or near 90°. This can be interpreted in terms of the K quantum number(s) at scission

and the M state populations.

In order to calculate the M state populations, the magnetic hyperfine interaction parameter, B, must be known. Within a given lattice BI/μ is constant for the isotopes of an element.[65] B for ^{255}Fm has been measured, but the nuclear magnetic dipole moments for ^{255}Fm and ^{257}Fm have been neither measured nor calculated. However, the experimentally known and theoretically calculated nuclear magnetic moments for odd-neutron actinide nuclei don't vary significantly, and therefore these two fermium nuclei can be assumed to have the same nuclear magnetic moment. From my measured value of B for ^{255}Fm, I obtain $B(^{257}Fm) \approx 0.28\ cm^{-1}$. The populations of the $\pm 1/2$ through $\pm 9/2$ nuclear magnetic substates at the average temperature of the experiment of $1/T = 70\ K^{-1}$ are then 0.418, 0.319, 0.180, 0.069 and 0.014.

Assuming that K is pure and specializing Eq. A.4a for I = 9/2 and k = 2 only, the angular distribution function for fission fragments becomes

$$W(\theta) = \frac{1}{4\pi} + \sum_M p(M)\ \frac{5}{4\pi}\ \frac{(12K^2 - 99)\ (12M^2 - 99)}{2^5 \cdot 3^3 \cdot 11}\ P_2(\cos\theta). \tag{A.7}$$

Upon inserting the above population factors, $A_2 = -0.0327\,(3K^2 - 99/4)/4\pi$. Because the experimental value of A_2 is negative, $(3K^2 - 99/4)$ must be positive; this is true only for K = 7/2 or 9/2. Before a choice can be made between the two possible K values, a more careful examination of the angular distribution function is in order.

For a pure M = 1/2, K = 9/2 state,

$$W(\theta) = [1 - \frac{2^2 \cdot 5}{11}\ P_2(\cos\theta) + \frac{2 \cdot 3^4}{11 \cdot 13}\ P_4(\cos\theta) - \frac{2^2}{11}\ P_6(\cos\theta) + \frac{7^2}{11 \cdot 13}\ P_8(\cos\theta)]\ /4\pi.$$

For a pure M = 1/2, K = 7/2 state,

$$W(\theta) = [1 - \frac{2^2 \cdot 5}{11} P_2(\cos\theta) - \frac{2 \cdot 3^2}{13} P_4(\cos\theta) - \frac{4}{3} P_6(\cos\theta) - \frac{7^2}{11 \cdot 13} P_8(\cos\theta)] / 4\pi .$$

In both cases the coefficient of the fourth- and sixth-order Legendre polynomials are not negligible with respect to the coefficient of the second-order Legendre polynomial. However, upon weighting by the population factors and assuming K = 9/2,

$$W(\theta) = [1 - 1.176P_2(\cos\theta) - 0.262P_4(\cos\theta) - 0.0157P_6(\cos\theta) + 0.0002P_8(\cos\theta)] / 4\pi .$$

For K = 7/2,

$$W(\theta) = [1 - 0.392P_2(\cos\theta) - 0.222P_4(\cos\theta) + 0.0241P_6(\cos\theta) + 0.0291P_8(\cos\theta)] / 4\pi .$$

The coefficients of the sixth- and eighth-order Legendre polynomials are small enough such that only the first two Legendre polynomials need be considered. Because the fourth-order Legendre polynomial has nodes at 31° and 70°, its average over the two segments of the mica strip is small. The average values of $P_4(\cos\theta)$ over the mica strip are 0.16 for $-15° < \theta < 55°$ and 0.088 for $55° < \theta < 105°$.

The anisotropy reduction factor, R, for the ^{257}Fm in NES source was not measured, but in general $R \approx 0.75$ for sources prepared in the same way. An additional factor of approximately 0.9 enters because

the mica was exposed to the warm source for 8 hr during apparatus set-up. Including these factors and considering only the second- and fourth-order Legendre polynomials, the theoretical values of the observed effect are 0.43 and 0.76 for K = 9/2 and K = 7/2 respectively. The experimental value of 0.55(28) favors K = 9/2 because errors in nuclear orientation experiments tend to reduce the anisotropy. However, in obtaining the theoretical values of the effect, the values of B and R had to be estimated. Errors in these estimates would either increase or decrease both theoretical values, and the theoretical value for K = 7/2 either would be shifted outside the experimental statistics or would become the more reasonable choice. Therefore I conclude that K at scission is probably 9/2, but K = 7/2 is not firmly excluded, nor is a mixture of K = 9/2 and K = 7/2.

A.6 ^{254}Es SPONTANEOUS FISSION HALF LIFE

As part of the process of purifying ^{254}Es on "but" columns for fission fragment angular distribution studies, the spontaneous fission half life was determined. There have been three earlier half life determinations. Ghiorso[142] obtained $t_{\frac{1}{2}sf} = 1.5\times10^5$y. McHarris[143] obtained $t_{\frac{1}{2}sf} = 6.8\times10^5$y. Diamond and co-workers[144] obtained a lower limit of $t_{\frac{1}{2}sf} \geq 2.5\times10^7$y. Ghiorso's value was obtained in 1955; and because he had a limited mass available, his result is probably not reliable. McHarris counted 111 fission events from a purified ^{254}Es source over a period of 171.5 h. Eight of these events were attributed to granddaughter ^{250}Cf. The corrected α/sf ratio together with the α half life yielded his $t_{\frac{1}{2}sf}$ value. (There is apparently a typographical error in McHarris's thesis in reporting the α/sf ratio. It should be 887000/1 not 88700/1). McHarris's method of integrated counting may not yield a reliable fission half life. Possible sources of error such as ^{253}Es, ^{250}Cf or ^{252}Cf contamination would give a spuriously short half life. In fact the spontaneous fission half life of ^{253}Es is 7×10^5 y.

^{254}Es α decays with a 276 d half life to ^{250}Bk which has a 3.2 h half life for β^- decay to ^{250}Cf. For ^{250}Cf $t_{\frac{1}{2}\alpha} = 13$ y and $t_{\frac{1}{2}sf} = 1.7\times10^4$ y (Ref. 123). Therefore ^{250}Cf rapidly grows into the ^{254}Es. The only reliable method for determining the ^{254}Es spontaneous fission half life is to follow the linear growth in the number of fissions per unit time resulting from the ^{250}Cf decay and then to extrapolate back to the time of ^{254}Es purification on the "but" column. This is the method that both Diamond and I used.

The procedure that I used is described below. An old sample of ^{254}Es vacuum deposited on an aluminum disk was obtained from Dr. Frank Asaro. α pulse height analysis revealed substantial ^{249}Cf, ^{250}Cf and ^{252}Cf contamination, but no ^{253}Es contamination. The energy of the main α group of ^{253}Es has a higher energy than that of ^{254}Es or the Cf isotopes, and therefore ^{253}Es is easily detected as even a trace contaminant.

Initial purification was done on an alcoholic HCl column and subsequent purifications were done on alternate "but" and "but" clean-up columns. For the final purification a quartz clean-up column having a polyethylene tip was used. The ^{254}Es activity was collected and evaporated on a Pt plate which had been previously counted for actinide element contamination which is generally present in Rad Lab Pt.

The number of spontaneous fissions was counted as a function of time in a Fission Alpha Preset Counter (19X1421). The results are presented as number of fissions per 1000 min. counting interval in Fig. 17. Extrapolating back to zero time yields 22 fissions/1000 min, 4 of which are counter background. The number of disintegrations/min (dpm) at zero time was 2.16×10^4 α dpm. Using the known α decay half life of 276 d (Ref. 123), I obtain $t_{\frac{1}{2}sf} = 9.0 \times 10^6$ y.

Herb Diamond has provided some of his data. His results extrapolate to zero fission events at the time of "but" column purification. Neither of us are able to explain the disagreement in our data and the factor of at least three difference in our values for the ^{254}Es spontaneous fission half life.

Whichever spontaneous fission half life is correct, ^{254}Es is unsuitable for fission fragment angular distribution studies. Even if my shorter half

life is correct, the ^{250}Cf fissions, which are isotropic, outnumber the ^{254}Es fissions after approximately one week following "but" column purification. Therefore by the time a clean-up column is run and the nuclear orientation source is prepared, at least half the observed events will be from ^{250}Cf.

The spontaneous fission half lives of actinide nuclei have been reviewed recently by Ledergerber and Pauli[145] and by Randrup et al.[146] The latter authors consider specifically the hindrance associated with the fission of the odd-A nuclei ^{257}Fm and ^{263}106. There have been no calculations of spontaneous fission half lives of odd-odd nuclei because of the difficulty of assigning theoretical inertial parameters and fission barriers. S. G. Nilsson[147] suggested that a fission half life of 10^{10} y for ^{254}Es is more reasonable than a half life of approximately 10^{6} y. The spontaneous fission half life of one other odd-odd nucleus; namely ^{242m}Am, has been measured to be $9.5(35)\times10^{11}$ y (Ref. 148); however, the fission barriers for shape isomer fission and ground state fission are quite different. Therefore no information about the expected ^{254}Es fission half life can be obtained from the known ^{242m}Am half life. In summary, the spontaneous fission half life of ^{254}Es is at least 9×10^{6} y.

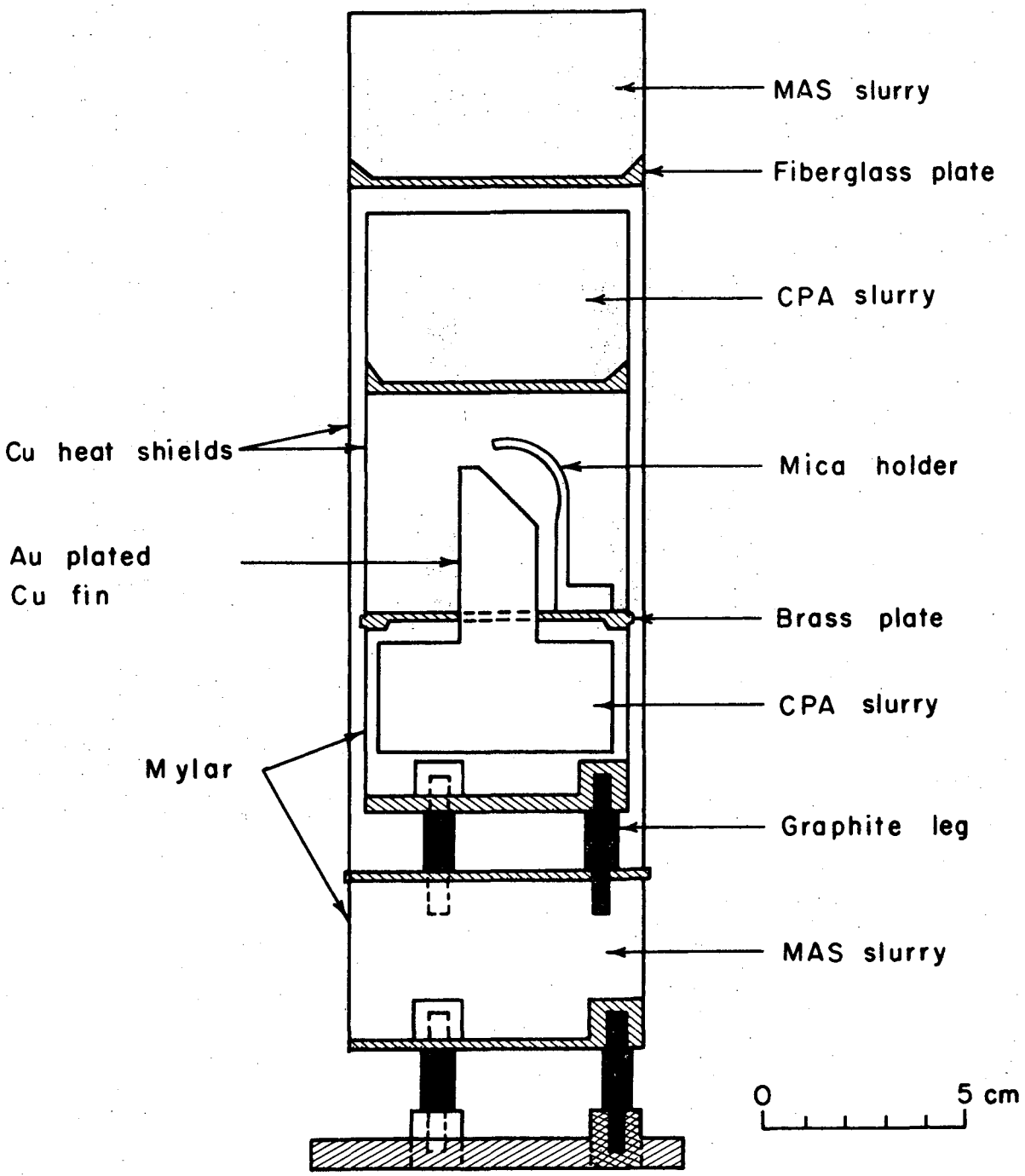

XBL747-3686

FIG. 13. Cross section of salt pill for spontaneous fission fragment angular distribution experiments.

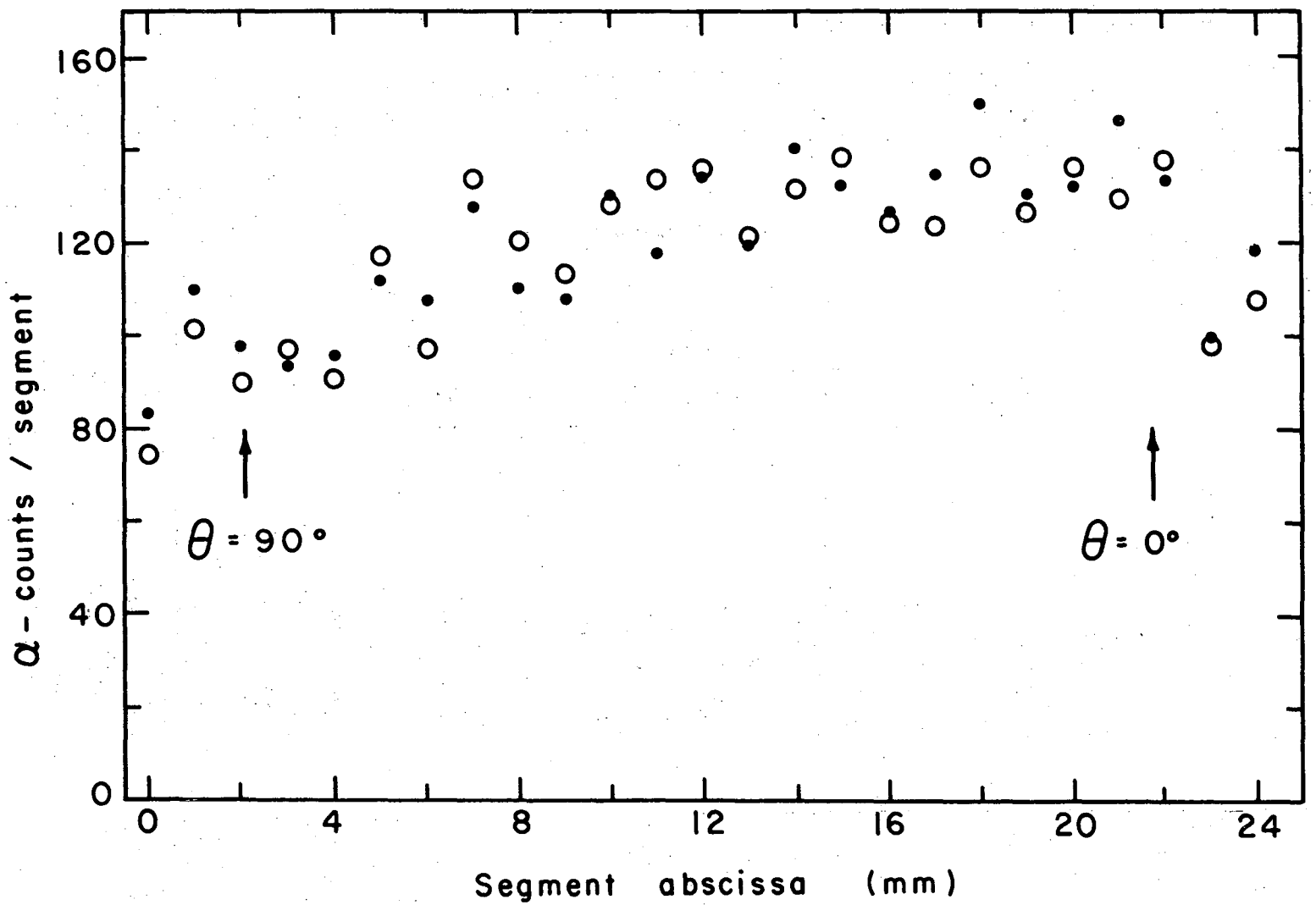

XBL747-3682

FIG. 14. α particles form ^{257}Fm in NES source registered in cellulose nitrate.

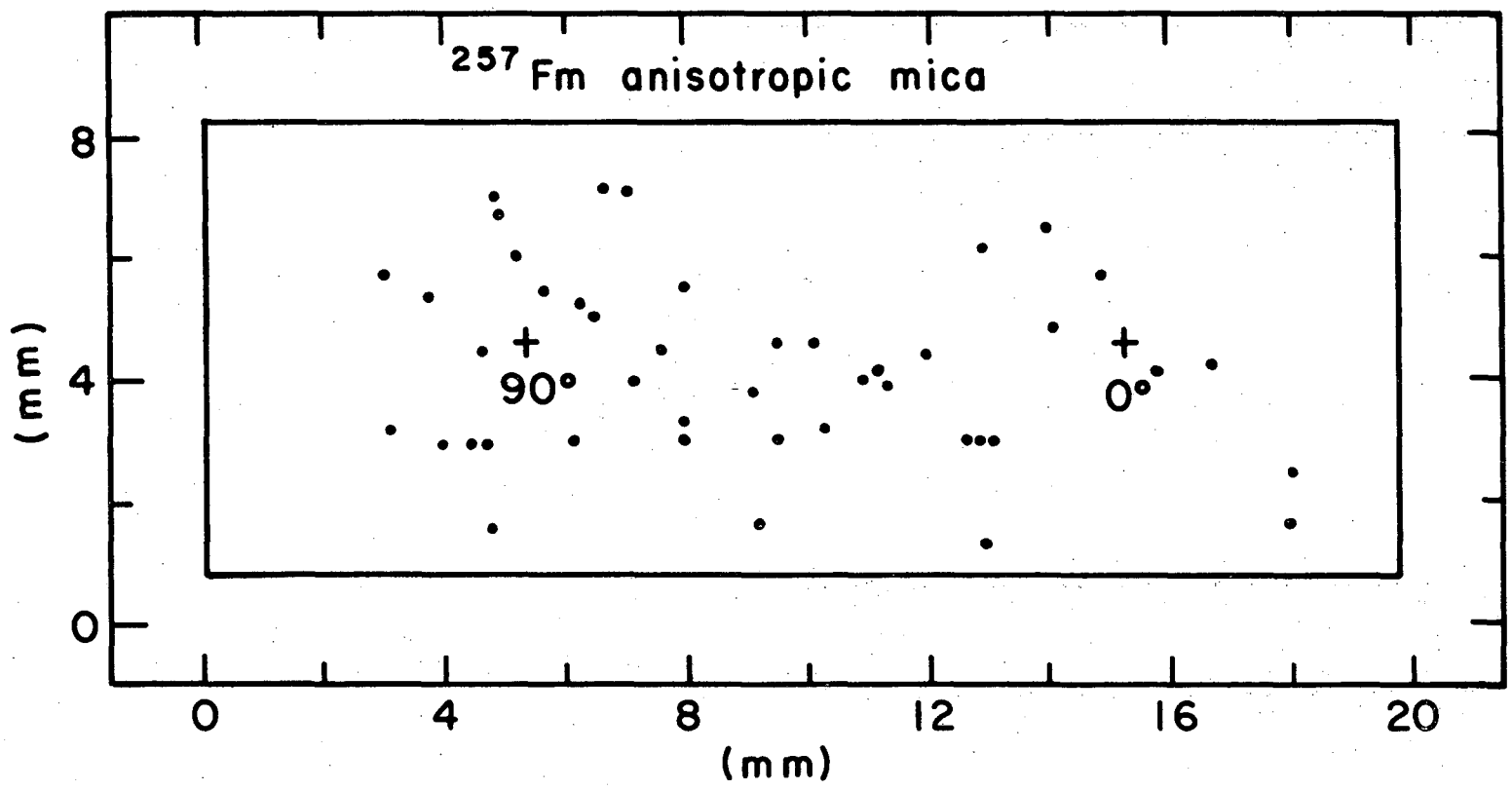

XBL747-3683

FIG. 15. Spontaneous fission tracks from oriented nuclei of ^{257}Fm in NES registered in mica.

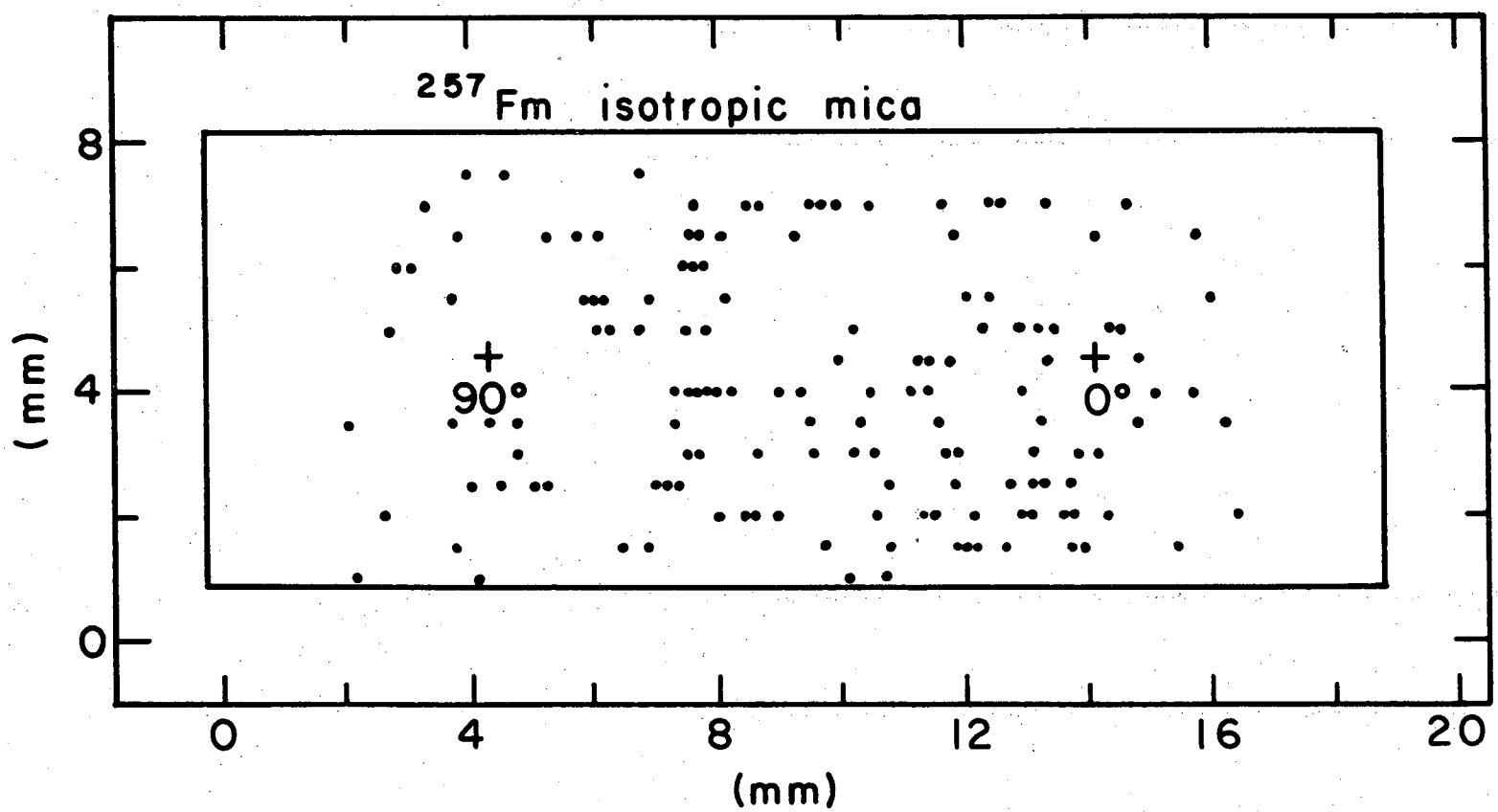

XBL747-3684

FIG. 16. Spontaneous fission tracks from non-oriented nuclei of ^{257}Fm in NES registered in mica.

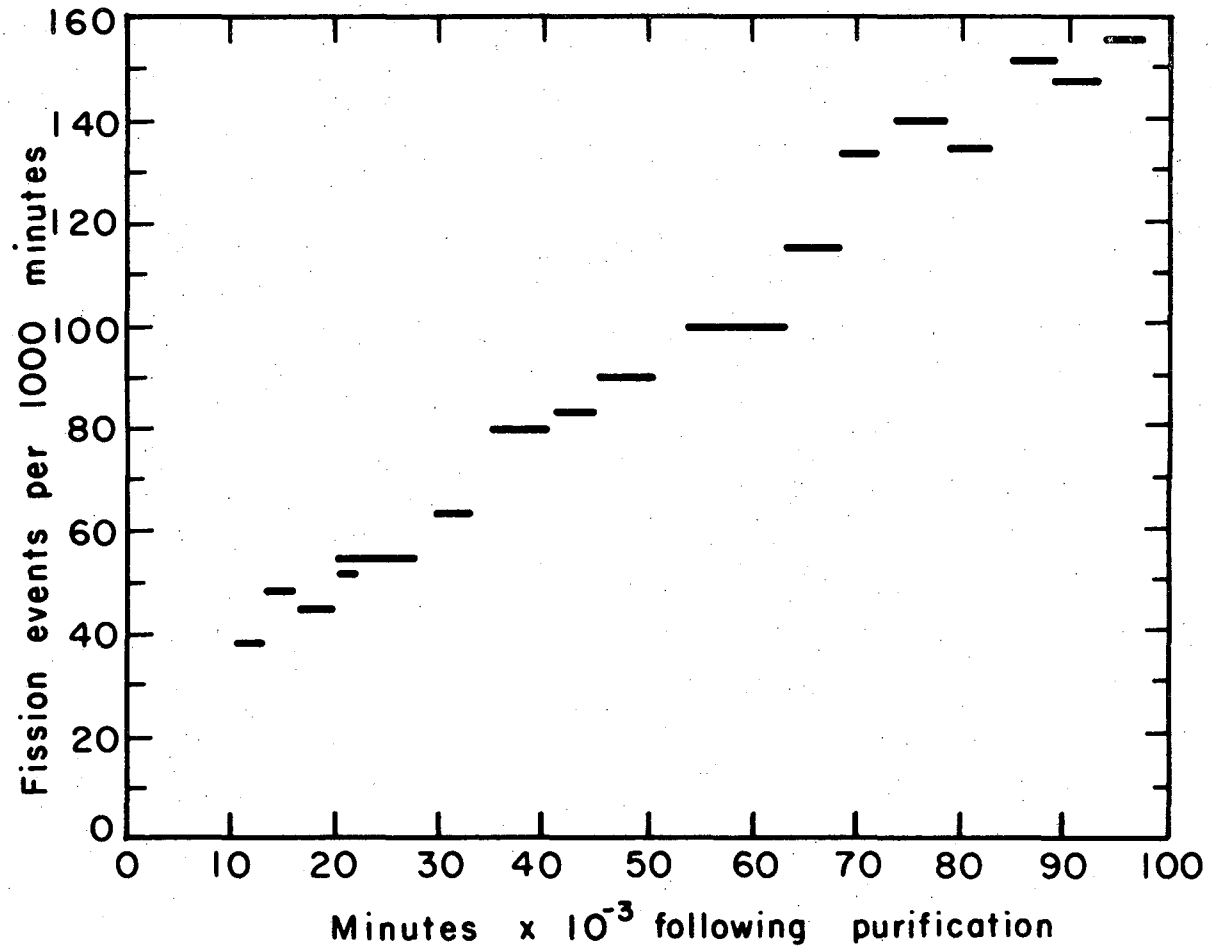

XBL747-3685

FIG. 17. ^{254}Es and granddaughter ^{250}Cf spontaneous fissions per 1000 minute interval as a function of time following ^{254}Es "but" column purification.

REFERENCES AND FOOTNOTES

1. J. A. Spiers, Nature 161, 807 (1948).
2. D. L. Hill and J. A. Wheeler, Phys. Rev. 89, 1102 (1953).
3. L. D. Roberts, J. W. T. Dabbs, and G. W. Parker, Oak Ridge National Laboratory Report No. ORNL-2204, 1956 (unpublished), p. 60.
4. J. W. T. Dabbs, L. D. Roberts, and G. W. Parker, Oak Ridge National Laboratory Report No. ORNL-2430, 1958 (unpublished), p. 50; Physica 24, S69 (1958).
5. S. H. Hanauer, J. W. T. Dabbs, L. D. Roberts, and G. W. Parker, Phys. Rev. 124, 1512 (1961).
6. R. R. Chasman and J. O. Rasmussen, Phys. Rev. 115, 1257 (1959).
7. Q. O. Navarro, J. O. Rasmussen, and D. A. Shirley, Phys. Letters 2, 353 (1962).
8. R. B. Frankel, Lawrence Radiation Laboratory Report No. UCRL-11871, 1964 (unpublished).
9. A. Bohr and B. R. Mottelson, Kgl. Danske Videnskab. Selskab, Mat.-Fys. Medd. 22, No. 16 (1953).
10. A. Bohr, P. O. Fröman, and B. R. Mottelson, Kgl. Danske Videnskab. Selskab, Mat.-Fys. Medd. 29, No. 10 (1955).
11. J. K. Poggenburg, Jr., Lawrence Radiation Laboratory Report No. UCRL-16187, 1965 (unpublished).
12. J. K. Poggenburg, H. J. Mang, and J. O. Rasmussen, Phys. Rev. 181, 1697 (1969).

13. B. R. Judd, C. A. Lovejoy and D. A. Shirley, Phys. Rev. 128, 1733 (1962).

14. R. M. Sternheimer, Phys. Rev. 159, 266 (1967). See also R. E. Watson and A. J. Freeman, Phys. Rev. 135, A1209 (1964).

15. R. P. Gupta and S. K. Sen, Phys. Rev. A7 850 (1973) and S. K. Sen, private communication, 1973.

16. Preliminary experiments were reported by D. A. Shirley, N. J. Stone and E. Matthias, Bull. Am. Phys. Soc. 10, 715 (1965).

17. L. D. Roberts and J. W. T. Dabbs, Ann. Rev. Nucl. Sci. 11, 175 (1961).

18. R. J. Blin-Stoyle and M. A. Grace, in Handbuch der Physik, edited by H. Geiger and K. Scheel (Verlag von Julius Springer, Berlin, Germany, 1957), Vol. 42, p. 555.

19. S. R. de Groot, H. A. Tolhoek, and W. J. Huiskamp, in Alpha-, Beta-, and Gamma-Ray Spectroscopy, edited by K. Siegbahn (North-Holland Publishing Company, Amsterdam, The Netherlands, 1965), Vol. 2, p. 1199.

20. D. A. Shirley, Ann. Rev. Nucl. Sci. 16, 89 (1966).

21. E. Ambler and R. P. Hudson, Rep. Prog. Phys. 18, 251 (1955).

22. N. Kurti, Nuovo Cim. Supp., Series X, 6, 1101 (1957).

23. E. Mendoza in Experimental Cryophysics, edited by F. E. Hoare, L. C. Jackson and N. Kurti (Butterworths, London, 1961), p. 165.

24. P. J. Brussard and H. A. Tolhoek, Physica 24, 233 and 263 (1958).

25. M. E. Rose, Elementary Theory of Angular Momentum (John Wiley & Sons, Inc., New York, 1957).

26. N. R. Steenberg and R. C. Sharma, Can. J. Phys. 38, 290 (1960).

27. R. M. Steffen in Angular Correlations in Nuclear Disintegration, edited by Hans van Krugten and Bob van Nooijen (Rotterdam University Press, The Netherlands, 1971), p. 1.

28. H. Frauenfelder and R. M. Steffen in Alpha-, Beta-, and Gamma-Ray Spectroscopy, edited by K. Siegbahn (North-Holland Publishing Company, Amsterdam, The Netherlands, 1965), Vol. 2, p. 997.

29. J. O. Rasmussen, Arkiv Fysik 7, 185 (1953).

30. M. A. Preston, Phys. Rev. 71, 865 (1947).

31. E. K. Hyde, I. Perlman, and G. T. Seaborg, Nuclear Properties of the Heavy Elements (Prentice-Hall, Inc., Englewood Cliffs, N. J., 1964), Vol. I, p. 201.

32. H. J. Mang, Z. Physik 148, 582 (1957); Phys. Rev. 119, 1069 (1960); and Ann. Rev. Nucl. Sci. 14, 1 (1964).

33. H. J. Mang and J. O. Rasmussen, Kgl. Danske Videnskab. Selskab, Mat.-Fys. Skrifter 2, No. 3 (1962).

34. P. O. Fröman, Kgl. Danske Videnskab. Selskab, Mat.-Fys. Skrifter 1, No. 3 (1957).

35. V. G. Nosov, Dokl. Akad. Nauk S.S.S.R. 112, 414 (1957).

36. F. Asaro, S. G. Thompson, F. S. Stephens and I. Perlman in Proceedings of the International Conference on Nuclear Structure, Kingston, edited by D. A. Bromley and E. W. Vogt (University of Toronto Press, Toronto, Canada, 1960), p. 581.

37. I. Ahmad, F. T. Porter, M. S. Freedman, R. F. Barnes, R. K. Sjoblom, F. Wagner, Jr., J. Milsted and P. R. Fields, Phys. Rev. C3, 390 (1971).

38. I. Ahmad, private communication, 1974.

39. A. J. Soinski, R. B. Frankel, Q. O. Navarro and D. A. Shirley, Phys. Rev. C2, 2379 (1970).

40. A. J. Soinski and D. A. Shirley, Phys. Rev., to be published.

41. I. Perlman and J. O. Rasmussen in Handbuch der Physik, edited by S. Flügge (Verlag von Julius Springer, Berlin, Germany, 1957), Vol. 42, p. 109.

42. S. G. Nilsson, C. F. Tsang, A. Sobiczewski, Z. Szymanski, S. Wycech, C. Gustafson, I. Lamm, P. Moeller and B. Nilsson, Nucl. Phys. A131, 1 (1969).

43. H. C. Pauli, Phys. Rep. 7C, 35 (1973).

44. J. O. Rasmussen in Alpha-, Beta-, and Gamma-Ray Spectroscopy, edited by K. Siegbahn (North-Holland Publishing Company, Amsterdam, The Netherlands, 1965), Vol. 1, p. 701.

45. L. S. Goodman, H. Diamond and H. Stanton, 166th National Meeting of the American Chemical Society, Chicago, Illinois, Aug. 1973. Abstract No.NUCL 35.

46. T. Tamura, Rev. Mod. Phys. 37, 679 (1965).

47. M. Abramowitz in Handbook of Mathematical Functions, edited by M. Abramowitz and I. A. Stegun (National Bureau of Standards, Washington, D. C., 1964), p. 537 and C. Fröberg, Rev. Mod. Phys. 27, 399 (1955).

48. J. O. Rasmussen and E. R. Hansen, Phys. Rev. 109, 1656 (1958).

49. S. Devons and L. J. B. Goldfarb in Handbuch der Physik, edited by S. Flügge (Verlag von Julius Springer, Berlin, Germany, 1957), Vol. 42, p. 415.

50. Y. A. Ellis and M. R. Schmorak, Nucl. Data B8, 345 (1972).

51. F. Falk, A. Linnfors, B. Orre and J. E. Thun, Physica Scripta 1, 13 (1970).

52. I am grateful to Dr. N. Glendenning of the Lawrence Berkeley Laboratory and to Dr. M. Gursky of the Los Alamos Scientific Laboratory for providing these computer codes.

53. A. Abragam and M. H. L. Pryce, Proc. Roy. Soc. (London) A205, 135 (1951).

54. B. Bleaney, Proc. Phys. Soc. (London) A64, 315 (1951) and Phil. Mag. 42, 441 (1951).

55. R. V. Pound, Phys. Rev. 76, 1410 (1949).

56. B. G. Wybourne, J. Opt. Soc. Amer. 55, 928 (1965).

57. J. P. Elliott, B. R. Judd and W. A. Runciman, Proc. Roy. Soc. (London) A240, 509 (1959).

58. Brian R. Judd, Operator Techniques in Atomic Spectroscopy (McGraw-Hill Book Company, Inc., N.Y., 1963).

59. Brian G. Wybourne, Spectroscopic Properties of Rare Earths (Interscience Publishers, N. Y., 1965).

60. W. T. Carnall, D. Cohen, P. R. Fields, R. K. Sjoblom and R. F. Barnes, J. Chem. Phys. 59, 1785 (1973).

61. J. G. Conway, private communication, 1970.

62. C. W. Nielson and George F. Koster, Spectroscopic Coefficients for the p^n, d^n, and f^n Configurations (The MIT Press, Cambridge, Massachusetts, 1963).

63. J. A. A. Ketelaar, Physica 4, 619 (1937).

64. K.H. Hellwege, Ann. Physik 4, 95, 127, 136, 143, 150, 357 (1949).

65. B. Bleaney in Hyperfine Interactions, edited by Arthur J. Freeman and Richard B. Frankel (Academic Press, N.Y., 1967), p. 1.

66. A. J. Freeman and R. E. Watson, Phys. Rev. 132, 706 (1963).

67. R. J. Elliott and K. W. H. Stevens, Proc. Roy. Soc. (London) A218, 553 (1953).

68. R. J. Elliott, Proc. Phys. Soc. (London) 70B, 119 (1957).

69. D. K. Fujita, Lawrence Radiation Laboratory Report No. UCRL-19507, 1969 (unpublished).

70. J. Blok, D. A. Shirley and N. J. Stone, Phys. Rev. 143, 78 (1966).

71. Rotating coil gaussmeter, model 203A, manufactured by George Associates, Berkeley, California.

72. Q. O. Navarro, Lawrence Radiation Laboratory Report No. UCRL-10362, 1962 (unpublished).

73. M. Kaplan, J. Blok and D. A. Shirley, Phys. Rev. 184, 1177 (1969).

74. J. M. Baker and B. Bleaney, Proc. Phys. Soc. (London) A68, 1090 (1950). and Proc. Roy. Soc. (London) A245, 156 (1958).

75. J. B. Gruber, J. Chem. Phys. 35, 2186 (1961).

76. J. G. Conway, J. Chem. Phys. 40, 2504 (1964).

77. W. F. Krupke and J. B. Gruber, J. Chem. Phys. 46, 542 (1967).

78. S. S. Bishton, M. M. Ellis, D. J. Newman and J. Smith, J. Chem. Phys. 47, 4133 (1967).

79. W. T Carnall, private communication, 1974.

80. S. Hüfner, Z. Physik 169, 427 (1962).

81. A. C. Larson and J. T. Waber, Los Alamos Scientific Laboratory Report No. LA-4297, 1969 (unpublished).

82. K. Rajnak and W. F. Krupke, J. Chem. Phys. 46, 3532 (1967).

83. E. Y. Wong and I. Richman, J. Chem. Phys. 36, 1889 (1962).

84. D. J. Newman, private communication, 1969.

85. W. Baer, J. G. Conway and S. P. Davis, J. Chem. Phys. 59, 2294 (1973).

86. A. J. Freeman and R. E. Watson, Phys. Rev. 127, 2058 (1962).

87. G. K. Woodgate, Proc. Roy. Soc. (London) A293, 117 (1966).

88. B. Bleaney, in Quantum Electronics, Proceedings of the Third International Congress, Paris, 1964, edited by P. Grivet and N. Bloembergen (Columbia University Press, New York, 1964) and Ref. 65.

89. P. G. H. Sandars and J. Beck, Proc. Roy. Soc. (London) A289, 97 (1965).

90. R. E. Watson and A. J. Freeman, in Hyperfine Interactions, edited by A. J. Freeman and R. B. Frankel (Academic Press, Inc., New York, 1967), p. 53.

91. P. G. H. Sandars and B. Dodsworth, in Hyperfine Interactions, edited by A. J. Freeman and R. B. Frankel (Academic Press, Inc., New York, 1967), p. 115.

92. W. B. Lewis, J. B. Mann, D. A. Liberman and D. T. Cramer, J. Chem. Phys. 53, 809 (1970).

93. E. F. Worden, R. W. Lougheed, R. G. Gutmacher, and J. G. Conway, J. Opt. Soc. Amer. 64, 77 (1974).

94. N. Edelstein, J. Chem. Phys. 54, 2488 (1971).

95. I. Lamm, Nucl. Phys. A125, 504 (1969).

96. S. Nagamiya and T. Yamazaki, Phys. Rev. C4, 1961 (1971).

97. R. Kalish, B. Herskind, J. Pederson, D. Shackleton and L. Strabo, submitted to Phys. Rev. Letters.

98. E. Bodenstedt and J. D. Rogers, in Perturbed Angular Correlations, edited by E. Karlsson, E. Matthias and K. Siegbahn (North-Holland Publishing Company, Amsterdam, The Netherlands, 1964), p. 91.

99. A. Bohr and B. R. Mottelson, Nuclear Structure (W. A. Benjamin, Inc., New York, 1969), Vol. I, p. 337.

100. Th. Lindblad, H. Ryde and D. Barneoud, Nucl. Phys. A193, 155 (1972).

101. S. A. Hjorth, A. Johnson and G. Ehrling, Nucl. Phys. A184, 113 (1972).

102. A. A. Kuliev and N. I. Pyatov, Soc. J. Nucl. Phys. 9, 185 (1969) [Yad. Fiz. 9, 313 (1969)].

103. M. I. Baznat, N. I. Pyatov and M. I. Chernej, Izv. Adad. Nauk S.S.S.R., Ser. Fiz 36, 789 (1972) and JINR Report E4-6265, Dubna, 1972.

104. M. I. Baznat, N. I. Pyatov and M. I. Chernej, Physica Scripta 6, 227 (1972).

105. Proceedings of the International Conference on Nuclear Moments and Nuclear Structure, Osaka, September 1972, edited by H. Horie and K. Sugimoto (Physical Society of Japan, Tokyo, 1973).

106. B. D. Dunlap, G. M. Kalvius and G. K. Shenoy, Phys. Rev. Letters 26, 1085 (1971).

107. J. Blok and D. A. Shirley, Phys. Rev. 143, 278 (1966).

108. D. Sengupta and J. O. Artman, Phys. Rev. B1, 2986 (1970).

109. H. Crosswhite, private communication, 1974.

110. B. R. Judd, Mol. Phys. 2, 407 (1959).

111. T. E. Manning, M. Fred and F. S. Tomkins, Phys. Rev. 102, 1108 (1956).

112. I am grateful to Dr. N. Edelstein for providing the computer codes for this calculation.

113. Y.A. Ellis, Nuclear Data B6, 635 (1971).

114. C. M. Lederer, J. K. Poggenburg, F. Asaro, J. O. Rasmussen and I. Perlman, Nucl. Phys. 84, 481 (1966).

115. J. E. Thun, in Angular Correlations in Nuclear Disintegration, edited by Hans van Krugten and Bob van Nooijin (Rotterdam University Press, The Netherlands, 1971), p. 78.

116. H. J. Mang, in Angular Correlations in Nuclear Disintegration, edited by Hans van Krugten and Bob van Nooijin (Rotterdam University Press, The Netherlands, 1971), p. 103.

117. V. E. Krohn, T. B. Novey and S. Raboy, Phys. Rev. 105, 234 (1957).

118. F. Asaro and K. Siegbahn, in Perturbed Angular Correlations, edited by E. Karlsson, E. Matthias and K. Siegbahn, (North-Holland Publishing Co., Amsterdam, The Netherlands 1964), p. 233.

119. J. M. R. Hutchinson, Phys. Rev. 157, 1093 (1967).

120. F. Falk, A. Linnfors, B. Orre and J. E. Thun, Physica Scripta 1, 13 (1970).

121. G. S. Bogle, H. F. Dufus and H. E. D. Scovill, Proc. Phys. Soc. (London) A65, 760 (1952).

122. F. Asaro, S. Bjørnholm and I. Perlman, Phys. Rev. 133, 3291 (1964).

123. C. M. Lederer, J. M. Hollander and I. Perlman, Table of Isotopes, 6th Edition (John Wiley and Sons, Inc., N.Y., 1967).

124. L. A. Malov and V. G Soloviev, Sov. J. Nucl. Phys. 5, 403 (1967) [Yad. Fiz. 5, 566 (1967)].

125. F. A. Gareev, S. P. Ivanova, L. A. Malov and S. G. Soloviev, Nucl. Phys. A171, 134 (1971).

126. W. Kelly, Ten Ever-Lovin' Blue-Eyed Years with Pogo (Simon and Schuster, New York, 1972), p. 18.

127. N. Bohr and J. A. Wheeler, Phys. Rev. 56, 426 (1939).

128. A. Bohr, in Proc. Int. Conf. on the Peaceful Uses of Atomic Energy (United Nations, New York, 1956), Vol. 2, p. 151.

129. R. Vandenbosch and J. R. Huizenga, Nuclear Fission (Academic Press, New York, 1973).

130. M. Rotenberg, B. Bivins, N. Metropolis and J. J. Wooten, Jr., The 3-j and 6-j Symbols (The Technology Press, Cambridge, Massachusetts, 1957).

131. A. R. Edmonds, Angular Momentum in Quantum Mechanics (Princeton University Press, Princeton, New Jersey, 1957).

132. J. R. Huizenga, A. N. Behkami and L. G. Moretto, Phys. Rev. 177, 1826 (1969).

133. J. A. Wheeler, in Fast Neutron Physics, edited by J. B. Marion and J. L. Fowler (Interscience Publishers, Inc., New York, 1963), Pt. II, p. 2051.

134. A. N. Behkami, Nucl. Data 10, 1 (1971).

135. J. A. Barclay, Lawrence Radiation Laboratory Report No. UCRL-18986, 1969 (unpublished).

136. R. L. Fleischer, P. B. Price and R. T. Woods, Phys. Rev. 188, 563 (1969) and P. B. Price and R. L. Fleischer, Ann. Rev. Nucl. Sci. 21, 295 (1971).

137. Cryogenics Resistance Bridge, manufactured by Oxford Instrument Co., Harwell, England.

138. W. C. Black, Jr., W. R. Roach and J. C. Wheatley, Rev. Sci. Instr. 35, 587 (1964).

139. D. H. Sinclair, H. G. Terbeek and J. H. Malone, Cryogenics and Industrial Gases 5, 15 (July/August 1970).

140. F. P. Kopp and T. Ashworth, Rev. Sci. Instr. 43, 327 (1972).

141. J. F. Wild, E. K. Hulet and R. W. Lougheed, J. Inorg. Nucl. Chem. 35, 1063 (1973).

142. A. Ghiorso, unpublished results cited in E. Hyde, Nuclear Properties of the Heavy Elements (Prentice-Hall, Inc., Englewood Cliffs, New Jersey, 1964), Vol. III, p. 77.

143. W. C. McHarris, Lawrence Radiation Laboratory Report No. UCRL-11784, 1965 (unpublished).

144. P. R. Fields, H. Diamond, A. M. Friedman, J. Milsted, J. L. Lerner, R. F. Barnes, R. K. Sjoblom, D. N. Metta and E. P. Horowitz, Nucl. Phys. A96, 440 (1967) and H. Diamond, private communications, 1973-74.

145. T. Ledergerber and H. C. Pauli, Nucl. Phys. A207, 1 (1973).

146. J. Randrup, C. F. Tsang, P. Möller, S. G. Nilsson and S. E. Larsson, Lawrence Berkeley Laboratory Report No. LBL-1944, 1973 (unpublished).

147. S. G. Nilsson, private communication, 1973.

148. J. T. Caldwell, S. C. Fultz, C. D. Bowman and R. W. Hoff, Phys. Rev. 155, 1309 (1967).

LEGAL NOTICE

This report was prepared as an account of work sponsored by the United States Government. Neither the United States nor the United States Atomic Energy Commission, nor any of their employees, nor any of their contractors, subcontractors, or their employees, makes any warranty, express or implied, or assumes any legal liability or responsibility for the accuracy, completeness or usefulness of any information, apparatus, product or process disclosed, or represents that its use would not infringe privately owned rights.

TECHNICAL INFORMATION DIVISION
LAWRENCE BERKELEY LABORATORY
UNIVERSITY OF CALIFORNIA
BERKELEY, CALIFORNIA 94720